N7920117

THEORY OF LOW FREQUENCY NOISE TRANSMISSION THROUGH TURBINES

GENERAL ELECTRIC CO., EVENDALE, OH.
AIRCRAFT ENGINE GROUP

MAR 1979

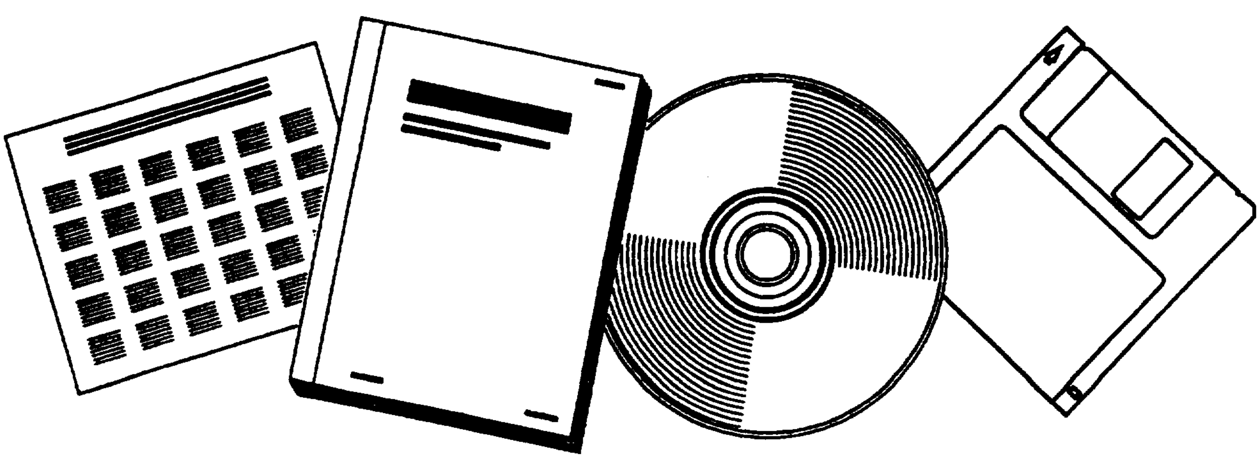

U.S. DEPARTMENT OF COMMERCE
National Technical Information Service

NASA CR-159457

R77AEG570

Theory of Low Frequency Noise Transmission through Turbines

by

R.K. Matta

R. Mani

GENERAL ELECTRIC COMPANY

Prepared For

National Aeronautics and Space Administration

NASA Lewis Research Center
Contract NAS3-20027

1. Report No. NASA CR-159457	2. Government Accession No.	3. Recipient's Catalog No.
4. Title and Subtitle THEORY OF LOW FREQUENCY NOISE TRANSMISSION THROUGH TURBINES		5. Report Date March, 1979
		6. Performing Organization Code
7. Author(s) R.K. Matta, R. Mani		8. Performing Organization Report No. R77AEG570
		10. Work Unit No.
9. Performing Organization Name and Address General Electric Company Aircraft Engine Group Evendale, Ohio 45215		11. Contract or Grant No. NAS3-20027
		13. Type of Report and Period Covered Final Contract Report
12. Sponsoring Agency Name and Address NASA Lewis Research Center 21000 Brookpark Road Cleveland, Ohio 44135		14. Sponsoring Agency Code
15. Supplementary Notes Program Manager: R.G. Huff Also see NASA CR-135219 - "Attenuation of Upstream Generated Low Frequency Noise by Gas Turbines," by V.L. Doyle and R.K. Matta, July 1977		

16. Abstract

This program was directed towards improvement of the existing theory of low frequency noise transmission through turbines and development of a working prediction tool.

The existing actuator-disk model and a new finite-chord model were utilized in an analytical study. The interactive effect of adjacent blade rows, higher order spinning modes, blade-passage shocks, and duct area variations were considered separately. The improved theory was validated using the data acquired in an earlier NASA program (NAS3-19435).

Computer programs incorporating the improved theory were produced for transmission loss prediction purposes. The programs were excercised parametrically and charts constructed to approximately define the low frequency noise transfer through turbines. The loss through the exhaust nozzle and flow(s) was also considered.

17. Key Words (Suggested by Author(s)) Combustor Noise; Core Noise Low Frequency Noise Attenuation Turbine Transfer Function Blade-Row Attenuation	18. Distribution Statement Unclassified - Unlimited

19. Security Classif. (of this report) UNCLASSIFIED	20. Security Classif. (of this page) UNCLASSIFIED	21. No. of Pages 146	22. Price*

* For sale by the National Technical Information Service, Springfield, Virginia 22151

TABLE OF CONTENTS

Section		Page
1.0	SUMMARY	1
2.0	INTRODUCTION	3
3.0	THEORY	5
	3.1 Background	5
	3.2 Finite-Chord Analysis	8
	3.3 Multistaging	15
	3.4 Secondary Effects	40
4.0	THEORY/DATA COMPARISON	48
	4.1 Background/Data Acquisition	48
	4.2 Comparison of the Data with the Improved Theory	63
5.0	USE OF THE THEORY AS A WORKING TOOL	72
	5.1 Conceptualization	72
	5.2 Computerized Prediction	72
	5.3 Approximate Estimation of the Transmission Loss	77
6.0	CONCLUSIONS	86
APPENDIX A - COMPUTER PROGRAM: MATRIX INVERSION SOLUTION		89
APPENDIX B - COMPUTER PROGRAM: ITERATIVE GENERALIZED SOLUTION		124
APPENDIX C - COUPLING OF A LINE SOURCE TO DUCT MODES		139
	NOMENCLATURE	142
	REFERENCES	145

LIST OF ILLUSTRATIONS

Figure		Page
1.	Geometry of Wave Incident on Stage Element.	6
2.	Blade-Row Attenuation Study (High Pressure Turbine).	7
3.	Dismantling of Transmission Process.	9
4.	Analyses Results.	14
5.	Comparison of Present Calculations with Actuator-Disk Analysis.	16
6.	Schematic of Sound Waves Encountered for a Three-Stage Turbine.	18
7.	Schematic of Wave Interaction at a Blade Row.	19
8.	Turbine Cascade Nomenclature.	32
9.	Schematic Representation of Area Variation for the Single-Stage, High Pressure Turbine Test.	41
10.	Shock and Acoustic Interaction (Reference 6).	46
11.	Shock Interaction with Sound Waves (Reference 6).	47
12.	Structure of Acoustic Tests to Accomplish the Program Objectives.	49
13.	Warm Air Turbine Facility.	51
14.	Schematic of Low Pressure Turbine Configurations.	52
15.	Schematic of NASA Core High Pressure Turbine Vehicle.	53
16.	Comparison of Upstream and Downstream Signals Showing Turbine Transmission Loss.	57
17.	High Pressure Turbine Design-Point Attenuation Spectra.	58
18.	Bathtub Spectrum Shape.	59
19.	Effect of Turbine Pressure Ratio on Attenuation of Single-Stage Low Pressure Turbine.	60

LIST OF ILLUSRATIONS (Continued)

Figure		Page
20.	Effect of Turbine Pressure Ratio on Attenuation of Three-Stage Low Pressure Turbine.	61
21.	Effect of Turbine Pressure Ratio on Attenuation of High Pressure Turbine.	62
22.	Comparison of Data and Prediction using Equal Energy Distribution.	65
23.	Comparison of Data and Prediction using Frequency Inverse Energy Distribution.	66.
24.	Comparison of Data and Theory using Frequency Inverse Distribution for the Low Pressure Turbine.	67
25.	Comparison of Theory and Data for the Single-Stage, Low Pressure Turbine.	69
26.	Comparison of Theory and Data for the Three-Stage, Low Pressure Turbine.	70
27.	Comparison of Theory and Data for the Single-Stage, High Pressure Turbine - Hot and Cold Inlet Flow.	71
28.	Flow Chart - Multistage, Multimode Computer Program.	73
29.	Typical Transmission Loss Spectrum.	76
30.	Approximate Prediction of Turbine Transmission Loss.	79
31.	Transmission Loss Spectrum for a Turboshaft Engine Turbine.	80
32.	Engine Data Correlation using Source Noise Parameters.	81
33.	Correlation for Turbine Transmission Loss Below Cut-On.	82
34.	Transmission Loss Through Exhaust Nozzle and Flow.	85
35.	Program Listing - Matrix Inversion Program.	90
36.	Flow Chart - Multistage, Multimode Computer Program. using Matrix Inversion.	101

LIST OF ILLUSTRATIONS (Concluded)

Figure		Page
37.	Input Sheet.	102
38.	Typical Output.	103
39.	Flow Chart - Multistage, Multimode Computer Program, Using Iterative Solution.	125
40.	Program Listing - Generalized Iterative Procedure.	126
41.	Sample Output.	135
42.	Coupling of Line Source to Duct Modes.	140

LIST OF TABLES

Table		Page
I.	Comparison of Successive Interaction and Multistage Solutions.	36
II.	Exhaust Duct Termination Effects.	43
III.	High Pressure Turbine Design Characteristics (NASA Core Turbine).	50
IV.	Low Pressure Turbine Design Characteristics (Highly Loaded Fan Turbine, HLFT-IVA).	50
V.	High Pressure Turbine Test Matrix (NASA Core Turbine).	54
VI.	Low Pressure Turbine Test Matrix (HLFT-IVA).	55
VII.	Typical Input Required for Multistage, Multimode Computer Program.	74
VIII.	Transmission Loss for Different Turbine Systems.	78

1.0 SUMMARY

Data acquired on the transmission of upstream-generated, low frequency noise transmission through aircraft engine-type turbines during NAS3-19435 showed the existing theory to be inadequate. This program, NAS3-20027, was directed towards improvement of the theory and evolution of a working tool to predict the low frequency noise transmission through turbines.

A comprehensive analytical study was performed to define the improved theory. Two approaches were utilized in the study: the existing, actuator-disk analysis and a new, finite-chord analysis. The frequency dependence was preserved through the latter, finite-element treatment of nozzle and rotor blades. However, it reproduced the results of the actuator-disk analysis for low frequencies and indicated that the simpler actuator-disk modeling was valid for frequencies as high as 0.4 to 0.5 of the blade passing frequency. This encompasses the entire frequency range of interest for combustor noise.

The existing, actuator-disk analysis and the new, finite-chord analysis both utilized an isolated blade row assumption. The effect of interaction with adjacent blade rows (multistaging) was added to the actuator-disk analysis, and due consideration was given to spinning modes by modeling these as equivalent plane waves. A frequency inverse energy distribution corresponding to the asymmetric sound introduction in the NAS3-19435 tests was specified for the multiple modes. The resulting analysis was compared with the bathtub spectrum specified in the experimental investigation and was found to be in very good agreement with the midfrequency floor, that is, nominally the 200 to 1200 Hz region. The lobe encountered in the data for this region was indeed shown to be caused by the first spinning mode cut-on. Subsequent cut-ons were found to be responsible for much of the data scatter noted previously about the nominal floor. In fact, the floor was found to extend beyond the frequency range first specified to about 2000-2500 Hz. The increase in transmission loss constituting the high frequency end of the bathtub spectrum was attributed to the diffraction by the blades.

The effect of area variations was studied and found to be responsible for a spurious increase in the transmission loss data at the very low frequencies (below 200 Hz). The apparent increase was caused by location of the downstream sensors at a pressure cancellation point in the turbine rig.

The interaction of the acoustic waves with blade passage shocks was analyzed and found to be a very weak, second-order effect.

The new theory was validated by comparison of the predicted and observed trends for the floor as a function of the pressure ratio and speed.

Two computer programs incorporating the new theory were written, and the program listings are provided in the Appendices, along with user instructions. One program is for unchoked turbines and uses an exact solution method. The other uses an iterative solution and is a generalized procedure for any combination of choked and unchoked rows.

The programs were exercised parametrically and charts constructed to approximately predict the low frequency noise transfer for single and multistage turbines. The transmission loss through the exhaust nozzle was found to merit consideration also, and was separately defined.

Recommendations were made for continuing work and include:

- Coupling of the turbine and exhaust nozzle wave systems.
- Completion of the modular prediction method for combustor noise.

2.0 INTRODUCTION

Studies of advanced aircraft propulsion systems indicate that combustor noise is a potential contributor to overall systems noise. This is especially true for propulsion systems with reduced fan and jet noise either due to cycle selection (for example, high bypass and turboshaft engines), or through incorporation of advanced acoustic treatment and/or mixed-flow exhaust systems as proposed for the Energy Efficient Engine. There has also been much speculation (see Reference 1) that "core," "tailpipe," or "excess" noise, all of which are generic terms for internally generated low frequency noise, constitute a floor in-flight for turbojet engines, such as used on the Concorde, or for low bypass engines that might be proposed for American AST application.

Accurate prediction of the different components is an important element of systems noise analysis. While General Electric's Unified Line combustor noise prediction method (Reference 2) has been found to be a reasonably accurate predictor of far-field levels for current engines, there is some question about adequacy for engines employing advanced combustors and turbines. The Unified Line method consists of a semiempirical correlation of <u>engine</u> data and makes no attempt to separate the individual elements. Recognizing that the problem is a great deal more complex than a black-box approach can cope with, General Electric has been engaged in defining an alternative, modular approach to combustor noise prediction under NASA and FAA sponsorship. The different modules consist of:

- Noise generation at the source
- Transmission through downstream turbine blade rows
- Transmission through the exhaust nozzle
- Propagation through the jet stream(s).

The acoustic characteristics of combustors at the source have been researched both experimentally and analytically in recent years (see References 1-6). Also, the investigation is continuing most actively at the NASA Lewis Research Center and at General Electric under NASA contract (NAS3-19736). The latter involves measurement of the source characteristics of an advanced, low emission combustor installed in an engine and the associated turbine transmission loss.

The salient features of low frequency noise transmission through turbines were determined on a component basis during an earlier NASA contract (Reference 7). Comparison of the data with an actuator-disk, isolated-blade-row, analytical model (Reference 3) showed the existing theory needed improvement. This program contained specific tasks to alleviate the shortcomings in the existing theory and to formulate an alternative theory free of the limitation associated with actuator-disk models.

The desired program goals were to:

1. Define an improved, validated theory for predicting the acoustic transfer function for low frequency noise propagating through aircraft engine turbines.

2. Provide working charts to predict the transfer of low frequency noise through single and multistage turbines.

3.0 THEORY

3.1 BACKGROUND

An analysis was performed previously (Reference 8) which examined the transmission and attenuation of sound waves through a turbine row on the basis that both the pitch and chord length of the turbine row were infinitesimally small compared to the wavelength of the sound impinging on it. In this limit, the turbine row may be modeled as an actuator disk which creates an abrupt discontinuity of the flow on either side of it (Figure 1). By employing conservation of mass flow and energy flux normal to the blade row, and by using the Kutta condition, the attenuation of a sound wave was calculated. This analysis was valid only for subsonic flow throughout but was later extended to include supersonic relative exit flow under NAS3-18551 (Reference 3). One of the key features of the new analysis was replacement of the Kutta condition by a choked-flow relationship. The analyses were programmed and exercised in a parametric study of the NASA Core, single-stage, high pressure turbine. The results are shown in Figure 2 in the form of the predicted attenuation for the plane-wave case as a function of the turbine stage pressure ratio with percent design speed as a parameter. The attenuation for the nozzle and rotor are shown separately and then summed to provide a stage attenuation. The supersonic and subsonic regimes are demarcated, and there is little discernible deviation going from one to the other. The predicted attenuation apparently increases slightly with pressure ratio over the subsonic range, remains flat in the transonic regime, and then decreases as the Mach number increases to well above unity.

An obvious problem with this analytical model was the loss of frequency content due to the actuator-disk assumption. Also, the upper frequency limit on the model was undefined. A second, more subtle problem was the "isolated blade row" assumption: that is, the use of anechoic terminations both upstream and downstream of the blade row in question. The effect of adjoining blade rows or discontinuities was not addressed.

An experimental investigation of low frequency noise through aircraft engine-type turbines was conducted under NAS3-19435, and the results are reported in Reference 7. The data from these scale-model-sized turbines were compared with the theory, and discrepancies between theory and data were noted. The experimentally determined transmission loss indicated a frequency dependence below 100 Hz and above 1500 Hz, increasing in both cases from a fairly constant value of attenuation in between. For single-stage turbines, the attenuation associated with this "bathtub" floor was found to correspond closely to the transmission loss predicted by the actuator-disk analysis. However, for a three-stage configuration, the attenuation was overpredicted by six to seven dB. An earlier check (Reference 3) of the analysis indicated that the attenuation for a six-stage arrangement was overpredicted by 20 dB. This clearly indicates that the attenuation for a multistage configuration cannot simply be obtained by summing up the attenuation for each individual

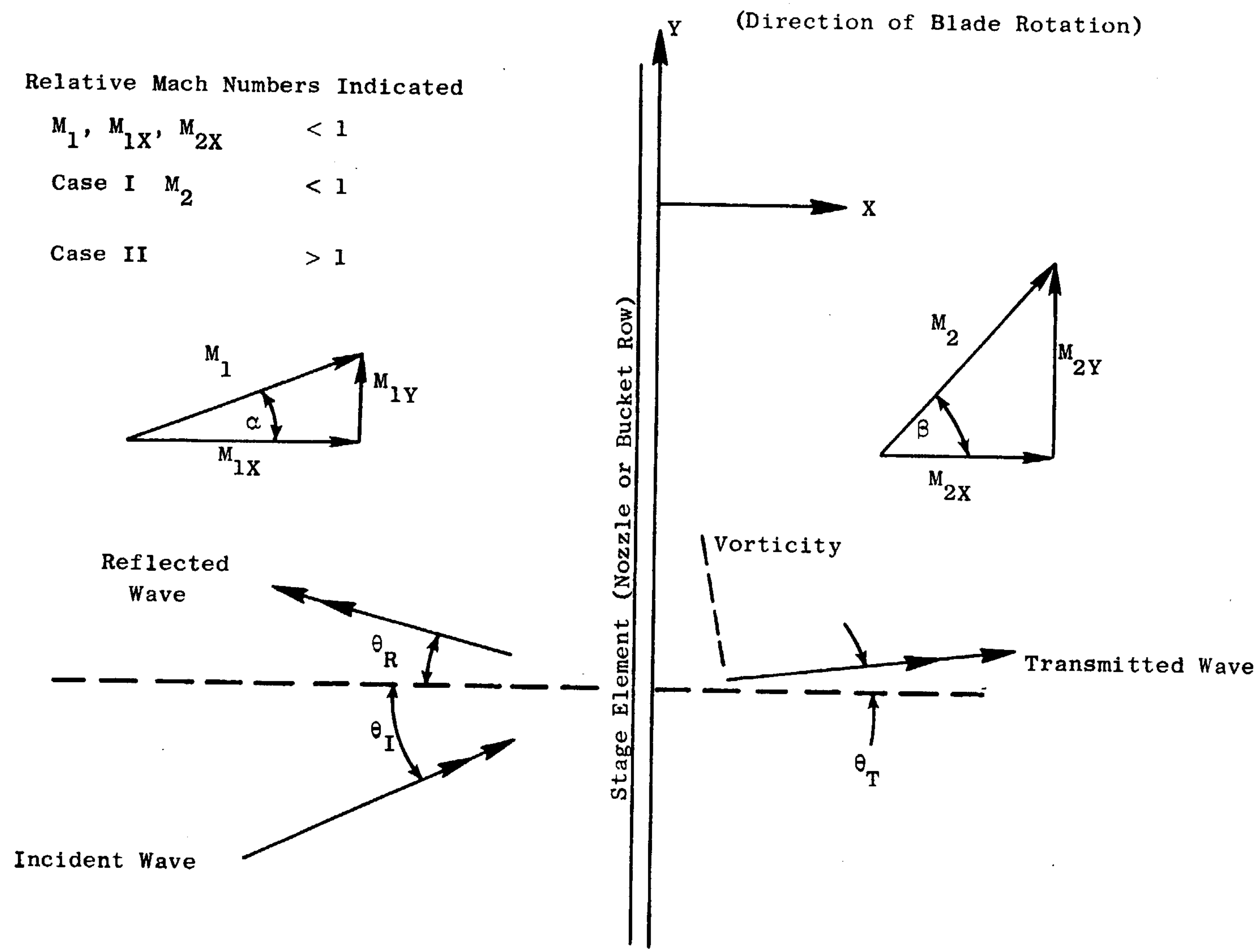

Figure 1. Geometry of Wave Incident on Stage Element.

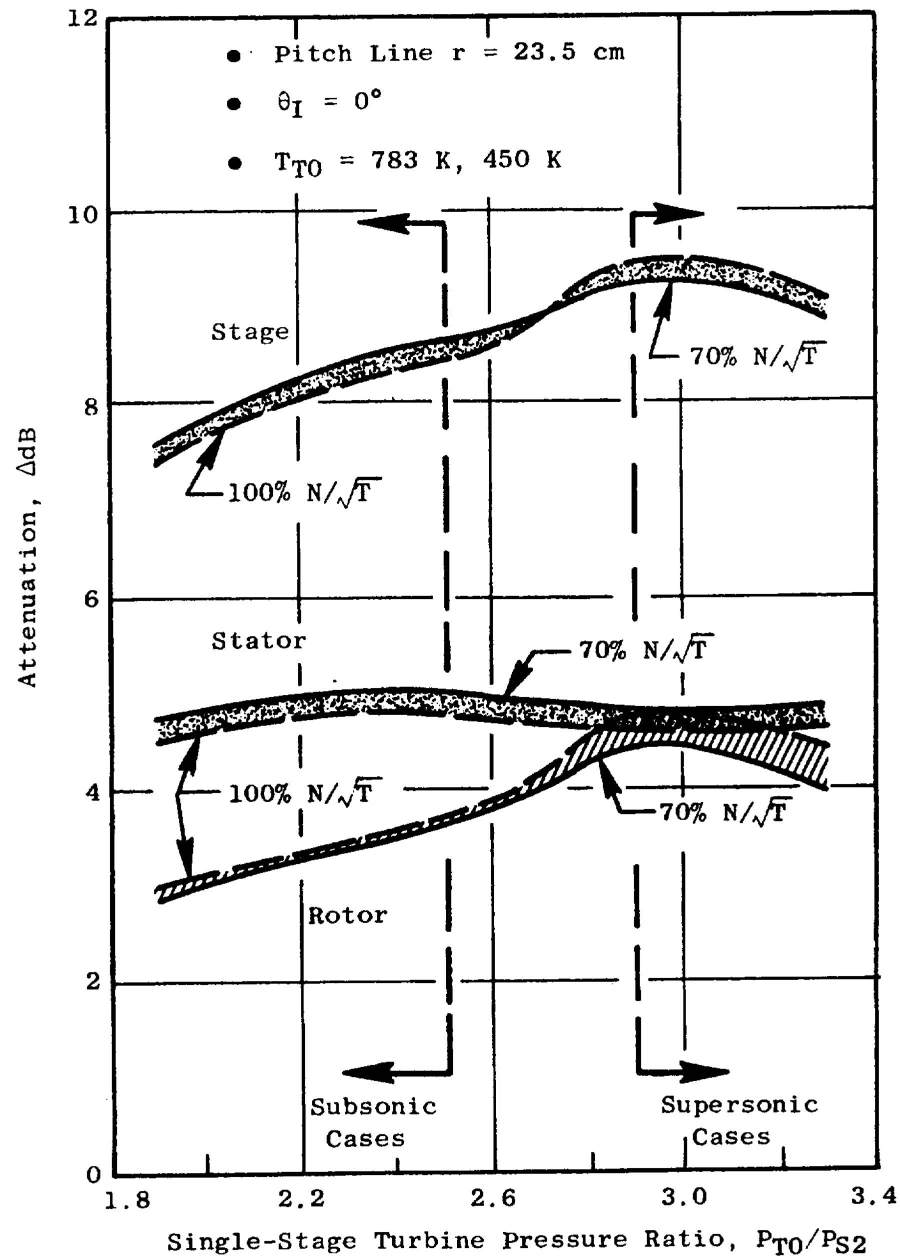

Figure 2. Blade-Row Attenuation Study (High Pressure Turbine).

blade row. The interactive effects of adjacent blade rows must be given due consideration. The interactive effect is integrated into the theory in the "multistaging" analysis in Section 3.3.

An analytical model utilizing a finite-chord-airfoil model, in order to preserve the frequency, is described in Section 3.2. The effect of acoustic wave interaction with the weak shock waves encountered in the flow passages is explored separately. The influence of abrupt area variations is examined in an attempt to discern associated frequency dependence, particularly effects which would influence the data obtained in NAS3-19435; that is, to note trends introduced by the unique facility used to obtain these data.

These data are compared with the theory in Section 3.4. A computer program incorporating the analysis is presented, along with operating instructions and sample printout. A simple, first-cut method of predicting turbine attenuation for preliminary design use is described. The method is the result of a parametric exercise of the analytical prediction program for a number of existing aircraft engine turbines. These include turbofans, turbojets, and turboshafts. The final section consists of conclusions and recommendations for future work.

3.2 FINITE-CHORD ANALYSIS

The basic idea adopted to consider the effect of finite-chord length (and finite, transverse pitch) is illustrated in Figure 3. The process of transmission of sound waves across the turbine blade row is "dismantled" into an "incidence" problem, a "passage" problem, and an "emission" problem. In other words, as in Reference 9, we assume: the incident sound wave first excites duct waveguide modes as if the blade row was a semi-infinite row of flat plates; secondly, these duct waveguide modes propagate through the turbine row as if it were a doubly infinite passage of varying area and a straight axis; finally, they reradiate plane waves on the emitted side as if the blade row was again a semi-infinite blade row of flat plates.

The above idealization considers, to a reasonable extent, the physics of the blade row; except, the curvature of the row is not being accounted for in the "passage" problem (though the curvature of the blade row is accounted for in treating the two semi-infinite blade rows corresponding to the incidence and emission problems as of different stagger angle). With "t" and "M_n" denoting the normal pitch at the inlet and inlet Mach number to the blade row, if the frequency of excitation in Hz is below [$a \sqrt{1 - M_n^2}/2t$] only the lowest duct waveguide mode of all the duct waveguide modes excited will be propagating. Under these circumstances, Cummins (in Reference 10) has shown experimentally (with no flow) that even curved bends with 180° turning produce very little transmission loss. We will restrict the analysis to frequencies below [$a \sqrt{1 - M_n^2}/2t$] (a is the speed of sound at the inlet to the row). The effects of variable area and variable Mach number in the passage problem are accounted for.

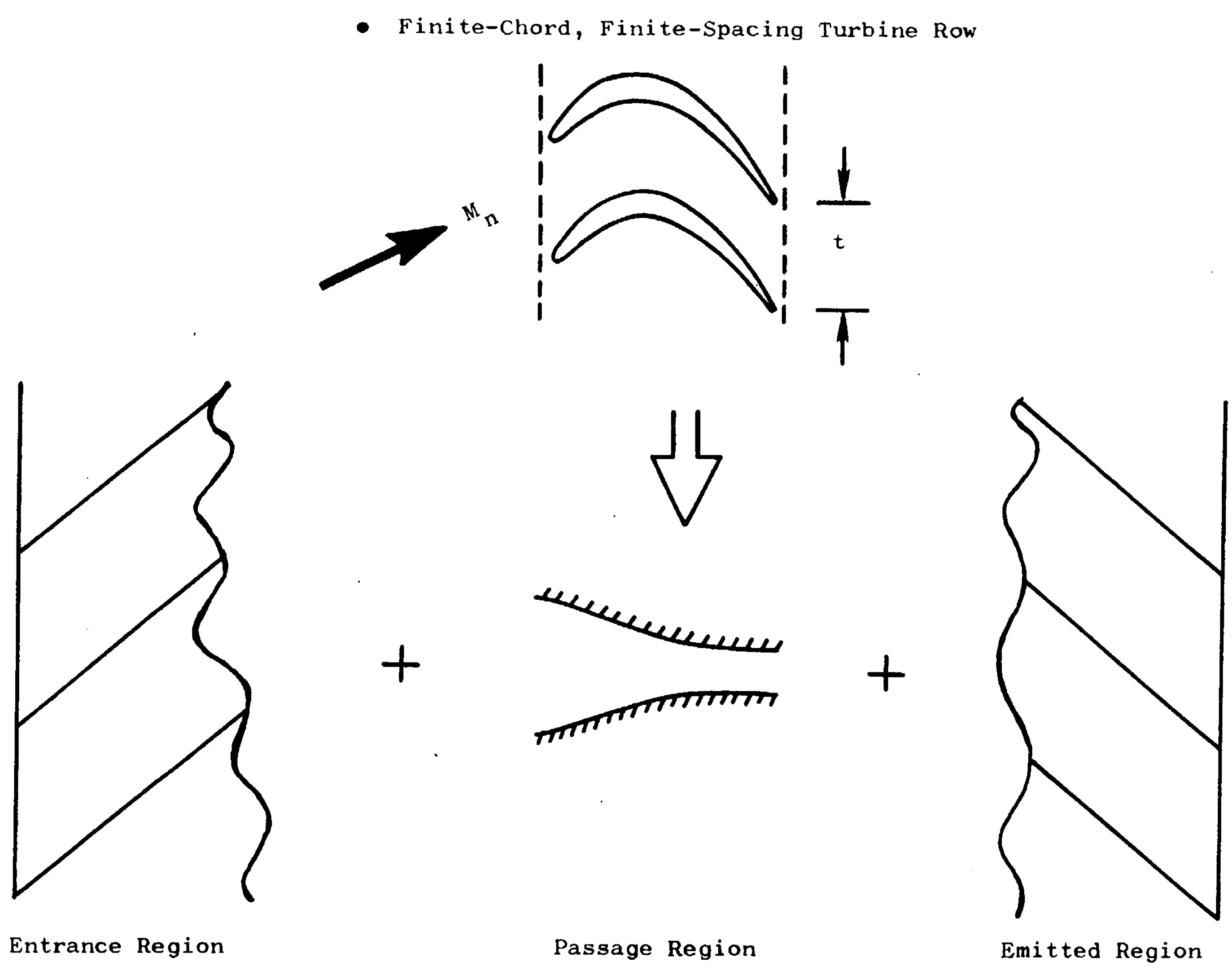

Figure 3. Dismantling of Transmission Process.

The incidence and emission problems are largely a matter of applying the results of Reference 9 and, hence, will not be discussed further here. The transmission of the lowest duct wave-guide mode through the variable area, variable Mach number, but straight passage region is discussed next.

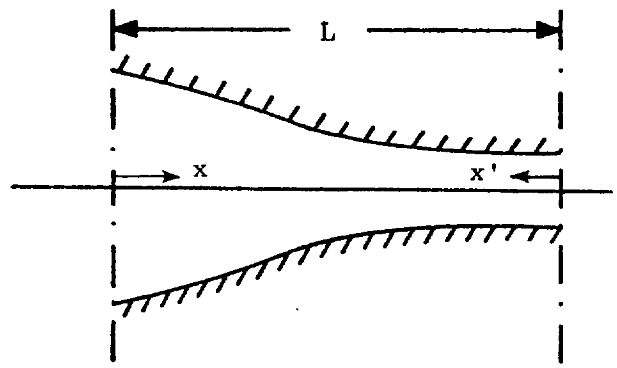

The equations governing the propagation of the lowest mode may be written in terms of a nondimensional acoustic pressure $\phi(p'/\gamma p)$ and nondimensional velocity $\nu(u'/U)$ as:

$$U \frac{d\nu}{dx} + U \frac{d\phi}{dx} - j \omega \phi = 0 \quad \text{(continuity equation)} \tag{1a}$$

$$\left(\frac{1}{M^2} - 1\right) U \frac{d\phi}{dx} - [(\gamma - 1) \frac{dU}{dx} - j \omega]\phi$$

$$+ [2 \frac{dU}{dx} - j \omega]\nu = 0$$

$$\text{(x-momentum equation)} \tag{1b}$$

In (1a) and (1b), a time dependence for all quantities of type exp $(-j \omega t)$ is assumed, $U(x)$ denotes the steady, average, axial velocity in the nozzle; $M(x)$ the associated steady, average, axial Mach number; and γ the specific heat ratio*. The above equations are given in References 11 to 14.

---

*p(x) is the average, steady, static-pressure distribution in the nozzle.

For convenience of the computational scheme to be used, we first introduce ϕ and $(\phi + \nu)$, rather than ϕ and ν as the dependent variables. We thus rewrite (1a) and (1b) as:

$$U \frac{d}{dx} (\nu + \phi) = j \omega \phi \tag{2a}$$

and

$$\left(\frac{1}{M^2} - 1\right) U \frac{d\phi}{dx} = \left[(\gamma + 1) \frac{dU}{dx} - 2 j \omega\right] \phi$$

$$- \left[2 \frac{dU}{dx} - j \omega\right] (\nu + \phi) \tag{2b}$$

Secondly, it will prove useful to choose the independent variable as $x' = (L - x)$ where L is the length from $U = 0$ to $U = a^*$, where a^* is the sonic velocity at the throat for the equivalent "linear" nozzle (following Reference 11). Equations (2a) and (2b) become:

$$U \frac{d}{dx'} (\nu + \phi) = -j \omega \phi \tag{3a}$$

$$U \frac{d\phi}{dx'} = \frac{M^2}{(1 - M^2)} \left\{\left[(\gamma + 1) \frac{dU}{dx'} + 2 j \omega\right]\phi\right.$$

$$\left. - \left[2 \frac{dU}{dx'} + j \omega\right](\nu + \phi)\right\} \tag{3b}$$

The "linear" nozzle approximation assumes that $U(x)$ varies linearly from the inlet to the outlet, that is: $\frac{U}{a^*} = \frac{x}{L}$. As stated in Reference 13, is a "suprisingly satisfactory approximation for conventional nozzles." We next nondimensionalize (3a) and (3b) by using a^* as a velocity scale and L as the length scale; (3a) and (3b) become:

$$(1 - \xi) \frac{d}{d\xi} (\nu + \phi) = - j \eta \phi \tag{4a}$$

$$(1 - \xi) \frac{d\phi}{d\xi} = \left\{[-(\gamma + 1) + 2 j \eta]\phi\right.$$

$$\left. + [2 - j \eta] (\nu + \phi)\right\} \frac{M^2}{(1 - M^2)} \tag{4b}$$

where $\eta = \omega L/a^*$ and $\xi = x'/L$

Now, for the linear nozzle, $M^2/(1 - M^2)$ may be shown to be

$$\frac{2(1 - \xi)^2}{(\gamma + 1)\ \xi(2 - \xi)}$$

so that we have to integrate the pair:

$$\frac{d}{d\xi}(\nu + \phi) = \frac{-j\ \eta\ \phi}{(1 - \xi)} \tag{5a}$$

$$\frac{d\phi}{d\xi} = \frac{2(1 - \xi)}{(\gamma + 1)\ \xi(2 - \xi)} \{[-(\gamma + 1) + 2j\ \eta]\phi$$

$$+ (2 - j\ \eta)\ (\phi + \nu)\} \tag{5b}$$

If M_i and M_f denote the initial and final Mach numbers in the nozzle (with $0 < M_i < M_f < 1$), the initial and final values of ξ are:

$$\xi_i = 1 - \left[\frac{M_f^{\,2}(\gamma + 1)}{2 + M_f^{\,2}\ (\gamma - 1)}\right]^{1/2} \tag{6a}$$

$$\xi_f = 1 - \left[\frac{M_i^{\,2}(\gamma + 1)}{2 + M_i^{\,2}(\gamma - 1)}\right]^{1/2} \tag{6b}$$

Note that if $0 < M_i < M_f < 1$, then $0 < \xi_i < \xi_f < 1$.

Suppose we start the integration near the nozzle throat at $\xi = \xi_i$. Assume there is only a transmitted wave in the nozzle; hence, we may show that if $\phi(\xi_i) = 1$, then $\nu(\xi_i) = 1/M_f$ and $\phi(\xi_i) + \nu(\xi_i) = [1 + 1/M_f]$. Equations (5a) and (5b) can be integrated by a Runge Kutta fourth-order scheme from $\xi = \xi_i$ to $\xi = \xi_f$ with the above initial values for ϕ and $(\phi + \nu)$ at $\xi = \xi_i$. If the terminal values of ϕ and $(\phi + \nu)$ at $\xi = \xi_f$ are known, by use of impedance relations for forward and reflected waves, $\phi_{inc.}$ at $\xi = \xi_f$ may be shown to be:

$$\frac{1}{2}\ \{(1 - M_i)\phi + M_i(\phi + \nu)\}$$

where ϕ and $(\phi + \nu)$ are the computed values at $\xi = \xi_f$ (where the Mach number is M_i).

The above describes the essence of the computation scheme that was adopted in the present study. Mesh size was normally taken as the smaller of $(\xi_f - \xi_i)/100$ or $\pi/20\eta$ so that it was the smaller of one-hundredth of the (nondimensional) nozzle length or one-fortieth of a wavelength (based on a^*, the speed of sound at the throat). However, for ξ small or ξ close to unity, the derivatives $d\phi/d\xi$ and $d/d\xi\ (\nu + \phi)$ can be quite large; hence, the mesh size was reduced to one-eighth times the lesser of ξ or $(1 - \xi)$ times the usual step size for $\xi < 0.125$ or $\xi > 0.875$.

The inputs are M_1, M_2*, and a frequency parameter taken here as f = [frequency in radians/sec] × actual nozzle curved length/speed of sound at stagnation conditions. Then η may be shown to be:

$$\eta = f \sqrt{(\gamma + 1)/2} \ / \ (\xi_f - \xi_i)$$

The analysis assumes $\gamma = 1.4$. It calculates the static pressure ratio (p_f/p_i) of the steady, ideal flow. Marble, in Reference 13, shows that as $\eta \to 0$ we may expect a result for $(p'_{transm.}/p'_{inc.})$ of

$$\left(\frac{2\ M_2}{(1 + M_2)}\right)\left(\frac{1 + M_1}{M_1 + M_2}\right)\left[\frac{\left(1 + \frac{\gamma - 1}{2} M_2^{\ 2}\right)}{\left(1 + \frac{\gamma - 1}{2} M_1\ M_2\right)}\right](p_f/p_i).$$

This is the result for "compact" nozzles. As $\eta \to \infty$ we may expect a limit from the point of view that the Blokhintsev energy is conserved at high frequencies (as pointed out in References 12 and 14, so that $(p'_{transm.}/p'_{inc.})$ would tend to

$$\left\{\left[\left(1 + \frac{\gamma - 1}{2} M_2^{\ 2}\right)^{1/2} M_2^{\ 1/2}\ (1 + M_1)\right] \div \left[\left(1 + \frac{\gamma - 1}{2} M_1^{\ 2}\right)^{1/2} M_1^{\ 1/2}\ (1 + M_2)\right]\right\} \quad \text{times } (p_f/p_i).$$

The results for $M_i = 0.05$, 0.1, and $M_f = 0.95$, 0.975, and for "f" ranging from 0.1 to 20, are shown in Figure 4. Notice the figure shows excellent agreement at high and low values of "f" with the theories of Blokhintsev and Marble.

The analysis described above for the passage problem was coupled to the solutions from Reference 9 for the incidence and emission problems to derive the complete, though approximate, solution.

---

*M_1 and M_2 are sometimes used to denote M_i and M_f respectively in what follows.

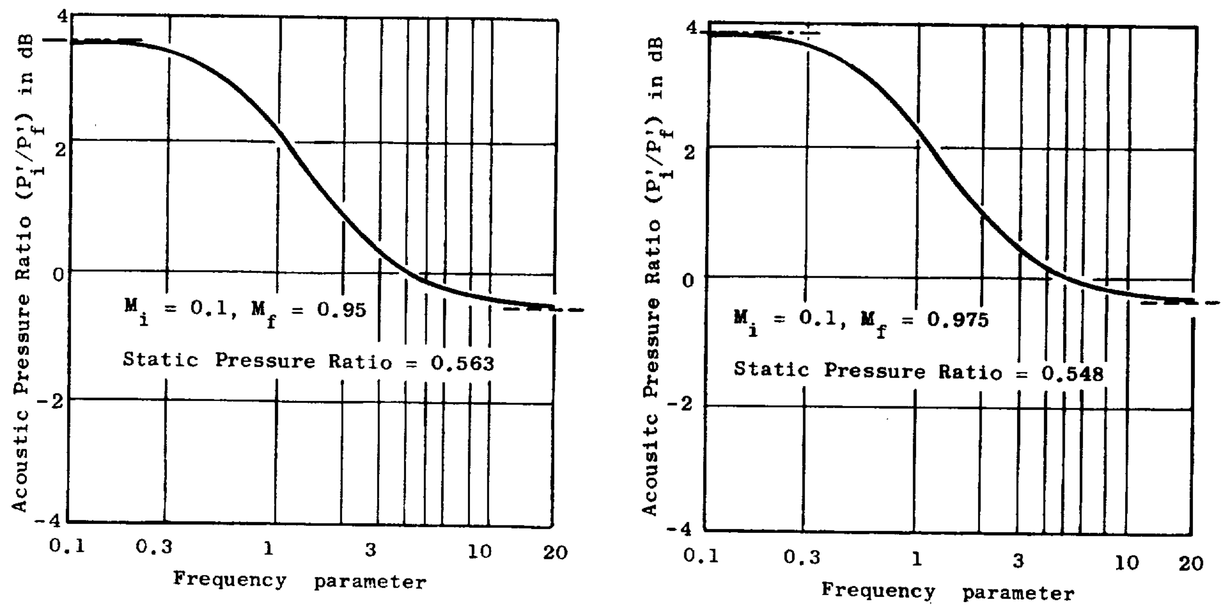

Frequency Parameter = (frequency in rad/sec) × (Nozzle Length)/(Stagnation Speed of Sound)
——— Current Calculations, —·— Marble Theory for "Compact" Nozzles (Zero Frequency Parameter), ------ Blokhintsev High Frequency Theory (Infinite Frequency Parameter)

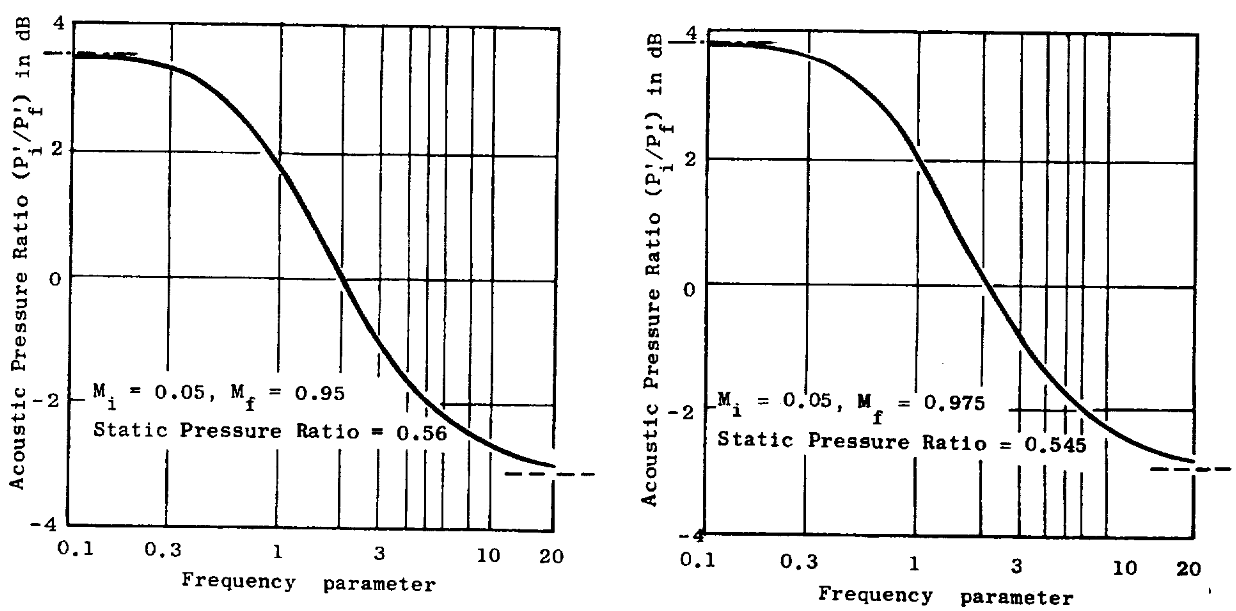

Figure 4. Analysis Results.

To check that such a "dismantling" process is valid, comparisons were made with the present method and with the actuator-disk method for a very low excitation frequency. Excellent agreement was obtained between the results of the two methods as shown in Figure 5.

Repeated calculations with the present method showed, however, that up to frequencies (f) defined by

$$f < \left[\frac{a\sqrt{1 - M_i^2}}{2t}\right]$$

the calculated results are rather insensitive to frequency. Since the rotor blade passing frequency can be taken as W_R/t, where W_R is the wheel tip velocity of the rotor and t the transverse pitch of the rotor, the above indicates that, up to half the rotor blade passing frequency, the results are rather insensitive to frequency. It should be pointed out that more exact calculations in Reference 15 for flat-plate cascades bear out these conclusions. The passage problem does have a frequency dependence, but it turns out that, once the initial Mach number (M_i) to a row exceeds 0.3, the frequency dependence is very slight with even the zero and infinite frequency limits being within a dB of each other.

Thus, the most important conclusion of Section 3.1 was that, in fact, the actuator-disk model has a high regime of validity; it is valid up to roughly (at least) one-half the blade passing frequency. In practical terms, for core noise interests which extend to less than one-half the blade passing frequency, there is no need to consider any frequency dependence insofar as the analysis of the transmission phenomenon is concerned; although, frequency dependencies may arise in a given experiment due to the fact that given source types couple into a duct in a frequency-dependent manner, and incidence angles on the blade row may be frequency dependent.

3.3 MULTISTAGING

3.3.1 Problem Formulation

A sound wave incident on a blade row will generally give rise to a reflected sound wave, a transmitted sound wave, and a shear (vorticity) wave. The latter two are formed downstream of the blade row and propagate in that direction. The former is encountered upstream of the blade row and will propagate in a direction opposite to that of the incident wave.

The transmitted wave will, in turn, be responsible for another set of three waves on encountering the next blade row. Further, the reflected wave from the second blade row interaction will interact with the first blade row giving rise to yet three more waves! It is convenient to collect all the upstream and downstream waves after a "steady state" has been attained such that there exist a pair of forward- and backward-propagating waves between

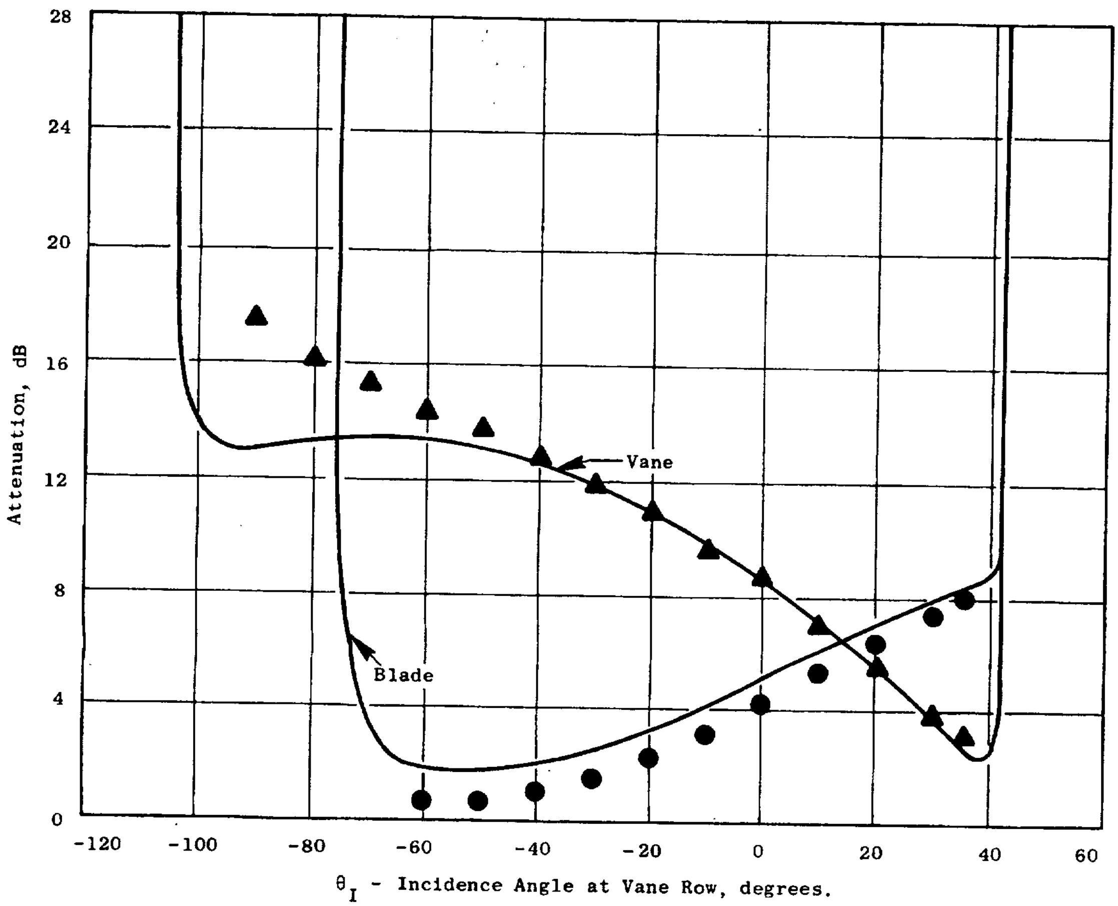

▲ New Calculations for Vane Row } at Low Frequencies
● New Calculations for Blade Row } at Low Frequencies
—— Actuator-Disk Results

	Upstream of Vane	Downstream of Vane	Upstream of Blade	Downstream of Blade
Axial Mach Number	0.25	0.27	0.27	0.38
Tangential Mach Number (Relative)	0	0.95	0.45	-0.84
Static Temperature K (° R)	1244 (2240)	1056 (1900)	1056 (1900)	1000 (1800)
Static Pressure MN/m^2 (psia)	0.81 (117)	0.41 (59)	0.41 (59)	0.28 (41)
	← Stage Press Ratio = 2.85 →			

Figure 5. Comparison of Present Calculations with Actuator-Disk Analysis.

each blade row (see Figure 6). Assuming anechoic terminations upstream and downstream of the turbine, the incident wave provides the only forward-propagating energy upstream, while a transmitted wave contains all the sound energy downstream and propagates away from the turbine.

In addition to the sound waves, there exist vorticity waves at each interface. These propagate with the flow and can only exist on the downstream side of each interaction; that is, the vorticity wave between an upstream nozzle and a rotor is determined by the interactions at the nozzle.

Since the wavelengths of interest here are of the order of a foot, while the blade chords and spacings are of the order of an inch, an actuator-disk analysis is conveniently applicable. Also, the phase differences between interfaces are small and can be neglected, considerably simplifying the problem.

A two-dimensional Cartesian coordinate system, fixed with respect to each blade row in turn, is used. Hence all quantities assume their relative values at each rotating blade row, as distinct from their absolute values. In this analysis, the relative inlet Mach number and the axial component of the exhaust Mach number are being limited to subsonic values. At any interface, upstream quantities will be denoted by the subscript n and downstream quantities by m. Hence, in a three-stage turbine, n can assume values from one to six, and m from two to seven, as is shown in Figure 6.

3.3.2 Wave Description

The wave interaction at each interface can be described schematically as in Figure 7. The direction of rotation defines the positive y-axis and the axial flow direction the positive x-axis. The flow angles are given by α and β upstream and downstream of the blade row respectively. Since alternate blade rows rotate and are fixed to each blade row in turn, α_n and β_n are not equal but are related by the rotor velocity component. Note that for turbines β will generally be negative downstream of a rotor and positive downstream of a nozzle.

The sign on the wave propagation angles is defined solely by the y-component of the velocity, as the x-components are predetermined by the forward- and backward-propagation terms. Hence all θ's shown in Figure 7 are positive.

The frequency across any interface is preserved. However, since the acoustic velocity varies and the wave number is defined by ω/a, upstream and downstream wave numbers are related by

$$\frac{k_m}{k_n} = \frac{a_n}{a_m} \tag{7}$$

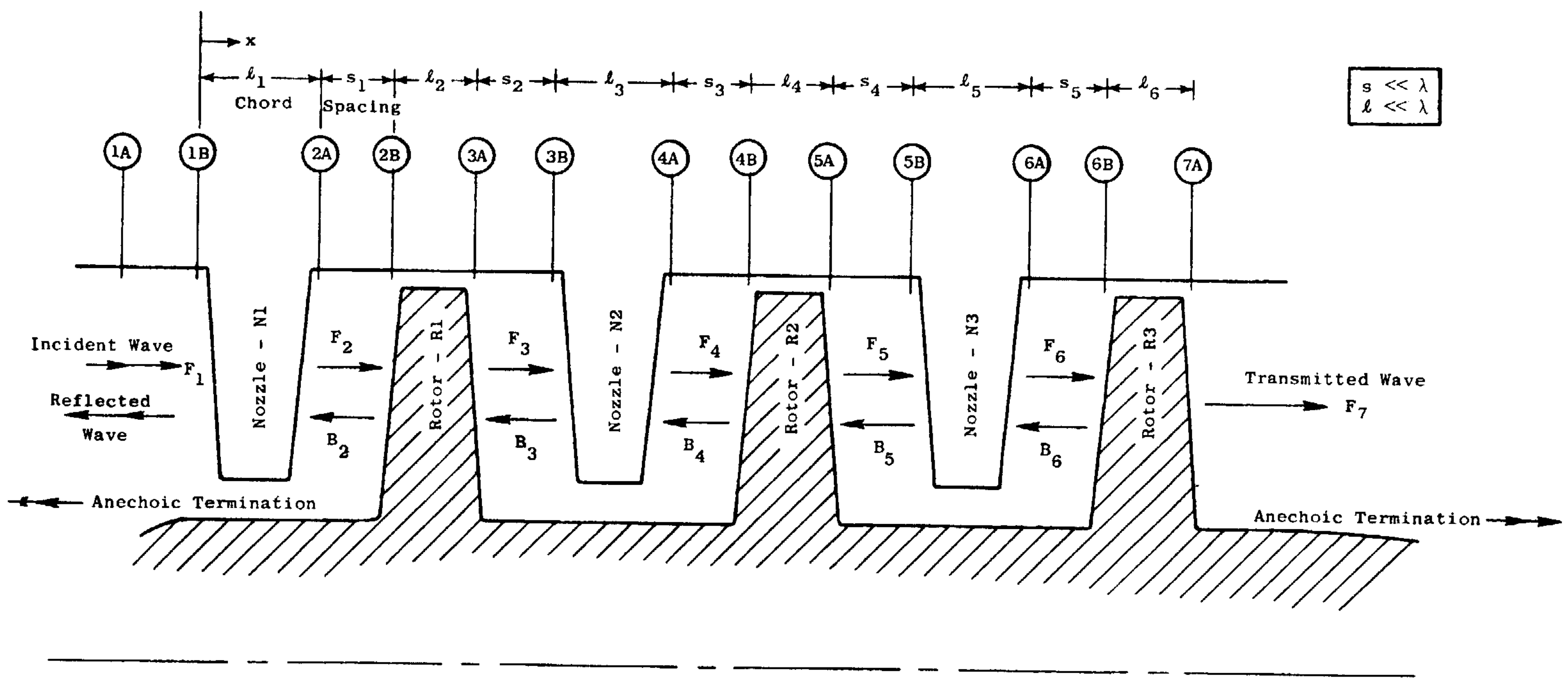

Figure 6. Schematic of Sound Waves Encountered for a Three-Stage Turbine.

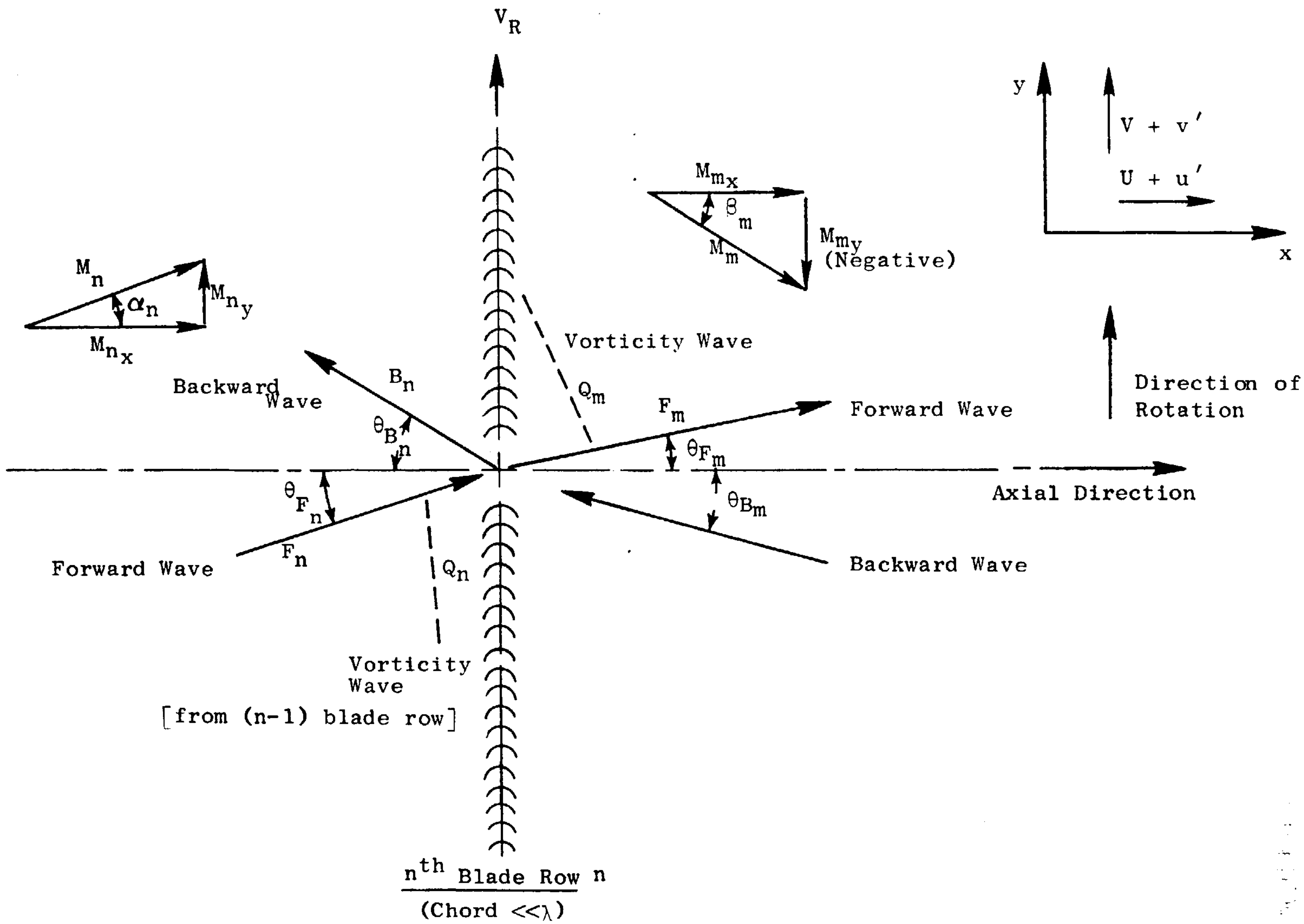

Figure 7. Schematic of Wave Interation at a Blade Row.

where a - ambient acoustic velocity

k - wave number, ω/a

ω - circular frequency, $2\pi f$

The pressure perturbation associated with forward- and backward-traveling sound waves can be expressed as:

$$p'_{F_n} = F_n \exp j \left[\frac{k_n (x \cos \theta_{F_n} + y \sin \theta_{F_n})}{1 + M_{nx} \cos \theta_{F_n} + M_{ny} \sin \theta_{F_n}} - \omega t \right] \quad (8)$$

and

$$p'_{B_n} = B_n \exp j \left[\frac{k_n (-x \cos \theta_{B_n} + y \sin \theta_{B_n})}{1 - M_{nx} \cos \theta_{B_n} + M_{ny} \sin \theta_{B_n}} - \omega t \right] \quad (9)$$

where the amplitudes F_n and B_n are fractions of the amplitude in the incident wave. That is, the incident wave is given by:

$$p'_I = \exp j \left[\frac{k_1 (x \cos \theta_I + y \sin \theta_I)}{1 + M_{1x} \cos \theta_I + M_{1y} \sin \theta_I} - \omega t \right] \quad (10)$$

The corresponding density and velocity perturbations are given by:

$$\rho'_{F_m} = \frac{p'_{F_m}}{a_m^2} \qquad m = 2, 3, \ldots 7 \quad (11)$$

The primed quantities denote a perturbation value, as distinct from steady-state values.

$$(u'_{F_m}, v'_{F_m}) = (\cos \theta_{F_m}, \sin \theta_{F_m}) \frac{p'_{F_m}}{\rho_m a_m} \quad (12)$$

$$\rho'_{B_n} = \frac{p'_{B_n}}{a_n^2} \qquad n = 1, 2, \ldots 6 \quad (13)$$

$$(u'_{B_n},\ v'_{B_n}) = (-\cos\theta_{B_n},\ \sin\theta_{B_n})\ \frac{p'_{B_n}}{\rho_n a_n} \qquad (14)$$

$$\rho'_I = \frac{p'_I}{a_I^2} \qquad (15)$$

$$(u'_I,\ v'_I) = (\cos\theta_I,\ \sin\theta_I)\ \frac{p'_I}{\rho_I a_I} \qquad (16)$$

There are no pressure or density perturbations associated with a vorticity wave, hence

$$p'_{Q_m} = \rho'_{Q_m} = 0 \qquad (17)$$

The velocity perturbations convect with the flow and assume the form:

$$(u'_{Q_m},\ v'_{Q_m}) = (K_{Qx},\ K_{Qy})\ Q_m\ \exp_j\ \{k_{mx}\ x + k_{my}\ y - \omega t\} \qquad (18)$$

where the direction cosines K_{Q_x} and K_{Q_y} remain to be defined.

The y-dependence of all the waves is determined by the incident wave:

$$\frac{k_n \sin\theta_{F_n}}{1 + M_{nx}\cos\theta_{F_n} + M_{ny}\sin\theta_{F_n}} = \frac{k_n \sin\theta_{B_n}}{1 - M_{nx}\cos\theta_{B_n} + M_{ny}\sin\theta_{B_n}} \qquad (19a)$$

$$= \frac{k_m \sin\theta_{F_m}}{1 + M_{mx}\cos\theta_{F_m} + M_{my}\sin\theta_{F_m}} \qquad (19b)$$

$$= \frac{k_m \sin\theta_{B_m}}{1 - M_{nx}\cos\theta_{B_m} + M_{my}\sin\theta_{B_m}} \qquad (19c)$$

$$= k_{my} \qquad (19d)$$

After some manipulation, the following expressions can be derived for θ_{B_n}, θ_{B_m}, and θ_{F_m} in terms of the "known" θ_{F_n} ($\theta_{F_1} \equiv \theta_I$):

$$\tan \theta_{B_n} = \frac{\left(1 - M_{nx}^2\right)\sin \theta_{F_n}}{\left(1 + M_{nx}^2\right)\cos \theta_{F_n} + 2 M_{nx}} \tag{20}$$

$$\tan \theta_{B_m} = \frac{- G_{mn} M_{mx} (1 - G_{mn} M_{my}) + G_{mn}\sqrt{\left[(1 - G_{mn} M_{my})^2 - (1 - M_{mx}^2) G_{mn}^2\right]}}{(1 - G_{mn} M_{my})^2 - G_{mn}^2} \tag{21}$$

$$\tan \theta_{F_m} = \frac{G_{mn} M_{mx} (1 - G_{mn} M_{my}) + G_{mn}\sqrt{\left[(1 - G_{mn} M_{my})^2 - (1 - M_{mx}^2) G_{mn}^2\right]}}{(1 - G_{mn} M_{my})^2 - G_{mn}^2} \tag{22}$$

$$\frac{k_{my}}{k_m} = G_{mn} \tag{23}$$

where $$G_{mn} = \frac{k_n}{k_m} \frac{\sin \theta_{F_n}}{1 + M_{nx} \cos \theta_{F_n} + M_{ny} \sin \theta_{F_n}} \tag{24}$$

The quantity k_{mx} is determined using the fact that the vorticity wave convects with the flow. That is, the wave will appear fixed (free of time dependence) in a coordinate frame moving with the fluid. The coordinate transformation is given by:

$$x_F = x - a_m M_{mx} t$$

$$y_F = y - a_m M_{my} t$$

The exponent in equation (18) becomes ...

$$\{k_{mx} (x_F + a_m M_{mx} t) + k_{my} (y_F + a_m M_{my} t) - \omega t\} \tag{25}$$

Since the time dependence must vanish,

$$k_{mx}\, a_m\, M_{mx} + k_{my}\, a_m\, M_{my} - \omega = 0$$

or $$k_{mx} = \frac{k_m - k_{my}\, M_{my}}{M_{mx}}$$

since $$k_m = \omega / a_m$$

Therefore $$\frac{k_{mx}}{k_m} = \frac{1 - (k_{my}/k_m)\, M_{my}}{M_{mx}}$$

or $$\frac{k_{mx}}{k_m} = \frac{1 - G_{mn}\, M_{my}}{M_{mx}} \qquad (26)$$

The direction cosines are determined from the fact that the vorticity wave is divergence free, so that

$$\frac{\partial u'_{Qm}}{\partial x} + \frac{\partial v'_{Qm}}{\partial y} = 0.$$

This requires

$$k_{mx}\, u'_{Qm} + k_{my}\, v'_{Qm} = 0.$$

Equation (18) can then be expressed as

$$(u'_{Qm}, v'_{Qm}) = \left(\frac{k_{my}}{\sqrt{k_{mx}^2 + k_{my}^2}}, \frac{-k_{mx}}{\sqrt{k_{mx}^2 + k_{my}^2}} \right) Q_m \exp j \left[k_{mx} x + k_{my} y - \omega t \right] \qquad (27)$$

The reflected and transmitted waves always appear on the opposite side of the axis from the incident wave. Using the sign convention of Figure 7, this means

$$\theta_R > 0 \text{ and } \theta_T > 0 \quad \text{when} \quad \theta_I > 0$$

$$\theta_R < 0 \text{ and } \theta_T < 0 \quad \text{when} \quad \theta_I < 0$$

$$\theta_R = \theta_T = 0 \quad \text{when} \quad \theta_I = 0$$

Cutoff Angles

There are two cutoff criteria for each blade row.

(a) Upstream Cutoff

On the upstream side of a blade row, the fact that a wave is forward propagating implies that

$$|\theta_{F_n}| < 90° + \sin^{-1} M_{nx} \tag{28a}$$

This condition can alternately be expressed as:

$$U_n + a_n \cos \theta_{F_n} \geq 0 \tag{28b}$$

Hence the upstream cutoff angles are determined by using an equality sign in expression (28). Waves exceeding $|\theta_{F_n}|$ cannot be incident on the blade row in question as they convect upstream.

(b) Downstream Cutoff

On the downstream side of a blade row, a forward-propagating wave implies that

$$|\theta_{F_m}| < 90° + \sin^{-1} M_{mx} \tag{29a}$$

This gives cutoff angles of:

$$\tan \theta_{F_m}, \text{cut-off} = \frac{\pm\sqrt{1-M_{mx}^2}}{-M_{mx}} \tag{29b}$$

This also defines the transmitted wave angle for which the radical in equation (22) becomes zero. For angles larger than this cutoff angle, the radical becomes negative and the wave decays exponentially.

Corresponding to the θ_{F_m} of equation (29) are θ_{F_n}, which can be derived using equation (19b)

$$\text{or } \tan \theta_{F_n}, \text{cut-off} = \frac{G_{nm}M_{nx}(1-G_{nm}M_{ny})+G_{nm}\sqrt{(1-G_{nm}M_{ny})^2-(1-M_{nx}^2)G_{nm}^2}}{(1-G_{nm}M_{ny})^2-G_{nm}^2} \tag{30}$$

$$\text{where } G_{nm} = \frac{k_m}{k_n} \; \frac{\sin\theta_{F_m}}{1+M_{mx}\cos\theta_{F_m}+M_{my}\sin\theta_{F_m}} \tag{31}$$

and θ_{F_m} is defined by equation (29b).

Real values of θ_{F_n} from equation (30) impose further limits on forward-propagating waves that are transmitted through any blade row.

3.3.3 Matching Conditions

Mass and energy conservation provide two sets of equations. A third set is derived from imposing the Kutta condition at the trailing edge (this is for subsonic relative exit flow; for supersonic flow, the choking condition is used instead).

Subsonic Relative Exhaust Flow

The linearized equation for mass conservation gives

$$[U\rho' + \rho u']_n = [U\rho' + \rho u']_m \tag{32}$$

where the subscripts indicate evaluation of the quantities in the square bracket on the upstream and downstream sides, respectively, of the actuator disk.

The linearized equation for energy conservation along with the adiabatic flow relation, p/ρ^γ = constant, in a frame of reference fixed to the blade yields:

$$[\frac{p'}{\rho} + U\ u' + V\ v']_n = [\frac{p'}{\rho} + U\ u' + V\ v']_m \tag{33}$$

If a stationary or laboratory coordinate system is used, the rotor energy must also be included.

Finally, the Kutta condition requires the flow to leave tangent to a trailing edge. Since the unit vector normal to the exit stream is given by $(-\sin\beta\ \hat{e}_x + \cos\beta\ \hat{e}_y)$, the Kutta condition gives

$$[\vec{v}' \cdot (-\sin\beta\ \hat{e}_x + \cos\beta\ \hat{e}_y)]_m = 0$$

or

$$[-u' \sin\beta + v' \cos\beta]_m = 0 \tag{34}$$

In general, the quantities both upstream and downstream will consist of a forward-propagating sound wave, a backward-propagating sound wave, and a vorticity wave. However, upstream of the first blade row there is no vorticity wave ($Q_1 = 0$), and downstream of the last blade row there is no backward-traveling sound wave ($B_{2N+1} = 0$), where N is the number of stages in the turbine. Since $F_1 \equiv 1$, that leaves 6N unknowns. However, there are 2N blade rows with three equations at each blade row. Therefore the problem can be solved.

Application of the matching conditions (32) - (34) to the first blade row gives the following equation set which can be expressed in matrix form as:

$$\begin{Bmatrix} \frac{a_1}{a_2}(M_{2x} + \cos\theta_{F_2}) & \frac{a_1}{a_2}(M_{2x} - \cos\theta_{B_2}) & \frac{a_1}{a_2}\frac{k_{2y}}{\left(k_{2x}^2 + k_{2y}^2\right)^{1/2}} \\ \frac{\rho_1}{\rho_2}[1 + M_2\cos(\beta_2 - \theta_{F_2})] & \frac{\rho_1}{\rho_2}[1 - M_2\cos(\beta_2 + \theta_{B_2})] & \frac{\rho_1}{\rho_2}\left[\frac{M_{2x}k_{2y} - M_{2y}k_{2x}}{\left(k_{2x}^2 + k_{2y}^2\right)^{1/2}}\right] \\ \sin(\beta_2 - \theta_{F_2}) & -\sin(\beta_2 + \theta_{B_2}) & \left[\frac{k_{2y}\sin\beta_2 + k_{2x}\cos\beta_2}{\left(k_{2x}^2 + k_{2y}^2\right)^{1/2}}\right] \end{Bmatrix} \begin{Bmatrix} F_2 \\ B_2 \\ Q_2 \end{Bmatrix}$$

$$= \begin{Bmatrix} (M_{1x} + \cos\theta_I) & (M_{1x} - \cos\theta_{B_1}) & 0 \\ [1 + M_1\cos(\alpha_1 - \theta_I)] & [1 - M_1\cos(\alpha_1 + \theta_{B_1})] & 0 \\ 0 & 0 & 0 \end{Bmatrix} \begin{Bmatrix} 1 \\ B_1 \\ 0 \end{Bmatrix} \tag{35a}$$

where $M_n = (M_{nx}^2 + M_{ny}^2)^{1/2}$

Using

$$(D_1) = \begin{Bmatrix} \frac{a_1}{a_2}(M_{2x} + \cos\theta_{F_2}) & \frac{a_1}{a_2}(M_{2x} - \cos\theta_{B_2}) & \frac{a_1}{a_2}\frac{(k_{2y}/k_2)}{\left[\left(\frac{k_{2x}}{k_2}\right)^2 + \left(\frac{k_{2y}}{k_2}\right)^2\right]^{1/2}} \\ \frac{\rho_1}{\rho_2}[1 + M_2\cos(\beta_2 - \theta_{F_2})] & \frac{\rho_1}{\rho_2}[1 - M_2\cos(\beta_2 + \theta_{B_2})] & \frac{\rho_1}{\rho_2}\left\{\frac{M_{2x}\left(\frac{k_{2y}}{k_2}\right) - M_{2y}\left(\frac{k_{2x}}{k_2}\right)}{\left[\left(\frac{k_{2x}}{k_2}\right)^2 + \left(\frac{k_{2y}}{k_2}\right)^2\right]^{1/2}}\right\} \\ \sin(\beta_2 - \theta_{F_2}) & -\sin(\beta_2 + \theta_{B_2}) & \frac{\left(\frac{k_{2y}}{k_2}\right)\sin\beta_2 + \left(\frac{k_{2x}}{k_2}\right)\cos\beta_2}{\left[\left(\frac{k_{2x}}{k_2}\right)^2 + \left(\frac{k_{2y}}{k_2}\right)^2\right]^{1/2}} \end{Bmatrix} \quad (36)$$

$$(A_1) = \begin{Bmatrix} (M_{1x} + \cos\theta_I) & (M_{1x} - \cos\theta_{B_1}) & 0 \\ [1 + M_1\cos(\alpha_1 - \theta_I)] & [1 - M_1\cos(\alpha_1 + \theta_{B_1})] & 0 \\ 0 & 0 & 0 \end{Bmatrix} \quad (37)$$

Then,

$$(D_1) \begin{Bmatrix} F_2 \\ B_2 \\ Q_2 \end{Bmatrix} = (A_1) \begin{Bmatrix} F_1 \\ B_1 \\ Q_1 \end{Bmatrix} \Bigg| \longrightarrow \quad (F_1 = 1,\ Q_1 = 0) \tag{35b}$$

and

$$\begin{Bmatrix} F_2 \\ B_2 \\ Q_2 \end{Bmatrix} = (D_1^{-1}\ A_1) \begin{Bmatrix} F_1 \\ B_1 \\ Q_1 \end{Bmatrix} \tag{38}$$

where D_1^{-1} is the inverse of D_1, that is in $D_1^{-1}\ D_1$ gives the identity matrix:

$$D_1^{-1}\ D_1 = \begin{vmatrix} 1 & 0 & 0 \\ 0 & 1 & 0 \\ 0 & 0 & 1 \end{vmatrix}$$

Similarly, for any blade row it can be written:

$$(D_n) \begin{Bmatrix} F_m \\ B_m \\ Q_m \end{Bmatrix} = (A_n) \begin{Bmatrix} F_n \\ B_n \\ Q_n \end{Bmatrix} \Bigg| \longrightarrow \quad \underline{m = n + 1} \tag{39}$$

and

$$\begin{Bmatrix} F_m \\ B_m \\ Q_m \end{Bmatrix} = (D_n^{-1}\ A_n) \begin{Bmatrix} F_n \\ B_n \\ Q_n \end{Bmatrix} \tag{40}$$

where

$$(D_n) = \begin{Bmatrix} \frac{a_n}{a_m}(M_{mx}+\cos\Theta_{F_m}) & \frac{a_n}{a_m}(M_{mx}-\cos\Theta_{B_m}) & \frac{a_n}{a_m}\frac{(k_{my}/k_m)}{K_m} \\ \frac{\rho_n}{\rho_m}[1+M_m\cos(\beta_m-\Theta_{F_m})] & \frac{\rho_n}{\rho_m}[1-M_m\cos(\beta_m+\Theta_{B_m})] & \frac{\rho_n}{\rho_m}\left[\frac{M_{mx}(k_{my}/k_m)-M_{my}(k_{mx}/k_m)}{K_m}\right] \\ \sin(\beta_m-\Theta_{F_m}) & -\sin(\beta_m+\Theta_{B_m}) & \frac{(k_{my}/k_m)\sin\beta_m+(k_{mx}/k_m)\cos\beta_m}{K_m} \end{Bmatrix}] \quad (41)$$

$$(A_n) = \begin{Bmatrix} (M_{nx}+\cos\Theta_{F_n}) & (M_{nx}-\cos\Theta_{B_n}) & \frac{(k_{ny}/k_n)}{K_n} \\ [1+M_n\cos(\alpha_n-\Theta_{F_n})] & [1-M_n\cos(\alpha_n+\Theta_{B_n})] & \left[\frac{M_{nx}(k_{ny}/k_n)-M_{ny}(k_{nx}/k_n)}{K_n}\right] \\ 0 & 0 & 0 \end{Bmatrix} \quad (42)$$

Where $K_n = [(k_{nx}/k_n)^2+(k_{ny}/k_n)^2]^{1/2}$ (43)

$K_m = [(k_{mx}/k_m)^2+(k_{my}/k_m)^2]^{1/2}$ (44)

For the last (2N) blade row, $F_{2N+1} = T$ and $B_{2N+1} = 0$, therefore

$$\begin{Bmatrix} T \\ 0 \\ Q_{2N+1} \end{Bmatrix} = (D_{2N}^{-1} A_{2N}) \begin{Bmatrix} F_{2N} \\ B_{2N} \\ Q_{2N} \end{Bmatrix}$$

$$= (D_{2N}^{-1} A_{2N})(D_{2N-1}^{-1} A_{2N-1}) \cdots (D_2^{-1} A_2)(D_1^{-1} A_1) \begin{Bmatrix} 1 \\ B_1 \\ 0 \end{Bmatrix} \tag{45a}$$

$$= \begin{Bmatrix} TC_{11} & TC_{12} & TC_{13} \\ TC_{21} & TC_{22} & TC_{23} \\ TC_{31} & TC_{32} & TC_{33} \end{Bmatrix} \begin{Bmatrix} 1 \\ B_1 \\ 0 \end{Bmatrix} \tag{45b}$$

(TC) provides the transition coefficients relating the transmitted and incident perturbations.

The second row of (45b) shows that

$$B_1 = -\frac{TC_{21}}{TC_{22}} \tag{46}$$

whereupon, it can be seen that

$$T = \left(TC_{11} - \frac{TC_{21}}{TC_{22}} TC_{12} \right) \tag{47}$$

A computer program to utilize this matrix-inversion technique can be found in Appendix A, along with a flow chart and typical output.

Supersonic Relative Exhaust Flow

When the relative flow exiting from a blade row becomes supersonic, the Kutta condition is replaced by the choked-flow condition. A discussion of application to disturbed flow at a blade row can be found in Reference 16. The interaction with the shock that occurs due to the locally supersonic conditions is considered separately in Section 3.4.

Supersonic flow actually implies two separate governing equations - one upstream of the blade row and the other downstream. The downstream condition is analogous to the Kutta condition in that it determines the relative exit angle. The Kutta condition states that the relative flow angle leaving the blade row is given by

$$\beta = \cos^{-1}(d_o/t) = \text{constant}$$

where d_o defines the cascade throat and t the blade-to-blade pitch (see Figure 8). However, when the critical pressure ratio is exceeded, the flow angle for low supersonic Mach numbers is given by:

$$\beta = \cos^{-1}\left(\frac{A}{A^*}\ \frac{d_o}{t}\right) \tag{48}$$

where A/A* is defined as in the usual sense (Reference 17):

$$\frac{A}{A^*} = \left[\frac{1}{M}\right]\left[\frac{2+(\gamma-1)M^2}{\gamma+1}\right] \quad \exp\left[\frac{\gamma+1}{2(\gamma-1)}\right] \tag{49}$$

The one-dimensional area function defined in (49) is valid only for small supersonic Mach numbers because it ignores shocks. The flow turning provides the extra area required to pass the flow defined in the throat.

However, the downstream choking condition and the mass conservation equation cannot both be used simultaneously as the former implicitly contains the latter and the resulting equations are no longer linearly independent.

The upstream choking condition requires that the corrected mass flow be dependent only on the upstream stagnation parameters (Reference 16). That is:

$$\frac{\dot{m}}{Ap_o}\sqrt{\frac{RT_o}{\gamma}} = \text{constant}$$

or

$$\rho U \frac{\sqrt{T_o}}{p_o} = \text{constant} \tag{50}$$

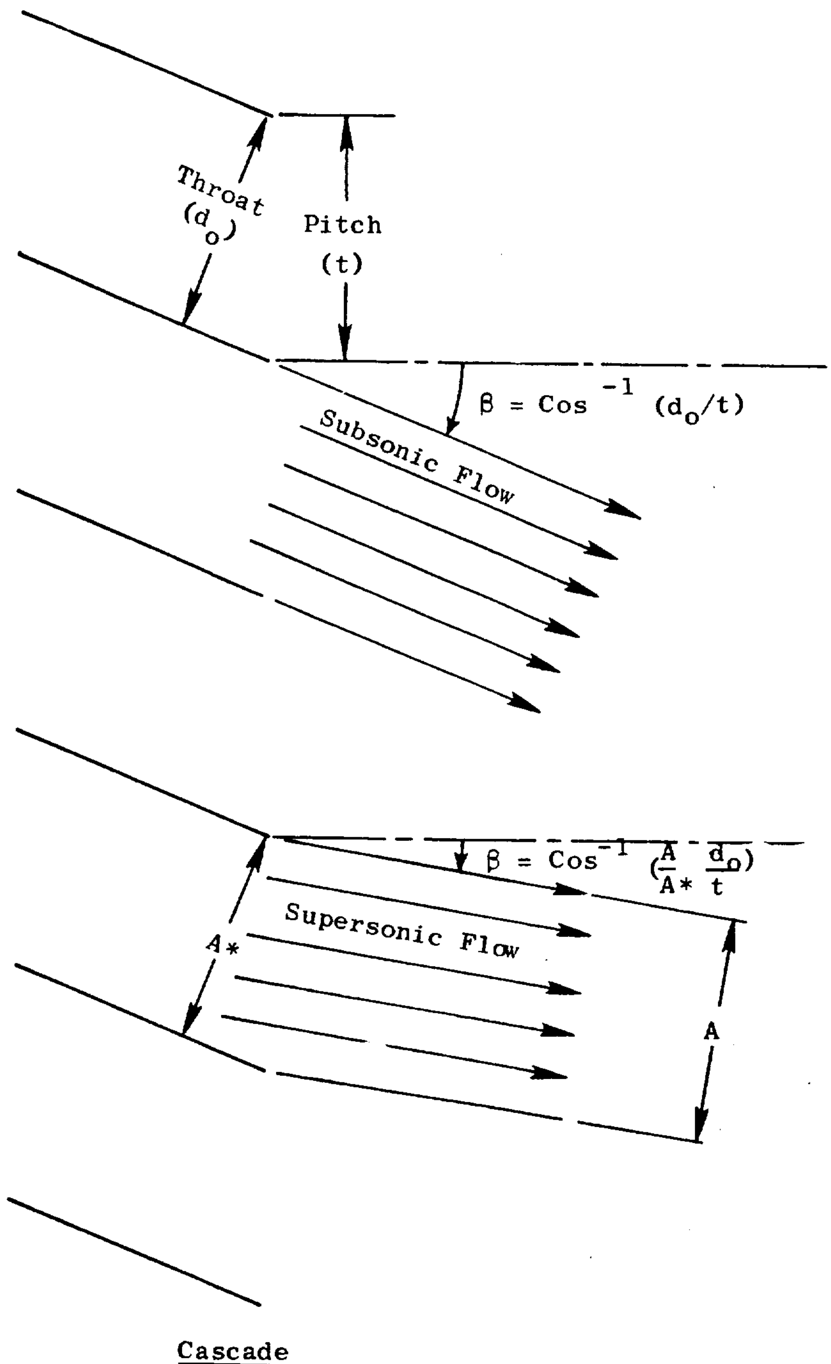

Figure 8. Turbine Cascade Nomenclature.

where: $\dot{m}$ = mass flow rate = ρUA

A = cross-sectional area

p_o = stagnation pressure

T_o = stagnation temperature

R = gas constant

γ = ratio of specific heats

Using conventional gas dynamic relationships and taking the logarithmic differential yields:

$$2\frac{u'}{U} - \frac{T'}{T} - \frac{\gamma+1}{\gamma-1}\frac{\mu'}{\mu} = 0 \qquad (51)$$

where: T' = temperature perturbation

$\mu = (1 + \frac{\gamma-1}{2} M^2_{abs})$

M_{abs} = absolute flow Mach number

After some further simplification and assumption of isentropic flow (see Reference 3), the following equation in u', v' and p' results:

$$\frac{\gamma-1}{\gamma}(M^2_{abs}-1)\frac{p'}{p} + \left[2\mu - (\gamma+1)\left(\frac{U}{a}\right)M_{abs}\cos\phi\right]\frac{u'}{U}$$

$$-\left[(\gamma+1)\left(\frac{V}{a}\right)M_{abs}\sin\phi\right]\frac{v'}{V} = 0 \qquad (52)$$

where ϕ = absolute flow angle.

Proceeding as in the subsonic flow case, with equation (52) replacing equation (34), the (A_n) and (D_n) matrices assume the following form:

$$(A_n) = \left\{\begin{matrix} (M_{nx}+\cos\theta_{F_n}) & (M_{nx}-\cos\theta_{B_n}) & \dfrac{k_{ny}/k_n}{K_n} \\ [1+M_n\cos(\alpha_n-\theta_{F_n})] & [1-M_n\cos(\alpha_n+\theta_{B_n})] & \dfrac{M_{nx}(k_{ny}/k_n)-M_{ny}(k_{nx}/k_n)}{K_n} \\ A_{31} & A_{32} & A_{33} \end{matrix}\right\} \qquad (53)$$

where

$$A_{31} = (\gamma-1)(M_{n_{abs}}^2-1) + \frac{2\mu}{M_{nx}}\cos\theta F_n - (\gamma+1)M_{n_{abs}}\cos(\phi_n-\theta F_n)$$

$$A_{32} = (\gamma-1)(M_{n_{abs}}^2-1) - \frac{2\mu}{M_{nx}}\cos\theta B_n + (\gamma+1)M_{n_{abs}}\cos(\phi_n'+\theta B_n)$$

$$A_{33} = \frac{2\mu}{M_{nx}}\ \frac{(k_{yn}/k_n)}{K_n} - (\gamma+1)M_{n_{abs}}\left[\frac{\frac{k_{yn}}{k_n}\cos\phi_n - \frac{k_{xn}}{k_n}\sin\phi_n}{K_n}\right] \qquad (54)$$

and

$$(D_n) = \begin{Bmatrix} \frac{a_n}{a_m}(M_{mx}+\cos\theta F_m) & \frac{a_n}{a_m}(M_{mx}-\cos\theta B_m) & \frac{a_n}{a_m}\ \frac{k_{my}/k_m}{K_m} \\ \frac{\rho_n}{\rho_m}\left[1+M_m\cos(\beta_{Bm}-\theta F_m)\right] & \frac{\rho_n}{\rho_m}\left[1-M_m\cos(\beta_{Bm}+\theta B_m)\right] & \frac{\rho_n}{\rho_m}\left[\frac{M_{mx}\frac{k_{my}}{k_m} - M_{my}\frac{k_{mx}}{k_m}}{K_m}\right] \\ 0 & 0 & 0 \end{Bmatrix}$$

(55)

It is obvious that (D_n) cannot be inverted any longer, and the solution method used for the subsonic case cannot be utilized here. Note, however, that (A_n) can be inverted. Hence, the solution can proceed from the last stage towards the first, if all the blade rows are supersonic. That is,

$$\begin{Bmatrix} 1 \\ B_1 \\ 0 \end{Bmatrix} = (A_1^{-1}D_1)(A_2^{-1}D_2)\ \ldots\ldots\ (A_{2N}^{-1}D_{2N})\begin{Bmatrix} F_{2N+1} \\ 0 \\ Q_{2N+1} \end{Bmatrix} \qquad (56a)$$

$$= \begin{Bmatrix} CT_{11} & CT_{12} & CT_{13} \\ CT_{21} & CT_{22} & CT_{23} \\ CT_{31} & CT_{32} & CT_{33} \end{Bmatrix}\begin{Bmatrix} F_{2N+1} \\ 0 \\ Q_{2N+1} \end{Bmatrix} \qquad (56b)$$

Here (CT) is the transition coefficient matrix for an all-supersonic exhaust flow turbine. Equation (56b) can be used to obtain

$$T = F_{2N+1} = \frac{CT_{33}}{CT_{11}CT_{33}-CT_{13}CT_{31}} \qquad (57)$$

Unfortunately, most turbine configurations incorporating supersonic exhaust flows do so only for the initial few blade rows. The matrices decouple at each subsonic/supersonic interface, and neither (TC) nor (CT) can be defined.

There are several alternative solution methods, including following acoustic waves through successive interactions with blade rows. This approach is used later on to validate the matrix-inversion technique for single-stage turbines. The implementation, however, becomes quite cumbersome and complex for multistage turbines.

A generalized solution results from the realization of the fact that, out of the six amplitudes involved at each blade, two are fully defined at the first blade row ($F_1 = 1$, $Q_1 = 0$). Guessing at one of the other four amplitudes, the other three unknowns can be obtained utilizing the three matching condition relationships at the first blade row. Since F_2, B_2, and Q_2 are now known, F_3, B_3, and Q_3 can be found by using the relationships at the second blade row. Finally, F_{2N+1} and Q_{2N+1} are calculated. Since an anechoic termination is assumed, $B_{2N+1} \equiv 0$. If the computed value of B_{2N+1} is not zero, a second iteration is made through the turbine. Note that this guessing routine allows for solutions of nonanechoic terminations. It is sufficient to define the relationship between F_{2N+1} and B_{2N+1} due to the termination. Then the computation loop-escape condition becomes (B_{2N+1}/F_{2N+1}) convergence to the ratio determined by the termination rather than $B_{2N+1} = 0$.

Implementation of this solution routine is made somewhat complex by supersonic exhaust blade rows because only two equations are available to define downstream quantities. Therefore it is necessary to start a new guess at each supersonic blade row. The solution scheme is outlined in Appendix B, along with a time-share program listing and typical output. An interesting result of supersonic-flow blade rows is that the sound waves move upstream slower than the flow moves downstream, and therefore negative values of the backward-traveling wave become possible.

Validation of Multistaging Approach

An acoustic wave incident on a multiblade-row vehicle will generally give rise to a system of acoustic and vorticity waves which can be evaluated in two different ways. The current, multistaging analysis postulates an "equilibrium" state solution; wherein, all the reflected and transmitted acoustic waves are combined into a pair of forward- and backward-travelling acoustic waves in each interblade-row space and the associated vorticity into a vorticity wave downstream of each blade row. The other approach considers each blade row interaction as an isolated blade-row impingement and then follows the resulting reflected, transmitted, and vorticity waves through successive interactions with adjoining blade rows. The solution in the limit of infinite interactions should approach that of the equilibrium model. This has been verified for a number of cases ranging from low to high pressure ratios, zero and nonzero acoustic wave incidence. Two representative comparisons are provided in Table I for the first stage only of the HLFT IVA low

Table I. Comparison of Successive Interaction and Multistage Solutions.

- HLFT IV A, First Stage Only
- $\theta_I = 0$

Case I: Stage $P_R = 1.53$, $N/\sqrt{T} = 100\%$

	Amplitude of Forward Waves							Amplitude of Backward Waves						
Station	Isol. Row	+ Velocity	+1 Inter.	+2 Inter.	+3 Inter.	+4 Inter	Multi-Stage	Isol. Row	+ Velocity	+1 Inter.	+2 Inter.	+3 Inter.	+4 Inter.	Multi-Stage
1 (inlet)	1.00	1.00	1.00	1.00	1.00	1.00	1.00	0.963	0.963	1.069	1.109	1.124	1.130	1.160
2	0.688	0.688	0.747	0.770	0.779	0.782	0.789	0.407	0.200	0.276	0.305	0.316	0.320	0.324
3 (exit)	0.505	0.618	0.639	0.647	0.650	0.651	0.653	0	0	0	0	0	0	0

Case II: Stage $P_R = 2.17$, $N/\sqrt{T} = 100\%$

1 (inlet)	1.00	1.00	1.00	1.00	1.00	1.00	1.00	1.517	1.517	1.527	1.534	1.540	1.544	1.556
2	0.522	0.522	0.601	0.660	0.703	0.735	0.826	0.541	0.224	0.388	0.509	0.598	0.663	0.848
3 (exit)	0.341	0.456	0.476	0.490	0.501	0.509	0.532	0	0	0	0	0	0	0

pressure turbine tested in NAS3-19435. Case I corresponds to the lowest pressure ratio tested for the full three-stage turbine, while Case II corresponds to the highest pressure ratio, at which the first stage was very nearly choked at 100% speed. The first column provides the acoustic wave amplitudes for the isolated blade-row interaction in which only the transmitted wave at each blade row is preserved; the reflected and vorticity waves are discarded immediately after the interaction. The second column gives the amplitudes if the vorticity wave from the first blade-row interaction were also preserved and made to interact with the next blade row. The succeeding columns contain the amplitudes due to successive interactions of the reflected wave from the second blade row. The last column gives the values predicted by the multistaging computer program. The convergence of the successive interaction solution to the multistage values is surprisingly rapid, particularly for low pressure ratios. For example, the final transmitted wave amplitude reaches a value of 99% of the multistage solution after only two interactions at the lower pressure ratio. At the higher pressure ratio, the transmitted wave amplitude reaches 92% of the multistage value after two interactions, and 96% after four.

3.3.4 Energy Transmission

The energy transmitted can be computed using the results of Blokhintsev (Reference 18). The energy density ε is given by

$$\varepsilon = \frac{p'^2}{\rho a^3}(a+\vec{V}_{abs}\cdot\hat{e}_p) \tag{58}$$

where $\vec{V}_{abs}$ is the absolute flow velocity and $\hat{e}_p$ the unit vector normal to the wave front. Also, the intensity flux vector $\vec{I}$ is given by

$$\vec{I} = \varepsilon\ (a\hat{e}_p+\vec{V}_{abs}) \tag{59}$$

Only the axial component is of interest here

$$I_x = \varepsilon(a\hat{e}_p+\vec{V}_{abs})\cdot\hat{e}_x$$

or $$I_x = \varepsilon(a\ \cos\theta_F+U)$$

also $$\vec{V}_{abs} = U\hat{e}_x+(V+W_R)\hat{e}_y$$

where W_R is the rotor wheel speed

therefore $$I_x = \frac{\tilde{p}^2}{\rho a^3}\left[a+U\cos\theta_F+(V_T+W_R)\sin\theta_F\right](a\cos\theta_F+U)$$

or $$I_x = \frac{\tilde{p}^2}{\rho a}\left[1+M_x\cos\theta_F+(M_y+M_R)\sin\theta_F\right](\cos\theta_F+M_x) \qquad (60)$$

The transmission loss through the turbine is then given by

$$TL = 10\log_{10}\frac{(I_x)_{incident}}{(I_x)_{transmitted}}$$

$$TL = 10\log_{10}\frac{1}{T^2}\,\frac{\rho_T a_T^2}{\rho_I a_I^2}\,\frac{[1+M_{Ix}\cos\Theta_I+(M_{Iy}+M_{IR})\sin\Theta_I]}{[1+M_{Tx}\cos\Theta_T+(M_{Ty}+M_{TR})\sin\Theta_T]}\times\frac{(\cos\Theta_I+M_{Ix})}{(\cos\Theta_T+M_{Tx})} \qquad (61)$$

where $M_R = W_R/a$, the blade tip Mach number, and the subscript T would denote conditions at exit from the last blade row, i.e., T = (2N+1), and I those at inlet to the first blade row, i.e., I = 1.

For a first approximation, annular spinning modes can be treated as plane waves propagating between infinite plates - as was demonstrated by Morfey (Reference 19).

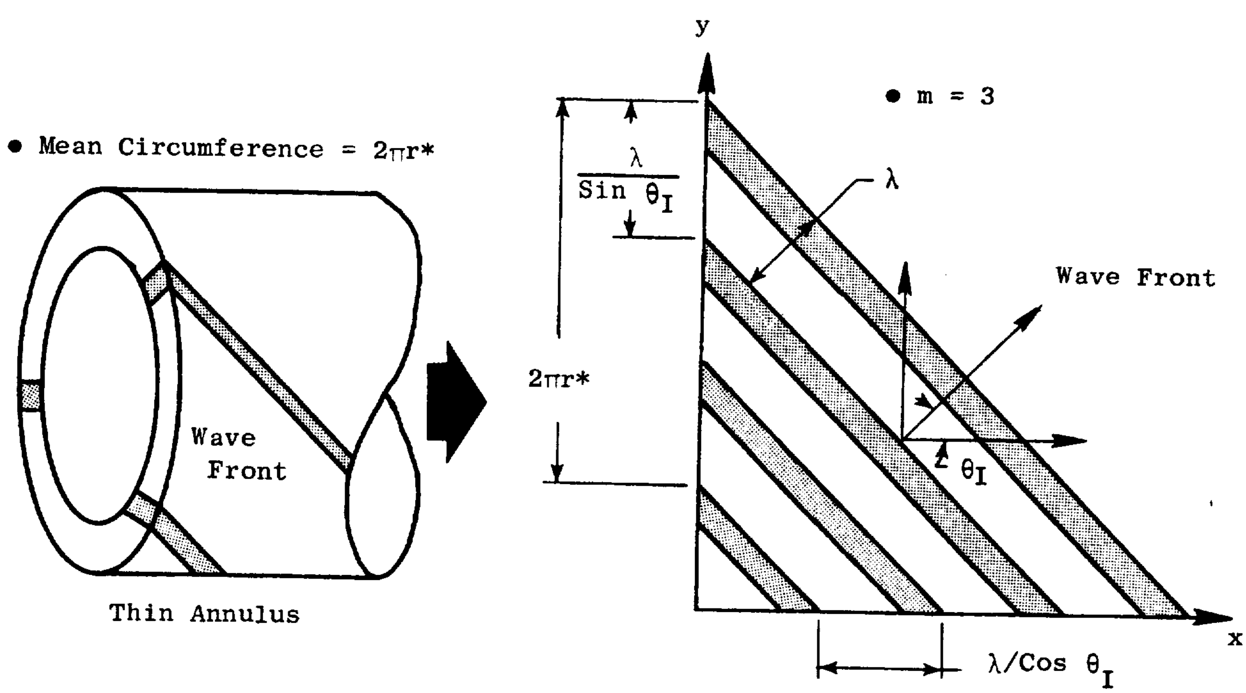

A plane wave approximation for m = 3 spinning lobe is provided as an example. The annulus is assumed to be cut and straightened out (unwrapped), so that the cylindrical walls become a plane sheet. Continuity in the circumferential (y) direction requires that the wave pattern be repeated every $2\pi r^*$ (mean circumference); that is,

$$M\left(\frac{\lambda}{\sin \theta_I}\right) = 2\pi r^*$$

or $$\sin \theta_I = \frac{m\lambda}{2\pi r^*} = \frac{m}{kr^*} \tag{62}$$

or $$\theta_I = \sin^{-1}\left(\frac{m}{kr^*}\right)$$

where m = circumferential lobe number

$= 0, 1, 2, \ldots \left(\frac{m}{kr^*}\right) \leq 1$

k = wave number

r^* = root mean square radius

$$= \left[\frac{(\text{tip radius})^2 + (\text{hub radius})^2}{2}\right]^{1/2}$$

When more than a single dimension is involved, the wave number k is the root mean square of the wave numbers associated with each of the dimensions, e.g. in the axial and circumferential directions.

Note that m = o corresponds to a plane wave propagating axially down the annulus and is the only cut-on mode for $kr^* < 1$. As soon as kr^* exceeds one, the first pair of spinning modes (one corotating and one counterrotating) appear - as was indeed observed during the NAS3-19435 tests.

Each mode is associated with a different incidence angle, and the corresponding transmission loss can easily be computed using (61). The question now arises as to the appropriate energy assignment. Equal energy distribution between all cut-on modes has been frequently postulated in fan noise and treatment work. Experimental observations indicate that this is not an unreasonable distribution for symmetric sources particularly. The siren tone injection into the turbine plenum during the NAS3-19435 tests corresponded closely to a point-source placed in an annulus. A simple, no-flow, analytical modeling (Appendix C) of the resulting duct coupling can be used to show that the energy distribution is given by

$$E_m \propto \frac{1}{(f^2 - f_c^2)^{1/2}} \tag{63}$$

where E_m = energy assignment to m^{th} mode

f = frequency of interest

f_c = cut-on frequency for m^{th} inverse

An obvious outcome of this frequency inverse dependence is that all the available energy is biased towards a mode just cutting-on. But θ_I for this mode is approximately 90° at cut-on, almost ensuring complete reflection at the blade row. Hence, cut-on should be associated with a sudden increase in transmission loss. This is not inconsistent with observations made during NAS3-19435, as will be shown in Section 4.

Once the energy assignment has been made, it is a simple matter to compute the summed transmission loss for any given frequency. The computer programs in Appendices A and B provide both the individual transmission losses for each cut-on mode and the summed transmission loss.

3.4 SECONDARY EFFECTS

3.4.1 Duct Termination and Area Changes

The area variations encountered in the turbine tests of NAS3-19435 may be modeled as shown in Figure 9. There is a gradual area change from the inlet plenum to the inlet casing (S_1 to S_2); there are sharp area changes associated with each blade row (S_3 and S_5), and then there is a sudden expansion as the exhaust flow dumps into the exhaust plenum (S_6 to S_7). Each area discontinuity is associated with reflected and transmitted waves. The answer being sought here is the effect on the transmission loss and, in particular, the unique or spurious effects imposed on the data acquired during NAS3-19435.

The area changes associated with the blade rows are properly accounted for in the analyses, but not the associated phase changes over the lengths ℓ_4, ℓ_5, ℓ_6, etc. The multistaging analysis, for example, assumes negligible change in phase over the interblade-row spacing ℓ_5. Since ℓ_5 = 1.31 cm for the turbine of Figure 9, the actual phase change [angle in degrees = (spacing/wavelength) x 360°] would be about 1° at 100 Hz and 18° at 2000 Hz, which represent the limits of the frequency range of major interest. Hence the assumption would be strictly valid only at the low frequency end.

The major impact would appear to be that of the area change at the exhaust plenum. It will be shown that the reflected wave at this termination is almost 180° out of phase with the incident wave for low frequencies and has an amplitude almost as large, making the duct termination a pressure node. Pressure measurements in this region would then indicate inflated values for the transmission loss. The exact degree of pressure cancellation at a given sensor is a function of the amplitude and phase of the reflected wave, the wave number, and the distance to the sensor (ℓ_9 or $\ell_8 + \ell_9$). To our knowledge, there are no exact solutions available in literature applicable to this particular geometry. However, several approximate methods are

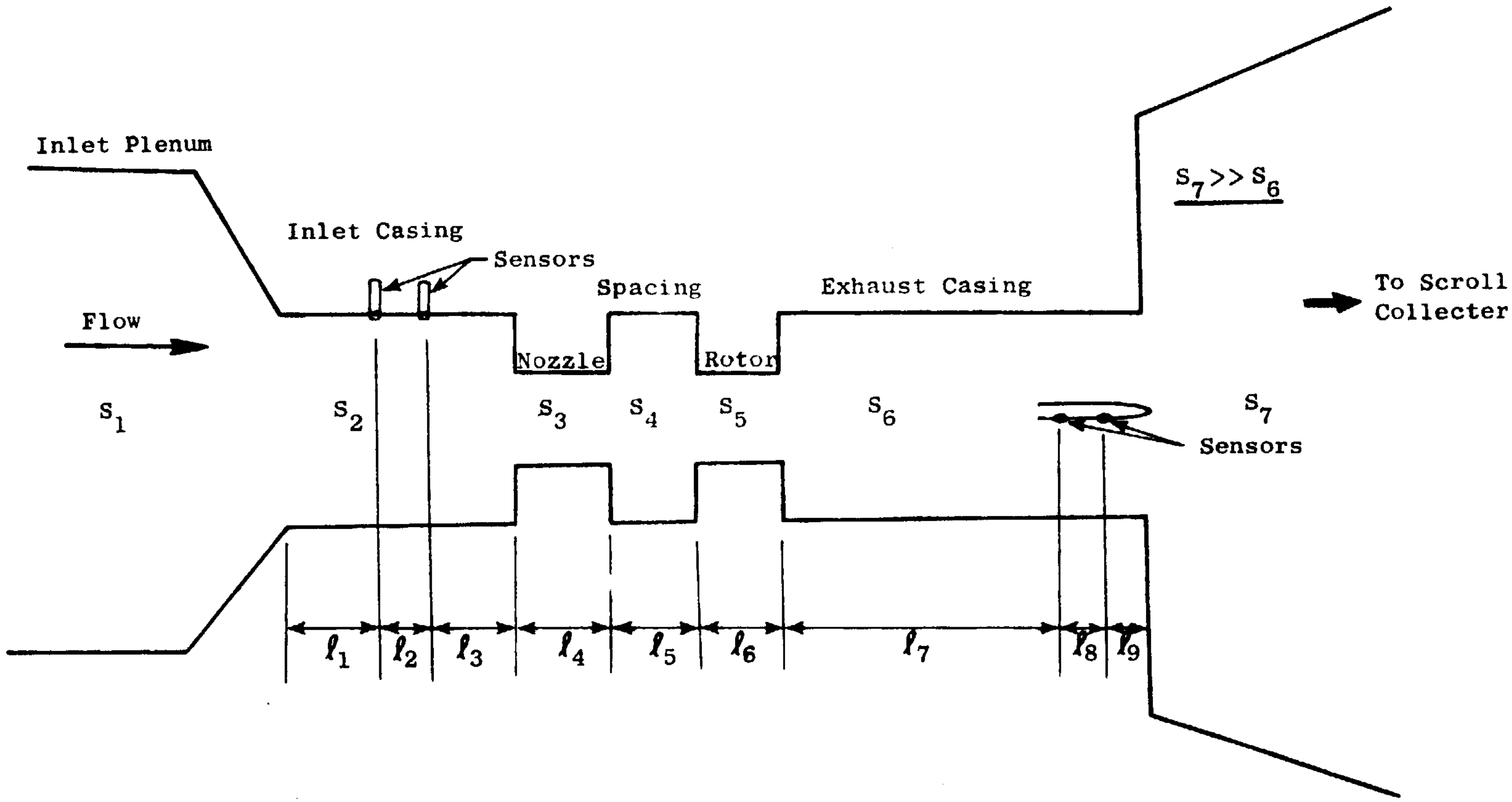

Figure 9. Schematic Representation of Area Variation for the Single-Stage, High Pressure Turbine Test.

available, such as the strip theory modeling by Mani (Reference 20) which includes flow effects, or the somewhat simpler no-flow models used to analog area changes in ducts or a pipe radiating into space (see, for example, Reference 21). A no-flow analysis is perfectly adequate here - as a demonstrator.

Assuming, for the moment, a cylindrical duct of radius r discharging into the plenum, the ratio of the reflected to incident wave can be written:

$$\frac{B_6}{F_6} = \frac{(R_o - \rho_o a/S_6) + j\,X_o}{(R_o + \rho_o a/S_6) + j\,X_o} \tag{64}$$

where R_o and X_o are the real and reactive components of the impedance at the interface and S is the cross-sectional area.

In the limit that (S_7/S_6) is finite, and the wavelength is large compared to the duct characteristic dimension, $R_o \simeq (\rho_o a/S_7)$ and $X_o \simeq 0$. Then,

$$\frac{B_6}{F_6} \simeq -\frac{S_7 - S_6}{S_7 + S_6} \tag{65}$$

using the values for S_6 given in Table II, and $S_7 = 5160\ cm^2$, the following results are obtained:

High Pressure Turbine	$\frac{B_6}{F_6} = -0.80,$	$\Delta TL = 14$ dB
One-Stage Low Pressure Turbine	$\frac{B_6}{F_6} = -0.62,$	$\Delta TL = 8.4$ dB
Three-Stage Low Pressure Turbine	$\frac{B_6}{F_6} = -0.37,$	$\Delta TL = 4$ dB

The ΔTL is the artificial increase in transmission loss due to pressure cancellation at the downstream sensors. Note that S_7 actually varied from 5160 cm^2 at the exhaust duct termination to about 13700 cm^2 at the scroll collector. Hence the ΔTL tabulated above are minimum increases in the transmission losses.

Table II. Exhaust Duct Termination Effects.

			Lengths, ℓ, for Sensors (cm)			
			Wall		Probe	
Turbine Configuration	Exhaust Duct Area, S_6 (cm^2)	Duct Height (cm)	K_5	K_6	K_9	K_{10}
High Pressure	562.5	3.81	---	---	4.06	6.60
1 Stage, Low Pressure	1206.5	6.60	19.05	16.51	5.84	3.30
3 Stage, Low Pressure	2387.2	12.45	14.73	12.19	7.37	4.83
Note: $S_7 \simeq 5160\ cm^2$ at the termination, but increased to about 13700 cm^2 at the exhaust scroll collector.						

For the case of very large (S_7/S_6), the impedance can be considered the same as that acting upon a piston mounted in an infinite baffle:

$$R_o = \frac{\rho_o a}{S_6} \tilde{R}\ (2\ kr)$$

$$X_o = \frac{\rho_o a}{S_6} \tilde{X}\ (2\ kr) \tag{66}$$

where

$$\tilde{R}(x) = \frac{x^2}{(2)(4)} - \frac{x^4}{(2)(4^2)(6)} + \frac{x^6}{(2)(4^2)(6^2)(8)} \cdots$$

$$\tilde{X}(x) = \frac{4}{\pi} \left[\frac{x}{(3)} - \frac{x^3}{(3^2)(5)} + \frac{x^5}{(3^2)(5^2)(7)} \cdots\right] \tag{67*}$$

and

$$\frac{B_6}{F_6} = \frac{\tilde{R}(2kr) - 1 + j\ \tilde{X}(2kr)}{\tilde{R}(2kr) + 1 + j\ \tilde{X}(2kr)} \tag{68}$$

For example, using the truncated series representation of Equation 67,

$$kr = 0.2 \text{ gives } \frac{B_6(o)}{F_6(o)} = 0.99 \exp\ [j\ (170°)]$$

where (o) mean kx = 0.0

---

* See Reference 21, page 146

That is, the reflected and incident waves provide almost complete cancellation at the duct termination. At higher frequencies, the cancellation is not as complete because of changes in both amplitude and phase:

$$kr = 2 \text{ gives } \frac{B_6(o)}{F_6(o)} = 0.554 \exp [j\ (107°)]$$

The effect at the measuring station can be computed using:

$$B_6(\ell) = B_6(o) \exp [j(-k\ell)]$$

$$F_6(\ell) = F_6(o) \exp [j(k\ell)] \qquad (69)$$

where $\ell = \ell_9 = 4.06$ cm for Kulite 10 (see NAS3-19435 Final Report, Reference 7) and $(\ell_8 + \ell_9) = 6.6$ cm for Kulite 9 in the case of the high pressure turbine tests. It is obvious that these measurements were very nearly in the pressure cancellation region. In contrast, the low pressure turbine transmission loss data were obtained largely with wall-mounted Kulites (K5 and K6) for which ℓ was much larger: 12.19 to 19.05 cm. The values of ℓ for both the wall and probe sensors are given in Table II.

Using either the assumption modeled by Equation (65) or the assumptions modeled by Equations (67) and (68) suggests that the sensor locations and the duct areas used in the NAS3-19435 tests should result in the spurious increases in apparent transmission loss which were observed in the low frequency end. In addition, either model also suggests that such distorted transmission loss increases should be evident to a greater degree in the high pressure turbine data because it has a more sudden expansion (larger area ratio). This is in agreement with observations made during the tests, as is discussed in Section 4. The conclusion is that it is very easy to structure a test to measure wave patterns generated by the geometry, rather than measuring real transmission characteristics.

The effect of the area changes on the inlet transducers is not as clear. The reflected wave from the S_2/S_3 interface reinforces the signal, but that from the S_2/S_1 interface provides a cancellation. Further, since ℓ_1 is very nearly equal to ℓ_3 in all cases, a good first estimate would be to assume a zero net effect.

The preceding manipulations are strictly valid only for no-flow and plane waves ($\theta_I = 0$). The latter restriction might be the more severe of the two. However, they clearly indicate a fictitious increase in the transmission loss, at frequencies below the initial mode cut-on, for the data measured in NAS3-19435.

It is clear that, in the case of combustor noise transmission in engine configurations, the major area variation influencing the transmission loss would be that at the core nozzle exit. The effect would be a nonzero B_{2N+1} for nozzles such that $(2kr) >> 1$. Even then, only a small decrease in the turbine transmission loss will result. However, there will be a comparatively large increase in the exhaust nozzle transmission loss which should not be overlooked.

There is also potential for a shift in the transmission loss spectrum due to the "gooseneck" sometimes encountered between the high pressure turbine exit and low pressure turbine inlet for high bypass turbofans. The gooseneck is typical of the CF6 family of engines and involves a large increase in the mean radius. The modal content of the acoustic energy propagating between the two turbines will change, since the first spinning modes will cut-on at a lower frequency (cut-on is computed using $kr^* = 1, 2, \ldots$ along with a Doppler correction for flow). That is, the sudden increase in transmission loss characterizing modal cut-on could shift to lower frequencies.

3.4.2 Shock Interaction

Since turbine blade passages are not normally designed as converging-diverging nozzles, the existence of supersonic flow results in shocks in the vicinity of the blade passage--but only at the trailing edge, as illustrated in Figure 10(a) (See Figure 21(c) of NACA RM EIK25 for Schlieren photograph of such shocks).

The interaction of acoustic waves with shocks has been investigated analytically by Landau and Lifshitz (Reference 22) for normal shocks and by Moore (Reference 23) for oblique shocks.

In general, the weak disturbance field resulting from shock interaction with an acoustic wave can be considered to include two components:

(a) an unsteady, isentropic, irrotational perturbation satisfying the wave equation, i.e., a sound wave

and (b) a steady (relative to the flow), rotational perturbation of constant pressure, i.e., a vorticity wave.

Strictly speaking, an entropy wave is also created (Reference 16). However, the acoustic perturbations are assumed to be small and the shock weak (the flow in turbine passages will rarely exceed $M = 1.2$). Under these circumstances, it would appear that the resulting entropy waves could be neglected.

As shows in Figure 10(b), Moore discusses the case of a shock overtaking a sound wave (Problem A), and that of a sound wave overtaking a shock (Problem B). The case of interest here corresponds to Problem A in his frame of reference. Within the blade passages only the zeroth order mode, an axially propagating wave, can be cut-on for the frequency range associated with combustor noise. Referring to Figures 10(a) and 10(c), one can see that the incidence angle ψ between shock and acoustic wave can then be taken as approximately zero. The case of interest here then corresponds to Problem A in Moore's frame of reference with $M \sim 1$ and $\psi_1 = 0$. Using the appropriate results, the net effect is a weak refraction of the incident sound wave, as shown in Figure 11(a) and (b). The associated vorticity wave occurs at $\psi_3 \sim \psi_1/2$ (approximately parallel to the shock in this case) (Figure 11(c)), but the velocity and density effects are very nearly zero, even for Mach numbers up to 1.5 (Figure 11(d)). The order of magnitude of the overall effect would appear to be much smaller than that resulting from the actuator-disk interaction and may be ignored for all practical purposes.

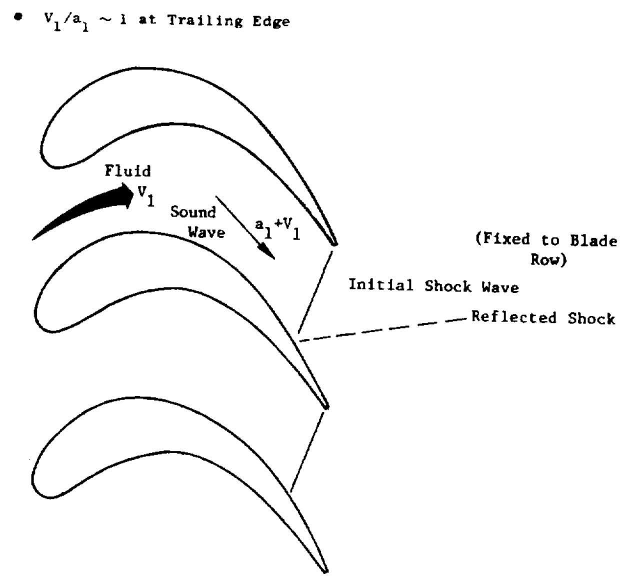

(a) Shock Patterns in a Transonic Turbine Cascade

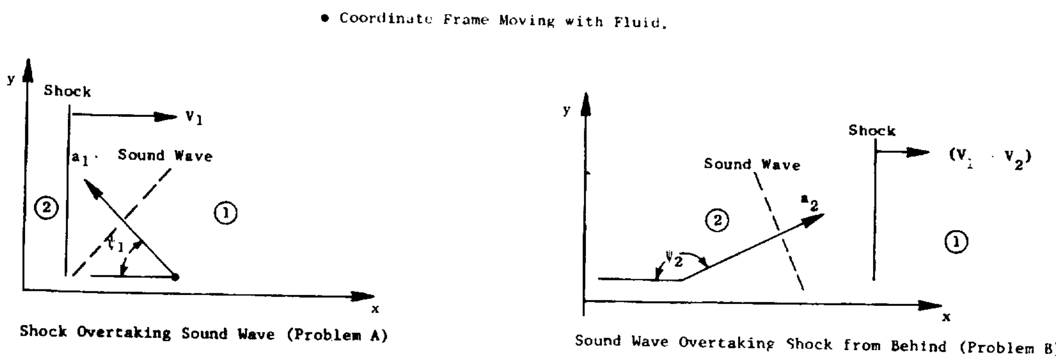

(b) Shock Interaction with Sound Waves (Reference 6)

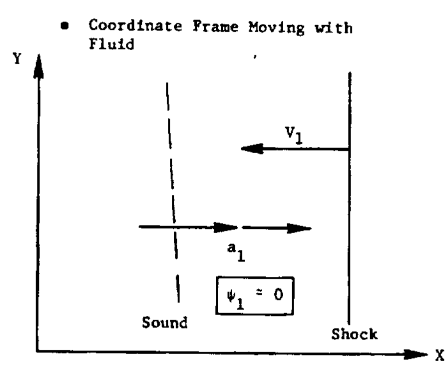

(c) Shock and Acoustic Interaction in a Moving Coordinate Frame

Figure 10. Shock and Acoustic Interaction.

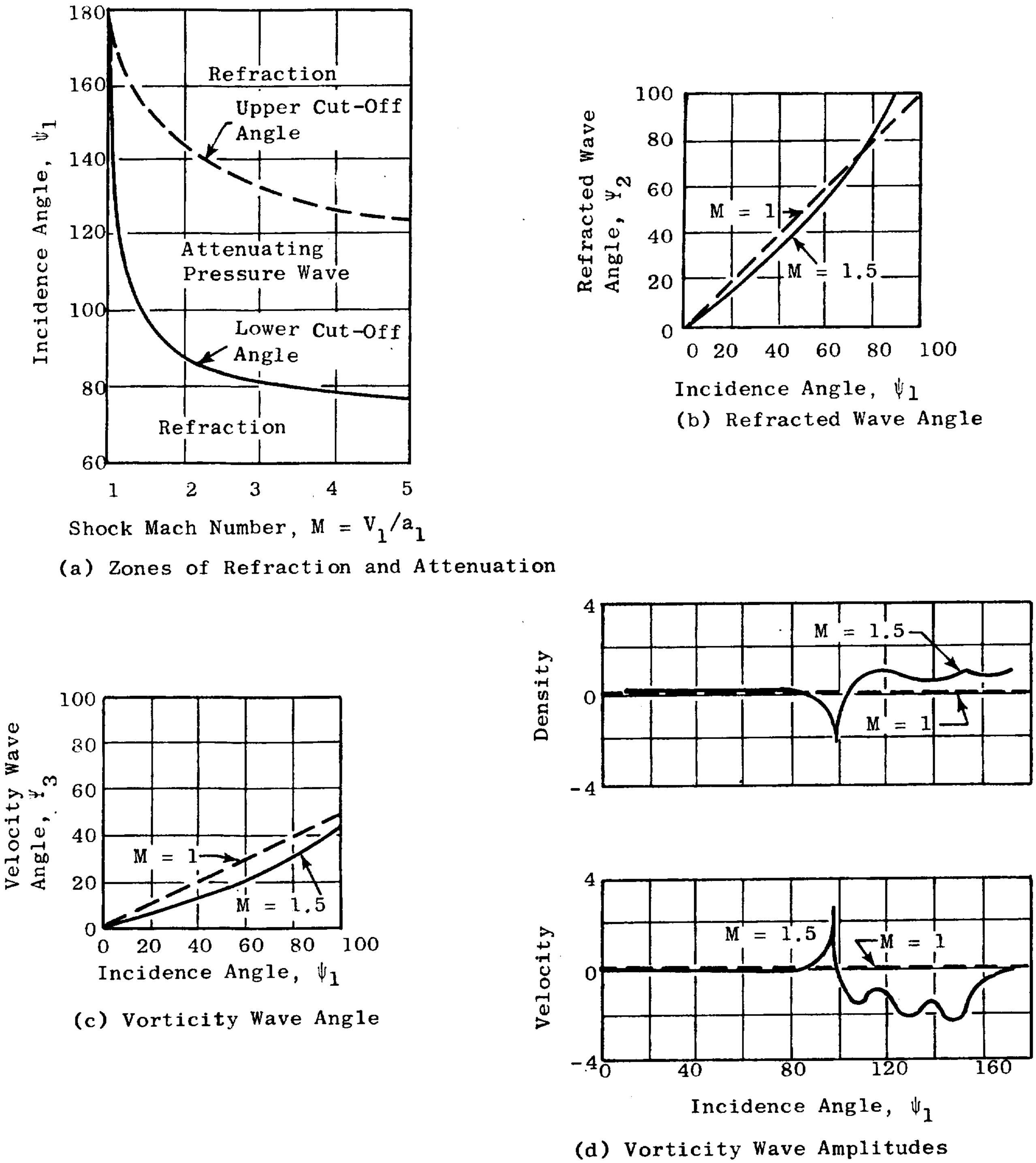

Figure 11. Shock Interaction with Sound Waves (Reference 6).

4.0 THEORY/DATA COMPARISON

4.1 BACKGROUND/DATA ACQUISITION

An experimental investigation of the low frequency noise transfer through aircraft engine-type gas turbines was conducted at General Electric under NASA Lewis Research Center sponsorship (NAS3-19435). Details of the test and the results obtained can be found in Reference 7. These data are compared below with predictions made using the analysis of the previous section. It is edifying to first obtain an understanding of the experimental setup and the effects that might be unique to the facility used to obtain the data.

The program objectives in NAS3-19435 were to (1) measure the acoustic transmission loss of sound injected upstream of the turbine as a function of the acoustic wave frequency and (2) compare these data with existing theory in order to assess the validity of the theory. The plan adopted in order to accomplish these objectives is outlined in Figure 12. Two turbines were tested: a single-stage, high-pressure turbine (NASA core) and a three-stage, low-pressure turbine. The design characteristics of these turbines are provided in Tables III and IV. The high pressure turbine was tested at two different inlet temperatures and the low pressure turbine in a single- (first stage only) and a three-stage configuration. Data were acquired at both choked and unchoked conditions.

The testing was conducted in General Electric's Warm Air Turbine Facility (Figure 13). The sound source consisted of a high intensity siren coupled to the inlet plenum through a transition horn and a radial-entry port. The entry point was several diameters upstream of the turbine and the sound first traversed through a diffuser section, flow-straightening screens, and a converging section accomplishing a change from cylindrical to annular flow path.

The sound level immediately upstream of the first blade row was measured using Kulite transducers mounted flush with the outside wall. Four transducers (K1 through K4) were employed in two axial pairings staggered about 180° circumferentially. The downstream levels were measured using two "sound separation" probes (each probe has two axially spaced Kulites) also staggered about 180° circumferentially. The low pressure turbine configurations also included one pair of wall-mounted Kulites (K5 and K6). The acoustic instrumentation and the turbine cross sections are displayed schematically in Figures 14 and 15.

Data were acquired at the turbine operating points shown in the test matrices of Tables V and VI. A range of siren frequencies was recorded at each turbine operating point. Nominally, seven siren settings were used (see Table V), which provided transmission loss information over a frequency range of 83 to 3525 Hz since the second and third harmonics of the siren tone were also readily discernible upstream in addition to the fundamental.

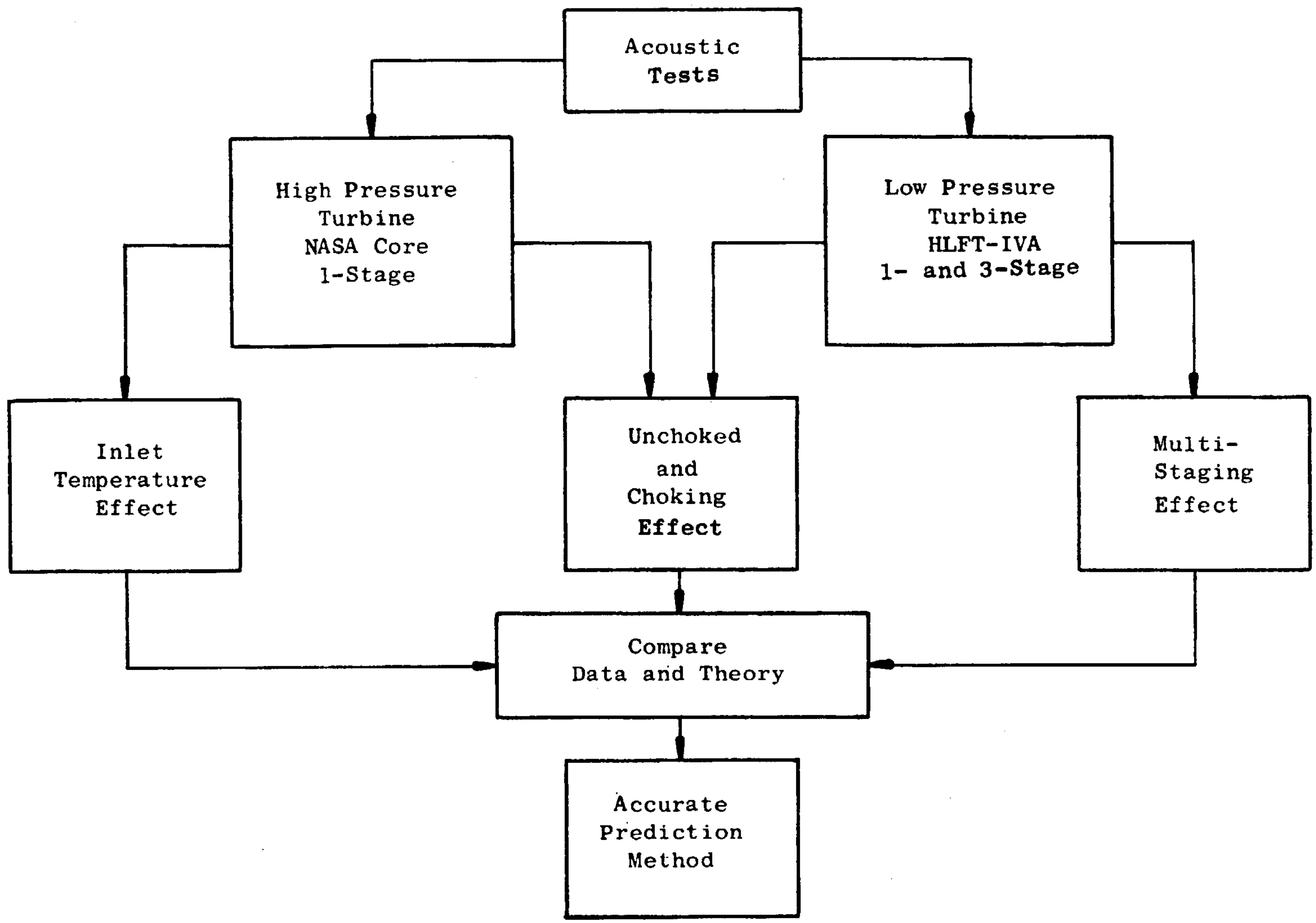

Figure 12. Structure of Acoustic Tests to Accomplish the Program Objectives.

Table III. High Pressure Turbine Design Characteristics (NASA Core Turbine).

Wt. Flow Function, $\frac{W\sqrt{T}}{P}$	0.81
Loading, $\frac{gJ\Delta H}{\Sigma U_P^2}$	1.66
Pressure Ratio (Total)	1.83
Speed, $N/\sqrt{T}$	362
Stator Vanes	36
Rotor Blades	64
Radius Ratio	0.85
Tip Diameter (Stage Exit), (cm)	50.8

Table IV. Low Pressure Turbine Design Characteristics (Highly Loaded Fan Turbine, HLFT-IVA).

	Stage			
	1	2	3	Overall
Wt. Flow Function, $\frac{W\sqrt{T}}{P}$	-	-	-	1.57
Loading, $\frac{gJ\Delta H}{\Sigma U_P^2}$	3.52	3.12	1.60	2.70
Pressure Ratio (Total)	1.73	1.81	1.41	4.72
Speed, $N/\sqrt{T}$	-	-	-	204
Stator Vanes	100	144	140	-
Rotor Blades	206	190	160	-
Radius Ratio	0.811	0.735	0.663	-
Tip Diameter (Stage Exit)(cm)	63.55	69.08	73.18	-

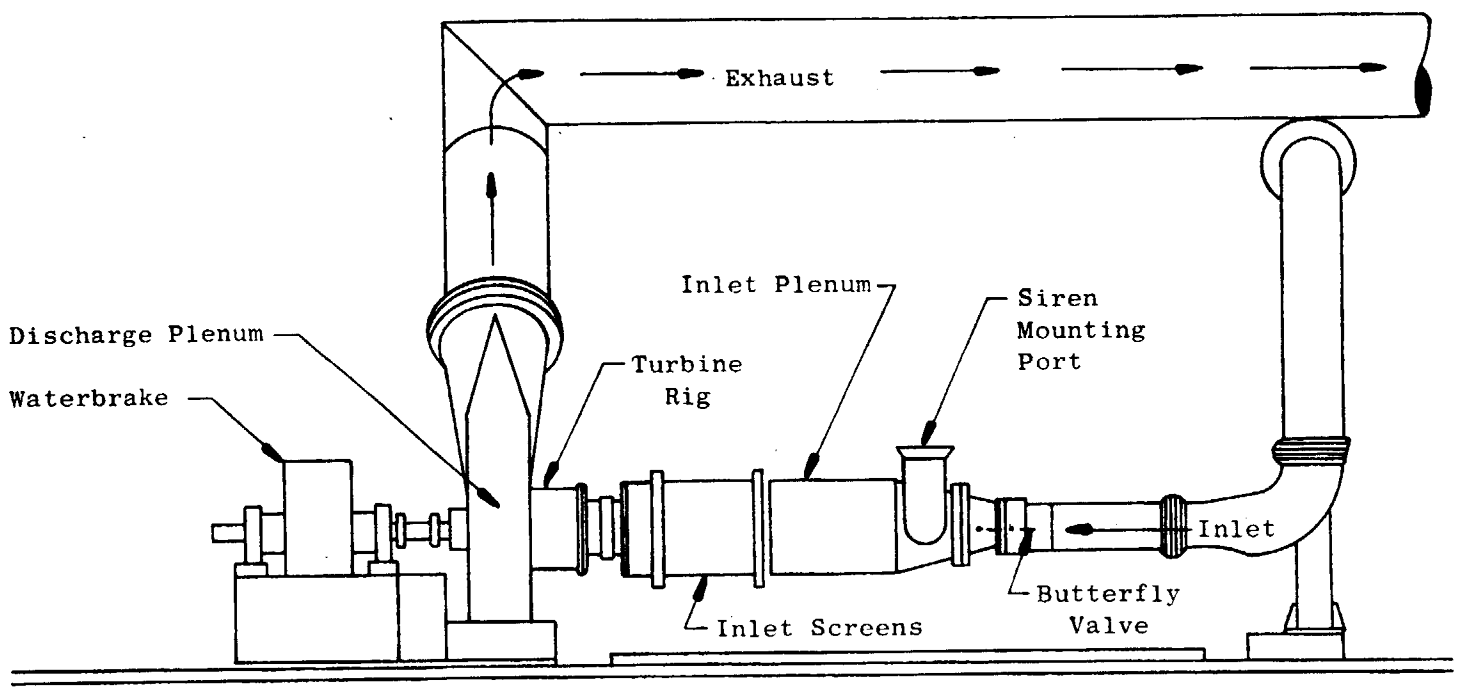

Figure 13. Warm Air Turbine Facility.

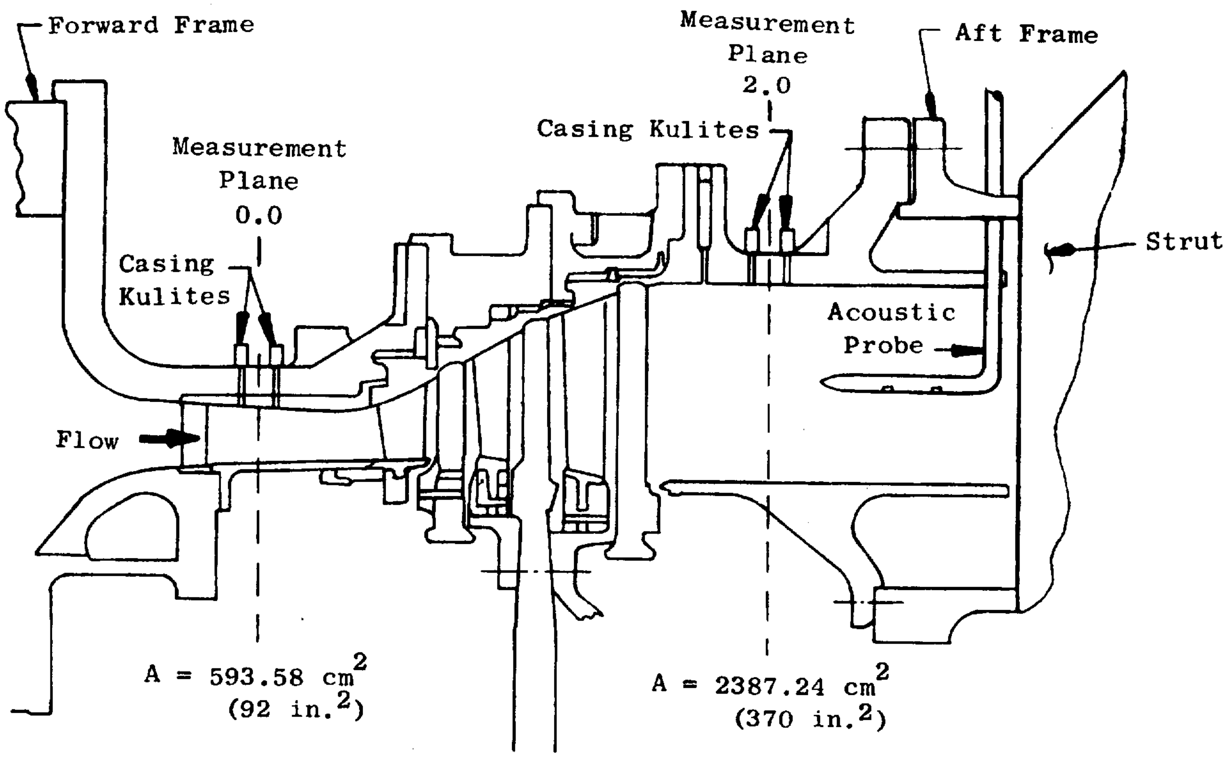

(a) HLFT-IVA Low Pressure Turbine, 3-Stage Build.

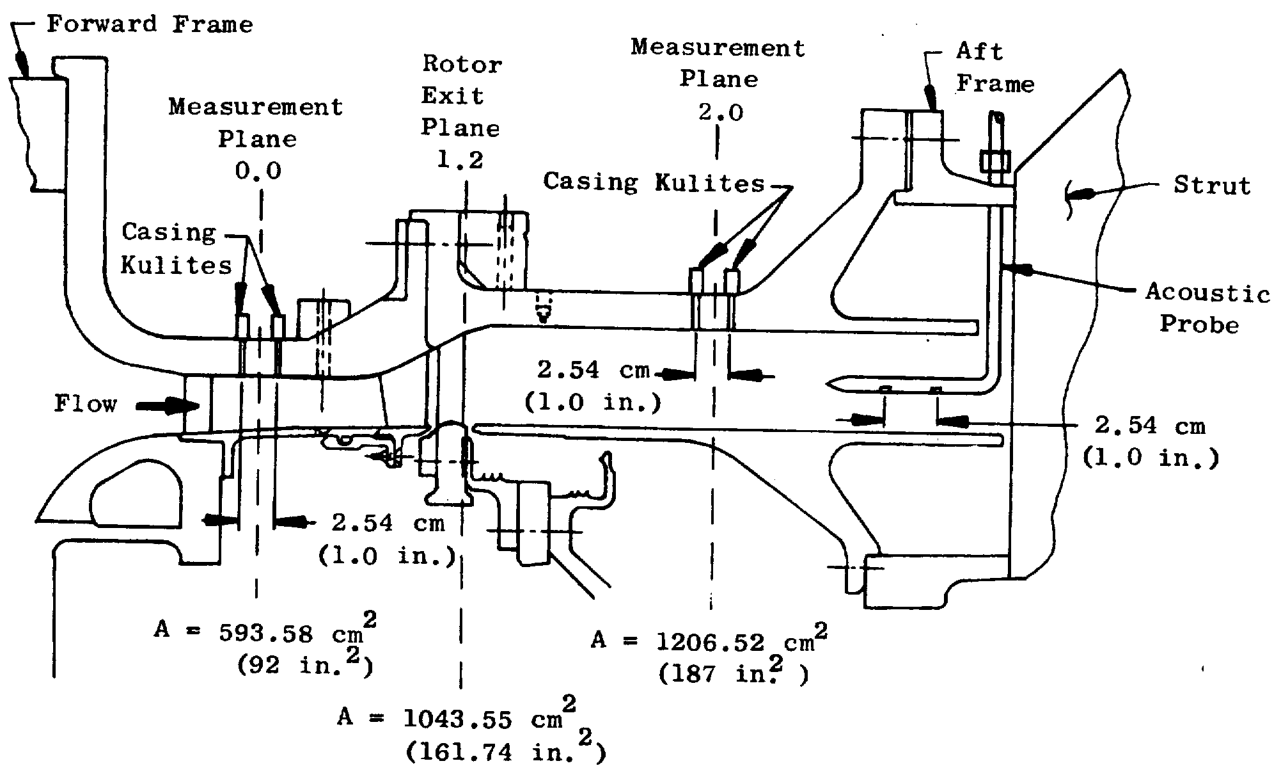

(b) HLFT-IVA Low Pressure Turbine, 1-Stage Build.

Figure 14. Schematic of Low Pressure Turbine Configurations.

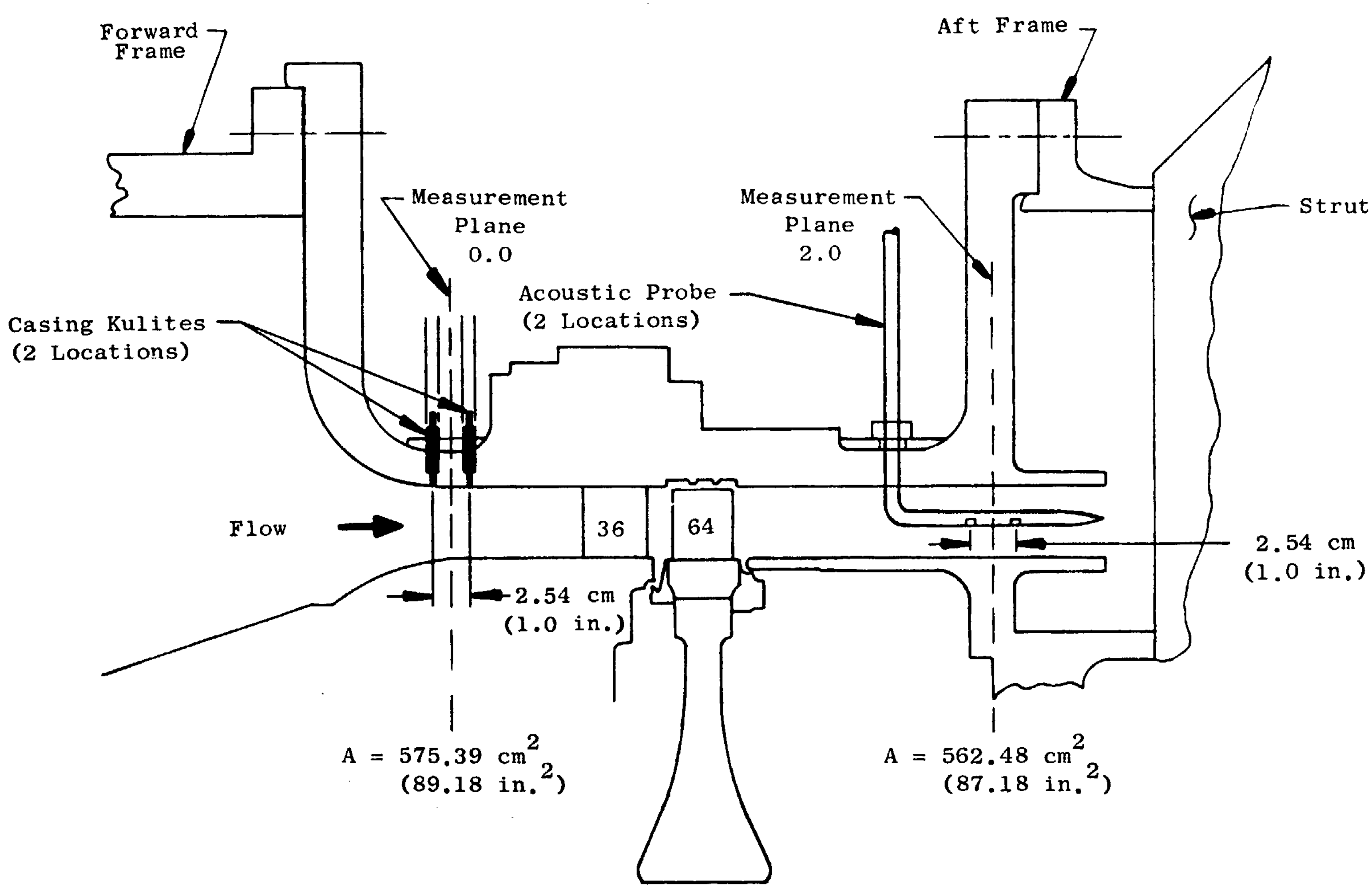

Figure 15. Schematic of NASA Core High Pressure Turbine Vehicle.

Table V. High Pressure Turbine Test Matrix (NASA Core Turbine)

- Design Speed, $N/\sqrt{T} = 362$
- Flow Function, $W\sqrt{T}/P = 0.81$
- Inlet Absolute Total Pressure, $P_{TO} = 389.5\ kN/m^2$

		Cold Inlet Test $T_{TO} = 450$ K P_{TO}/P_{S2}						Hot Inlet Test $T_{TO} = 783$ K P_{TO}/P_{S2}				
% $N/\sqrt{T}$	rpm	1.9	2.14	2.49	2.68	3.03	rpm	1.9	2.14	2.49	2.68	3.03
70	5380	X	X	X	X	-	7100	X	X	X	X	-
90	6920	X	(X)	X	X	-	9130	X	X	X	X	-
100	7690	X	(X)	(X)	-	X	10146	X	X	X	-	X
110	8460	X	(X)	X	-	X	11160	-	X	X	-	X

○ - Repeat Point

Table VI. Low Pressure Turbine Test Matrix (HLFT-IVA).

- Desigr Speed, $N/\sqrt{T}$ = 204
- Flow Function, $W\sqrt{T}/P$ = 1.57
- Inlet Total Pressure P_{T0} = 275.8 kN/m^2
- Inlet Total Temperature, T_{T0} = 422 K

% Design Speed	Speed (rpm)	Pressure Ratio (P_{T0}/P_{S2}) Single-Stage Build				Three-Stage Build			
		1.6	1.9	2.2	2.5	2.0	3.0	4.0	5.2
50	2100	X	-	-	-	X	-	-	-
70	2940	X	X	X	-	X	X	X	-
90	3780	X	X	(X)	X	X	(X)	X	X
100	4200	X	(X)	(X)	(X)	X	X	X	(X)
110	4615	X	X	X	X	X	(X)	X	X

◯ - Repeat Point

Data analysis techniques included very high resolution data reduction and coherence analysis between upstream and downstream sensors in an effort to unmask the siren tones downstream of the turbine. The latter was found to be more successful. A typical coherent spectral comparison is shown in Figure 16. The figure clearly shows large transmission losses for the 400 and 800-Hz tones, but a much smaller value for the 1200-Hz tone. The comparison of Figure 16 is on a SPL basis. A more meaningful result was obtained by correcting the data for flow, specific impedance, and area to arrive at the corresponding power levels (see Reference 7). The area correction assumed zero-th order, radial-mode distribution, that is, constant energy distribution from hub to tip. This has been found to be a reasonable assumption for low frequency noise measured in an engine core (Reference 2).

Typical plots of the siren tone attenuation as a function of the tone frequency are shown in Figure 17 for the high pressure turbine at design point. The spectra display a very distinct, bilobed shape, with large increases in attenuation below 100 Hz and above 2000 Hz and a secondary peak between 350 and 400 Hz. This secondary peak was found to correspond to cut-on of the first spinning mode. How this cut-on increases the transmission loss has already been discussed in Section 3.

The data appeared to exhibit a fairly large amount of random scatter, possibly as a consequence of duct-related phenomena and interference between forward- and backward-propagating acoustic waves. The 2.54-cm axial spacing between sensors was found to be inadequate to separate the two wave systems because of the large wavelengths and high broadband "noise" levels. Ultimately, the only viable option available was data averaging - use of large samples and as many of the sensors as possible. The midlobe, however, remained readily discernible, even for the low pressure turbine data where the siren frequency corresponding exactly to the first modal cut-on was assiduously avoided. Partly because the size of the midfrequency lobe was believed to be a consequence of the asymmetric sound injection into the turbines, and partly to facilitate comparison with the existing theory at that time (1976), a bathtub spectrum shape was postulated as shown in Figure 18. The attenuation spectrum was divided into three distinct regions as shown in the figure: very low frequencies (below 100 Hz), midfrequency floor (200 to 1200 Hz), and high frequencies (above 1500 Hz). It was hypothesized that there were mechanisms involved at the low and high frequency ends which either invalidated the basic theoretical (actuator disk) assumptions or involved phenomenon not considered in the analysis. The bathtub floor was found to correspond closely to the actuator-disk theory. Coincidently, the floor spans the major frequencies of interest for combustor noise. The frequency span of the floor could easily be extended to 2000 Hz without any loss of generality, as is obvious from Figures 17 and 18.

A single value of transmission loss corresponding to the floor was obtained for each turbine operating point by averaging the attenuation values of all siren tones within the midfrequency region. This technique proved to be remarkably successful in collapsing the data and revealing trends. The collapse achieved is shown in Figures 19 through 21 for the

- High Pressure Turbine
- Siren = 1204 rpm
- Inlet Temperature = 450 K
- Inlet Pressure = 389.6 kN/m^2

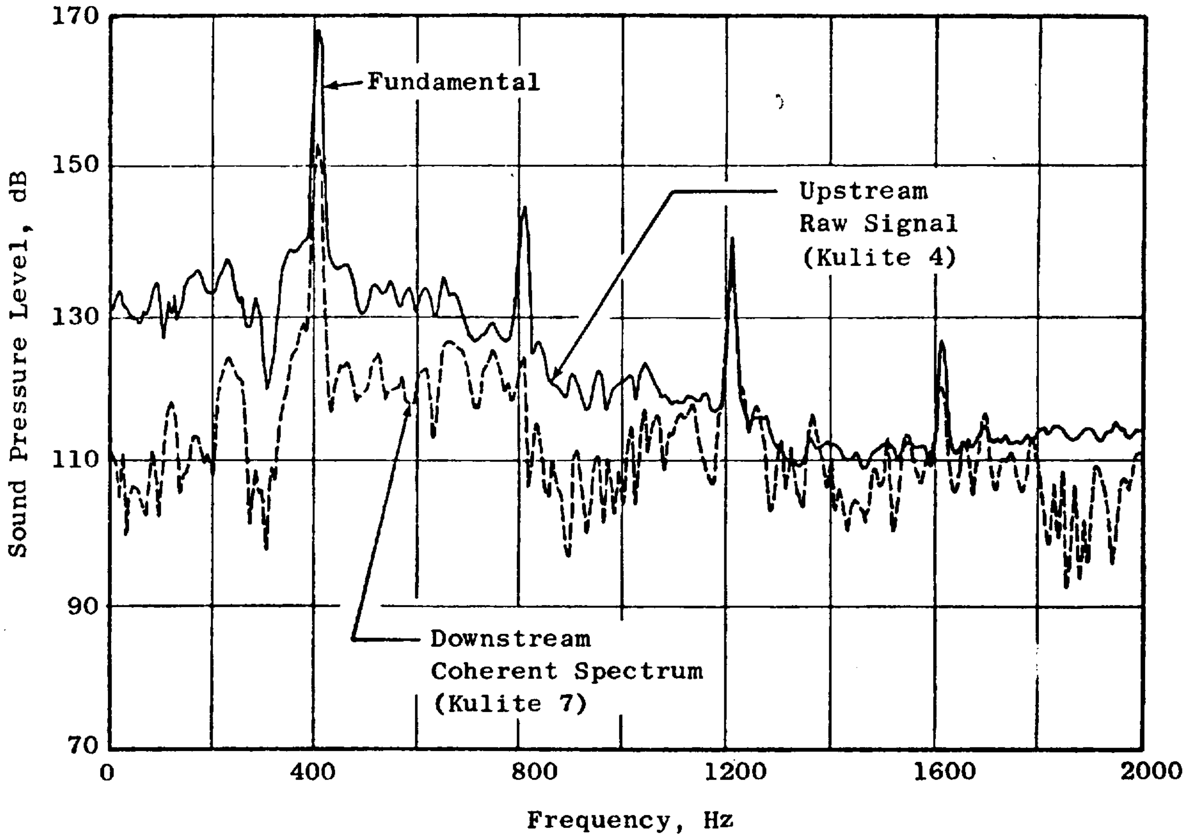

Figure 16. Comparison of Upstream and Downstream Signals Showing Turbine Transmission Loss.

• NASA Core High Pressure Turbine
• Averaged Values from Coherent Spectra
• Inlet Temperature = 450 K
• P_{T_0}/P_{S_2} = 2.14, $N/\sqrt{T}$ = 100%

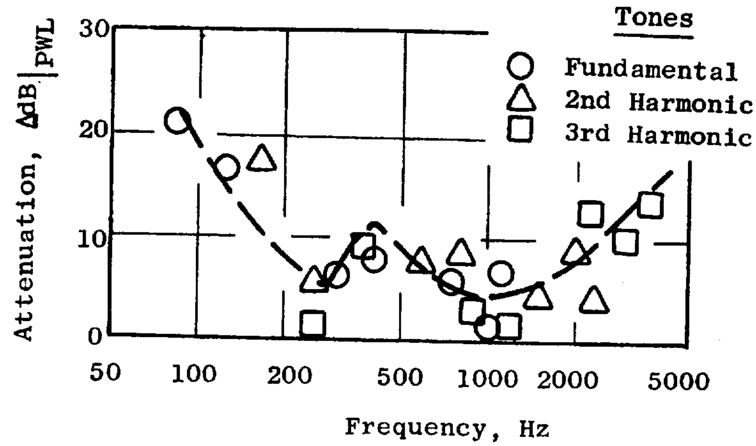

(a) HPT Cold Design-Point Attenuation Spectra

• NASA Core High Pressure Turbine
• Averaged Values from Coherent Spectra
• Inlet Temperature = 783 K
• P_{T_0}/P_{S_2} = 2.14, $N/\sqrt{T}$ = 100%

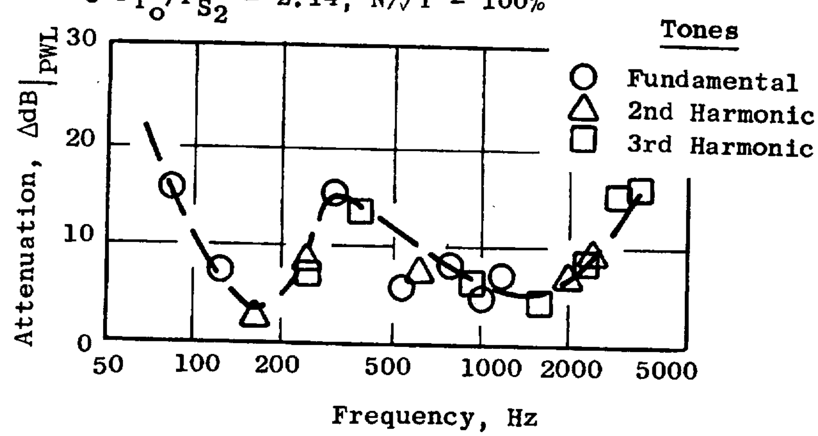

(b) HPT Hot Design-Point Attenuation Spectra

Figure 17. High Pressure Turbine Design-Point Attenuation Spectra.

ORIGINAL PAGE IS
OF POOR QUALITY

- 1-Stage Low Pressure Turbine
- Average Attenuation for Design Point

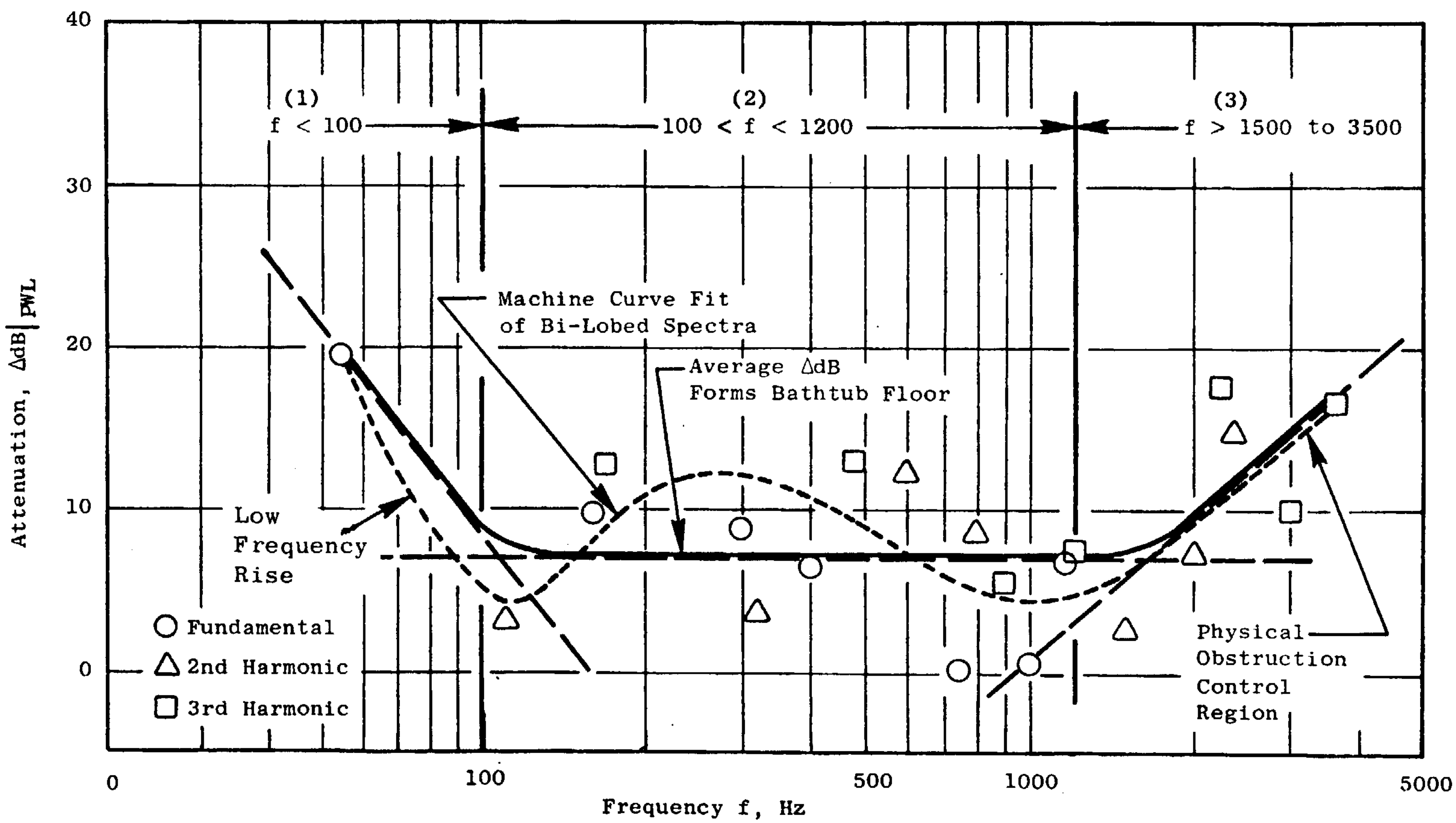

Figure 18. Bathtub Spectrum Shape.

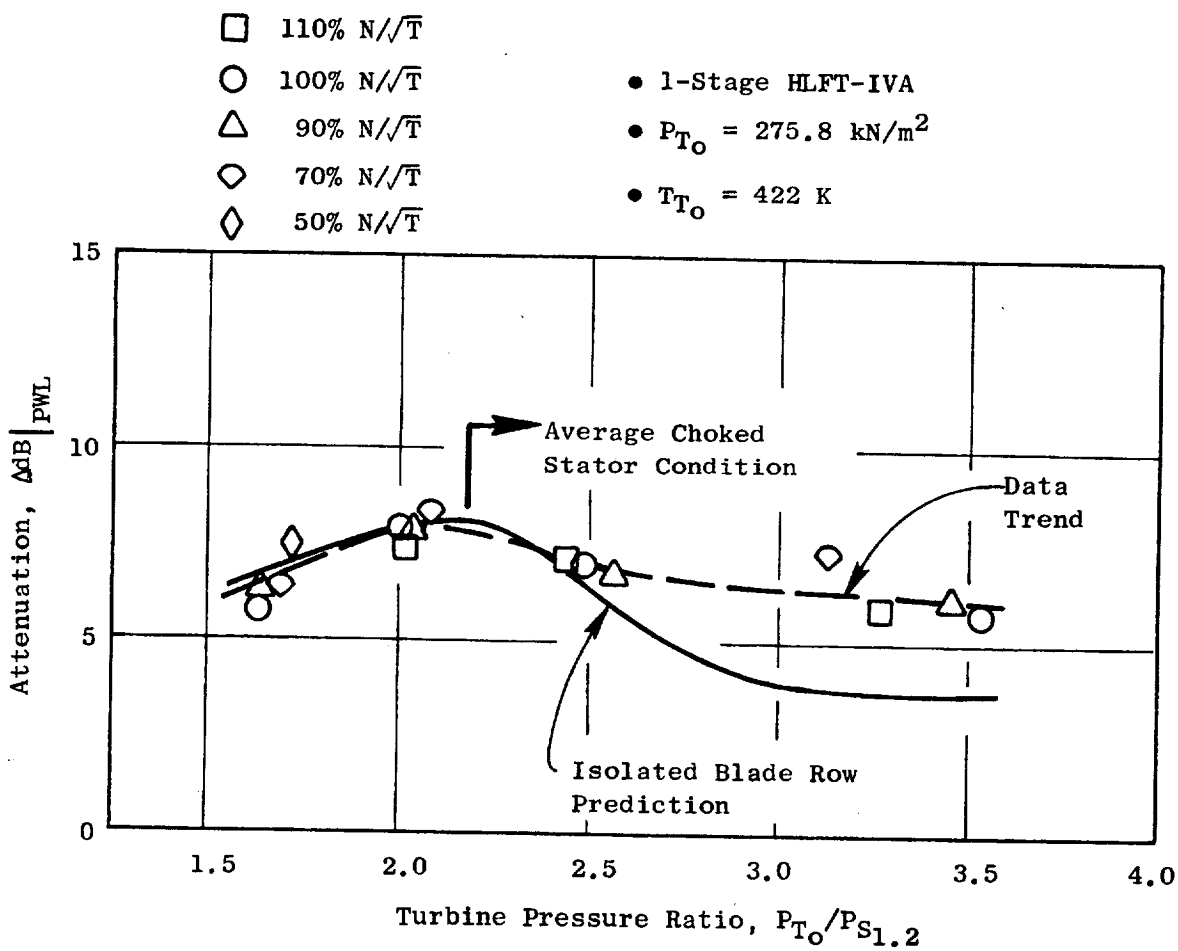

Figure 19. Effect of Turbine Pressure Ratio on Attenuation of Single-Stage Low Pressure Turbine.

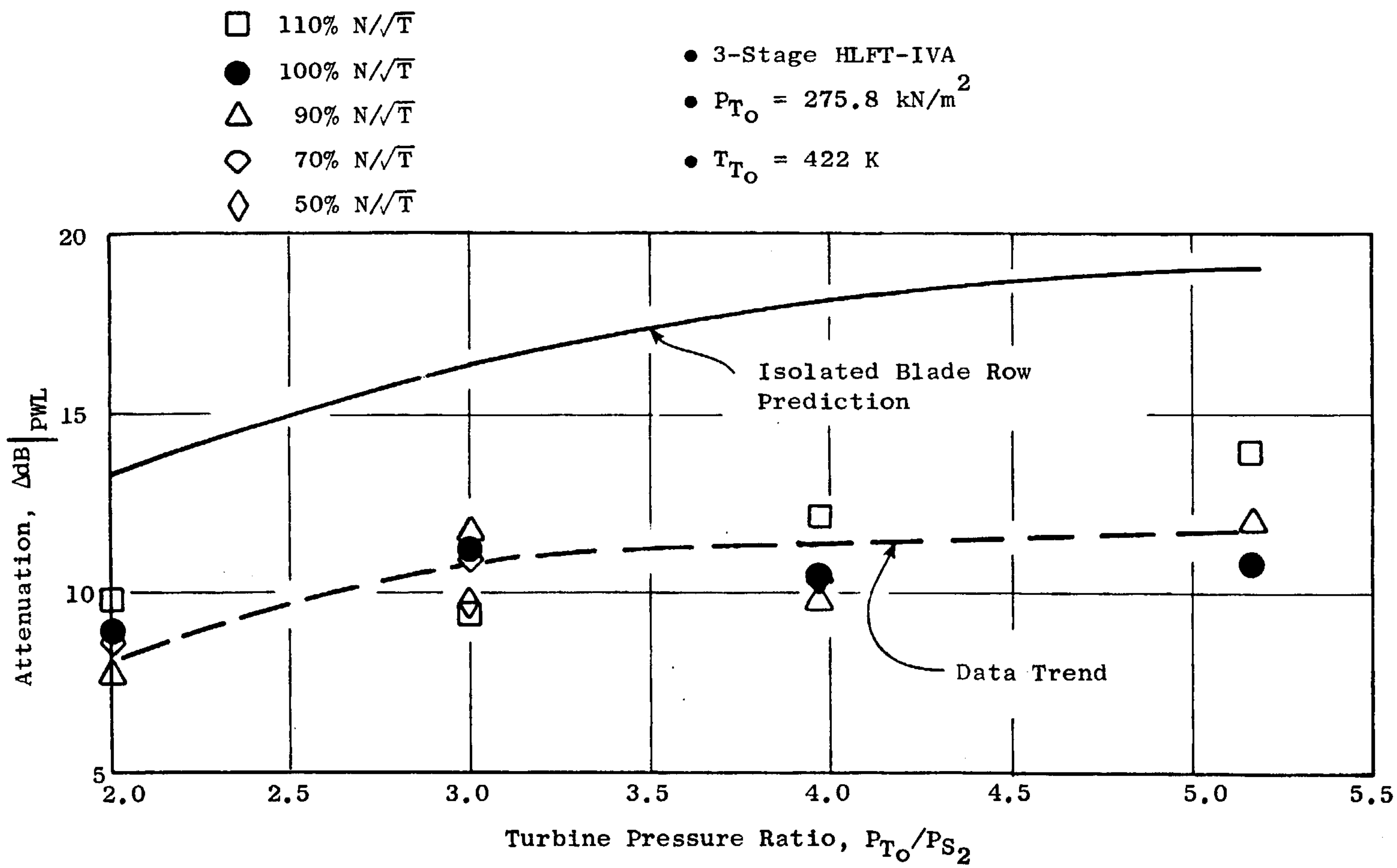

Figure 20. Effect of Turbine Pressure Ratio on Attenuation of Three-Stage Low Pressure Turbine.

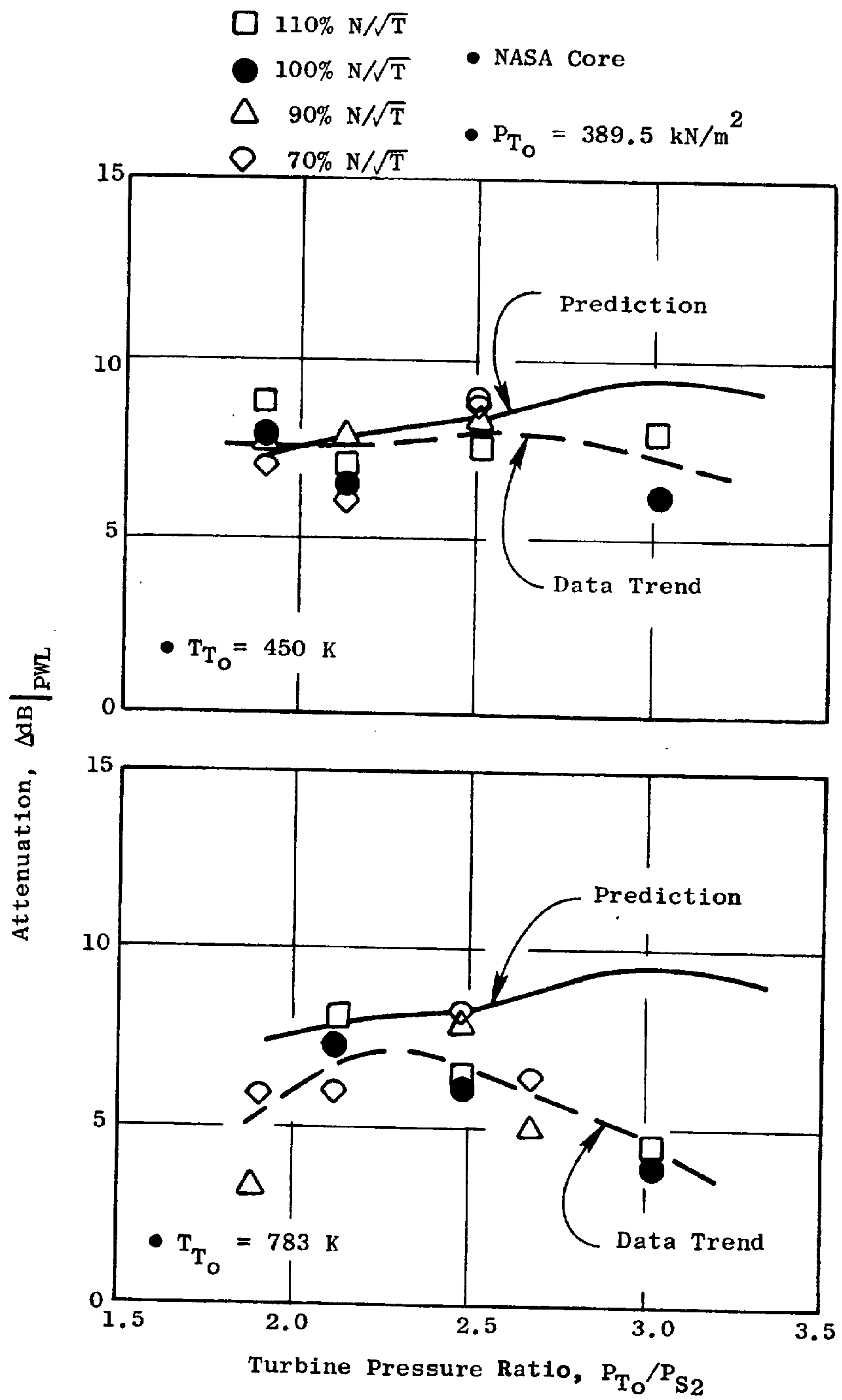

Figure 21. Effect of Turbine Pressure Ratio on Attenuation of High Pressure Turbine.

turbines tested. The plots* show the floor transmission loss as a function of the turbine pressure ratio, with the turbine speed as a separate parameter. Clearly, the turbine speed is not a significant variable. The data trends did indicate a pressure dependency in that the attenuation increased (very slightly) with the pressure ratio for subsonic flows, flattening out, and even decreased by a small amount for choked flows. However, the total variation observed for any turbine was about 3 dB or less over the entire test matrix. The test matrices for these component tests represented far greater excursions from design than would be encountered for turbines installed in engines. Hence, the data trends would suggest very minor, certainly less than 3 dB, changes in midfrequency transmission loss over the normal operating range for aircraft engine turbines.

These figures also show the analytical predictions using the actuator-disk theory of Reference 3. The prediction involved two major assumptions in addition to the actuator-disk modeling. First, only the plane wave propagating axially down the duct was considered ($\theta_I = 0$); spinning modes were ignored because of the low frequency nature of the sound. Secondly, it was assumed that the attenuation due to each blade row could be computed separately with anechoic terminations both upstream and downstream and the individual attenuations were additive in arriving at the attenuation for the turbine. Both assumptions were necessary in order to maintain a viable mathematical model and extract a solution. Comparison of the predictions with the data trends in Figures 19 and 20 left little doubt that the existing analysis needed further modification. Figure 19 shows remarkable agreement for pressure ratios below choking, but the pronounced dip in predicted attenuation above choking was not matched by the data trend, and a 3-dB discrepancy resulted. Further, while good agreement was found for single-stage turbines in the subsonic flow regime, the three-stage turbine data were overpredicted by 3.5 to 7 dB proceeding from the lowest to highest turbine pressure ratio tested. The question then became: could the actuator-disk theory be modified sufficiently through recognition of higher order (spinning) modes, multistaging, etc., to obviate the discrepancies noted above and explain the observed frequency spectrum?

4.2 COMPARISON OF THE DATA WITH THE IMPROVED THEORY

The predictions used here were generated using the computer programs listed in Appendices A and B. The program in Appendix A can be exercised only for subsonic turbines, while that in Appendix B is a generalized program which can accommodate both choked and unchoked blade rows. However, the Appendix A program provides an exact solution and is considerably cheaper to execute.

---

*The values are slightly different from those shown in Reference 7. The ΔSPL to ΔPWL conversion in Reference 7 was made using average values (one for each turbine) of the specific impedance and Mach number in order to facilitate data reduction. The data shown here have been corrected using the exact values for each different operating point.

Figures 22 and 23 provide data comparisons with predictions using the multistaging program of Appendix A for the single-stage, high pressure (NASA Core) turbine. The prediction in Figure 22 uses an equal energy distribution and is seen to skim along the bottom of the data points. There is an increase in attenuation at each modal cut-on frequency. The effect of the first one is most pronounced; suddenly two-thirds of the incident energy is transferred into the two new waves that are completely reflected. At the second modal cut-on, two-fifths of the incident energy is transferred into the new waves; therefore, the indicated increase in transmission loss is correspondingly smaller. As the number of existing modes increases, the effect of subsequent cut-on naturally diminishes. The variations in the measured transmission losses, however, are somewhat larger than predicted.

A logarithmic scale was used for the frequency in Figure 22 and throughout NAS3-19435 in order to facilitate comparison with one-third-octave band spectra characteristically utilized in the analysis of combustor noise. It is more instructive to evaluate these turbine test results on a linear frequency scale for current purposes. Such a linear plot is shown in Figure 23, along with a prediction made with the frequency inverse energy assignment discussed in Section 4. This energy distribution model biases the available acoustic energy into the highest cut-on mode and, in fact, assigns all the incident energy to a new mode at the instance of cut-on ($f = fc$). The associated propagation angle, $\theta_I = \pm 90°$, almost ensures complete reflection and therefore infinite transmission loss. The program assumes a more reasonable finite value of 20 dB at this point. The prediction can be seen to be in very close agreement with the measured data, particularly in picking up the increased transmission loss points due to modal cut-on. Filled-in data point symbols in the figures denote masking of the downstream tone by broadband noise. Hence the actual transmission loss was at least as much as shown by such a symbol, but it could have been significantly higher.

The good match between the data and saw-toothed prediction implies that the apparent scatter in the data about the "mean" bathtub floor was, in part, a manifestation of a modal cut-on, due to asymmetric noise injection, and not a random error in the measurements. The fact that greater scatter was observed for the low pressure turbine data (see Figure 24) than for the high pressure turbine data provides further verification of this thesis. Because cut-on occurred earlier in the low pressure turbine as a consequence of the larger mean radius there would, therefore, be more cut-ons over a given frequency range. The large jump associated with the first modal cut-on is obvious in the high pressure turbine transmission loss spectra but conspicuous by its absence from the low pressure turbine data only because the onset became apparent during the testing and was carefully avoided by moving the siren to adjacent frequencies. It was recognized then, and is emphasized here, that the prominence of the cut-on effect in the test data was most probably due to the method of sound injection into the turbines. A symmetric sound source, such as provided by aircraft engine combustors, should result in equal energy modal distribution and a flatter transmission loss spectrum such as shown by the solid line in Figure 22.

ORIGINAL PAGE IS OF POOR QUALITY

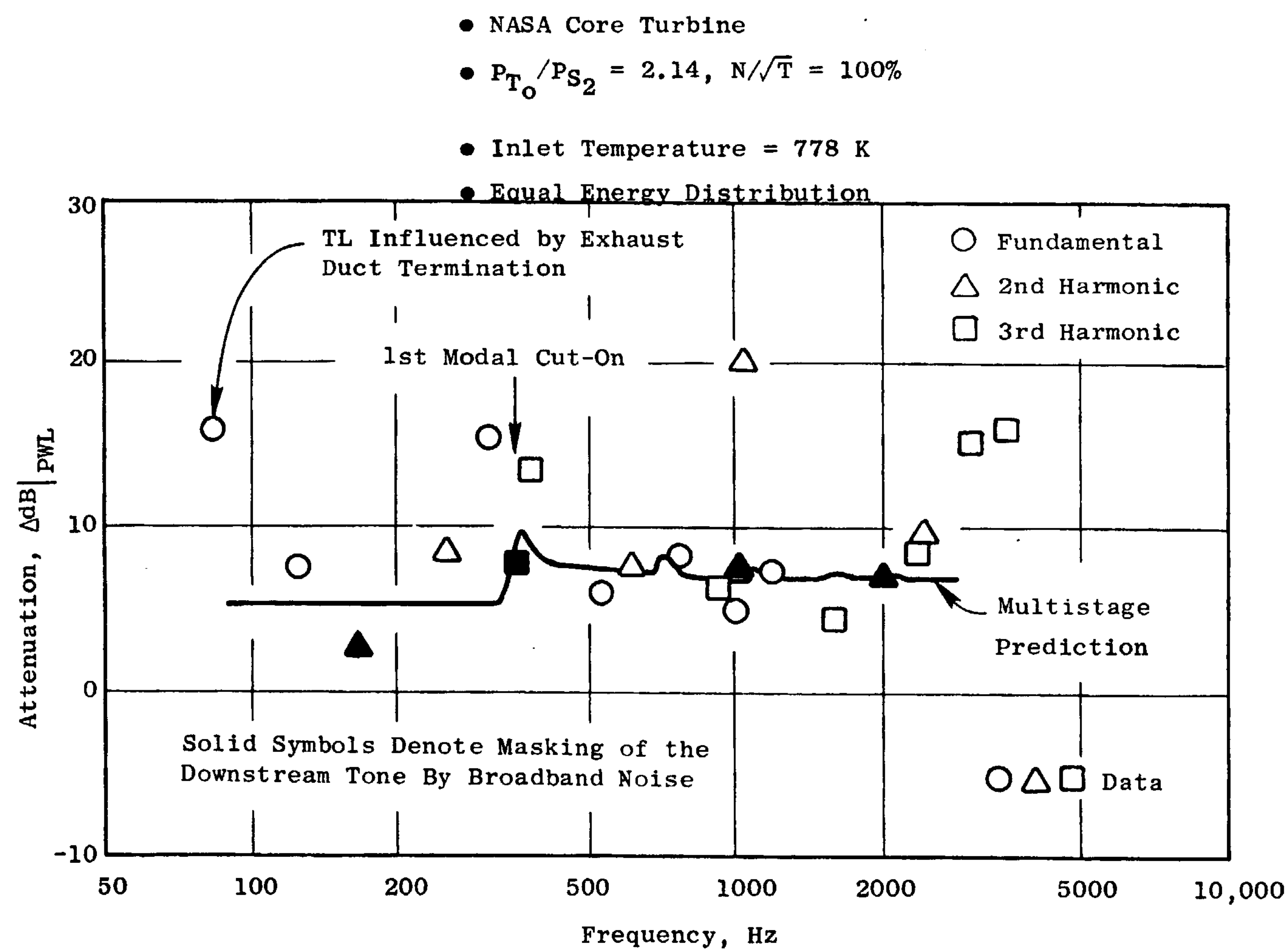

Figure 22. Comparison of Data and Prediction Using Equal Energy Distribution.

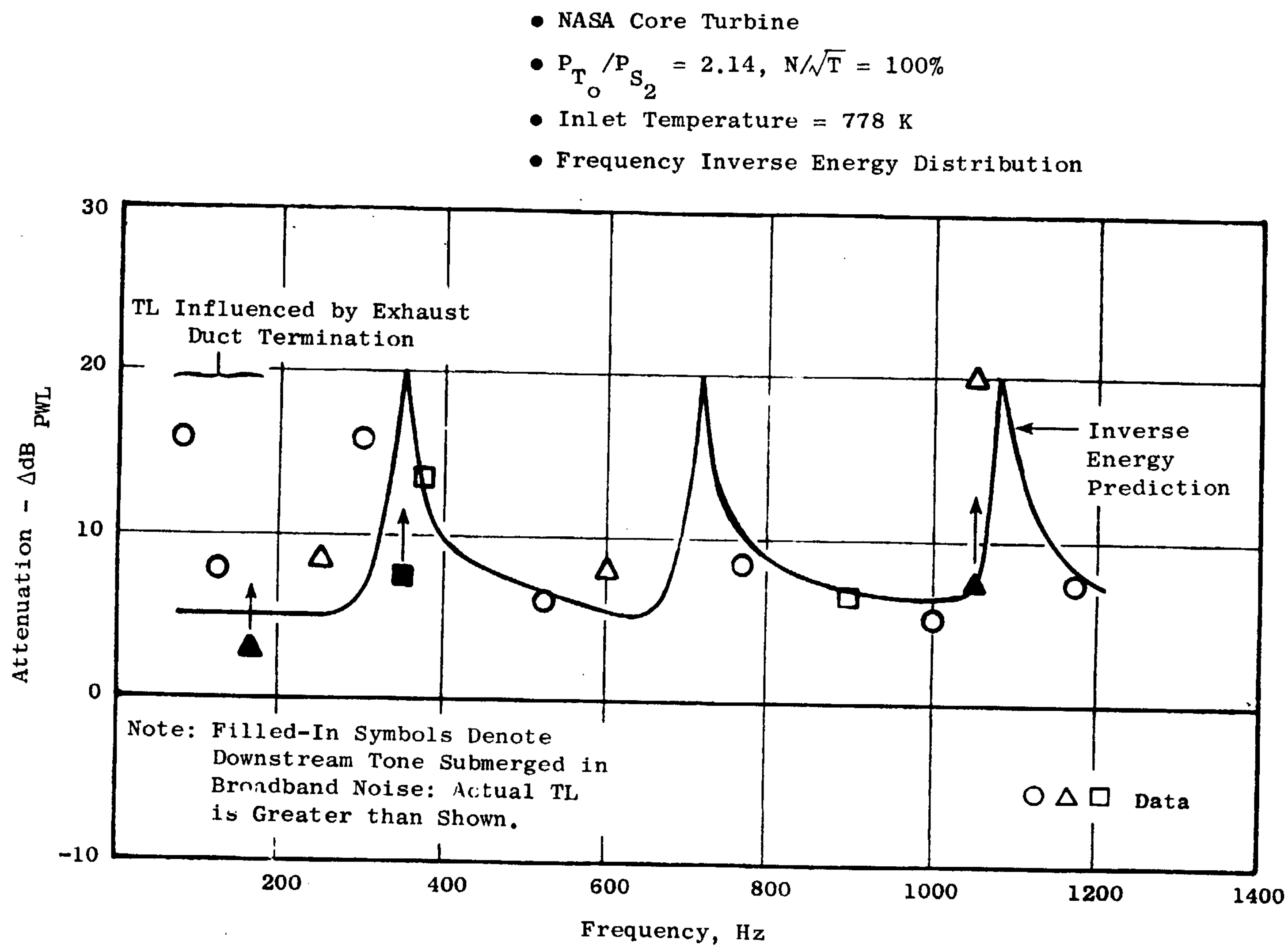

Figure 23. Comparison of Data Prediction Using Frequency Inverse Energy Distribution.

- 1-Stage HLFT IVA
- $P_{T_O}/P_{S_{1.2}} = 2.5$, $N/\sqrt{T} = 100\%$
- Inlet Temperature = 778 K
- Frequency Inverse Energy Distribution

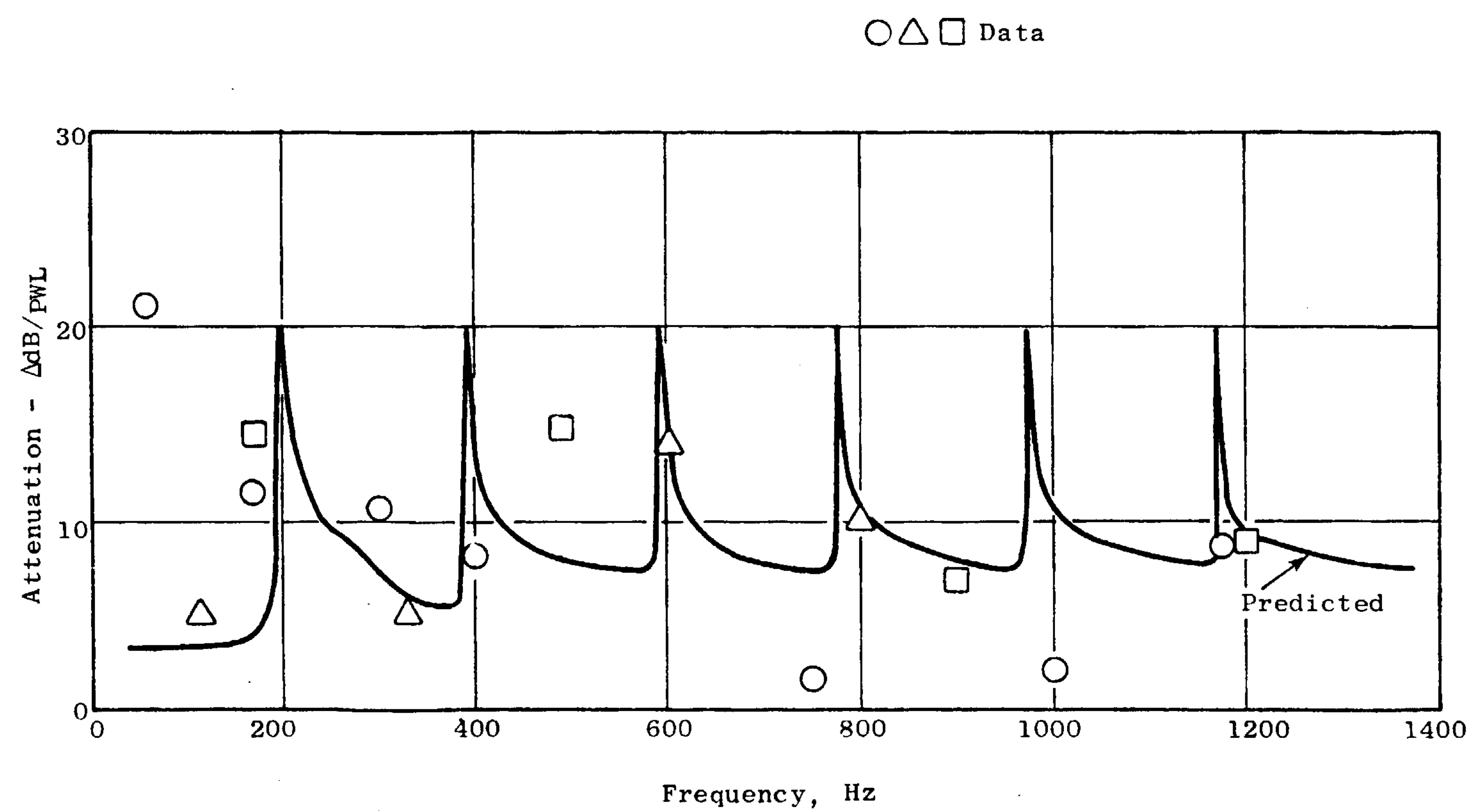

Figure 24. Comparison of Data and Theory Using Frequency Inverse Distribution for the Low Pressure Turbine.

Recognizing the influence of the modal cut-on phenomenon in the test data, a case could be made for the extension of the bathtub floor to 2500 Hz, or greater, from the original 1200 Hz used in NAS3-19435. The gradual increase in transmission loss for frequencies above 3000 Hz could be attributed to the diffraction effect discussed in the finite-chord modeling of Section 3.2. The increase in transmission loss at the very low frequencies has been shown to be a spurious effect due to the location of the exhaust sensors near the turbine exhaust duct termination. That is not to say that there will not be any increase in the very low frequency transmission loss for a gas turbine engine, merely that any such increase will probably be due to the exhaust nozzle, not the turbines.

The following figures provide comparisons of the predicted and measured transmission loss variations with pressure ratio and speed. The measured transmission losses represent the bathtub floors for the test matrix points, as discussed earlier in Section 4.1. Each predicted value corresponded to the asympototic transmission loss floor of the spectrum for frequencies above the first cut-on. For example, referring to Figure 22, the transmission loss at design point for the NASA core turbine would be 7.2 dB.

Figure 25 shows the results for the single-stage configuration of the low pressure turbine. There is very close agreement between data and measurement, including the small increase with pressure ratio before the onset of choking and the slight decrease for pressure ratios higher than critical. In contrast, the isolated blade-row predictions using only the axial plane wave had indicated a very large decrease in transmission loss above choking (see Figure 19). The difference is mainly due to the incorporation of the spinning modes into the current prediction method.

On the other hand, the improvement in the theory/data comparison for the three-stage configuration (see Figure 26) is a consequence also of the multistaging analysis wherein the influence of adjacent blade rows was included. The predicted transmission loss is of the same order as that measured: 10 dB. The data do indicate a small increase, about 3 dB, between the 2.0 and 5.2 pressure ratios, but only for speeds other than design.

The data for the high pressure turbine are compared with the new theory in Figure 27. Both the hot and the cold inlet data show agreement with theory. As in the case of the single-stage, low-pressure turbine, the slight increase in transmission loss with pressure ratio below choking and decrease above choking is reproduced.

In brief summary, the inclusions of higher order modes and incorporation of the interactive influence of adjacent blade rows into the actuator-disk model provided the critical elements to successfully explain the trends in the available data.

ORIGINAL PAGE IS OF POOR QUALITY

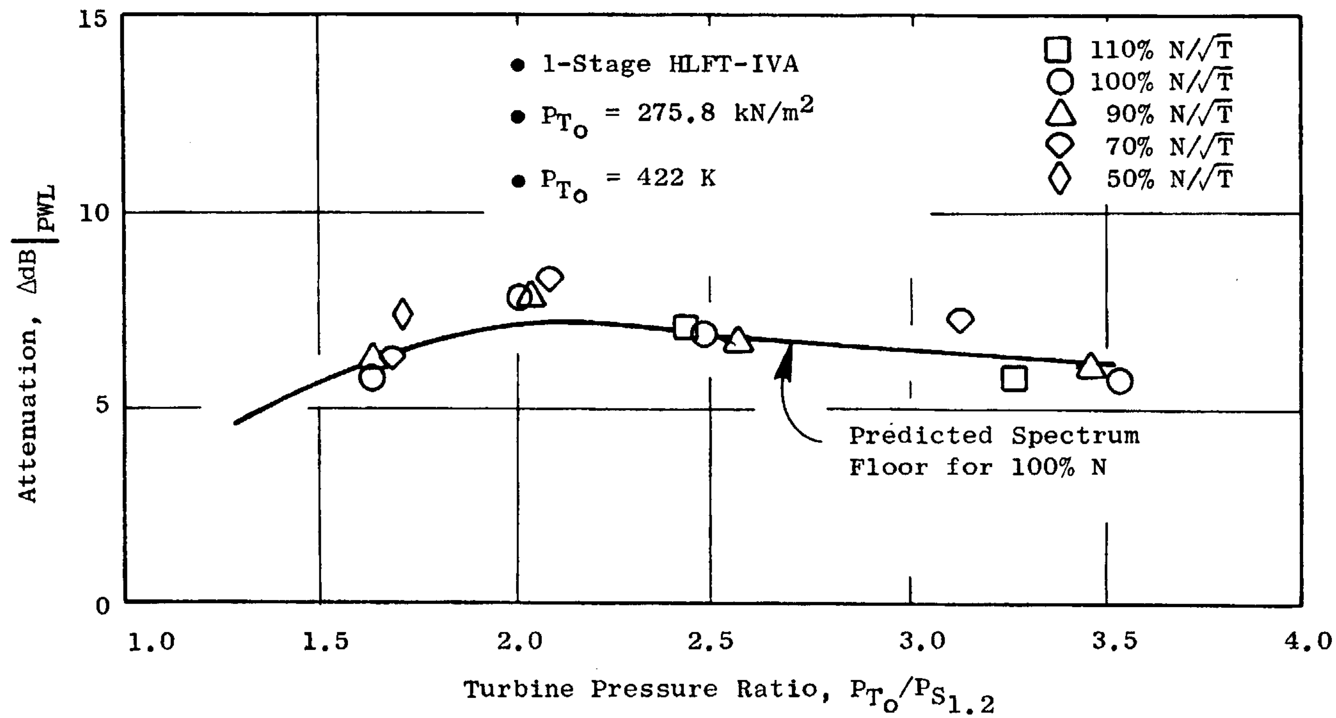

Figure 25. Comparison of Theory and Data for the Single-Stage, Low Pressure Turbine.

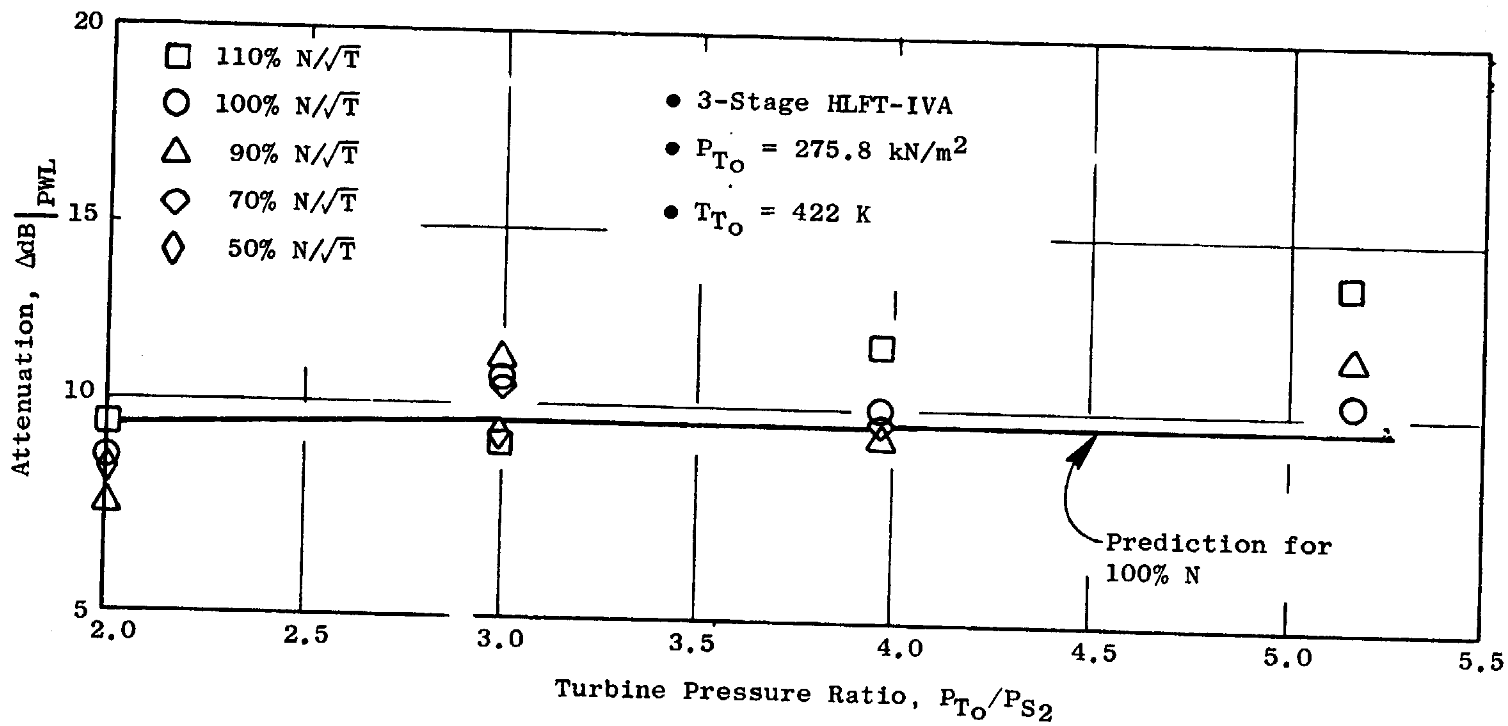

Figure 26. Comparison of Theory and Data for the Three-Stage Low Pressure Turbine.

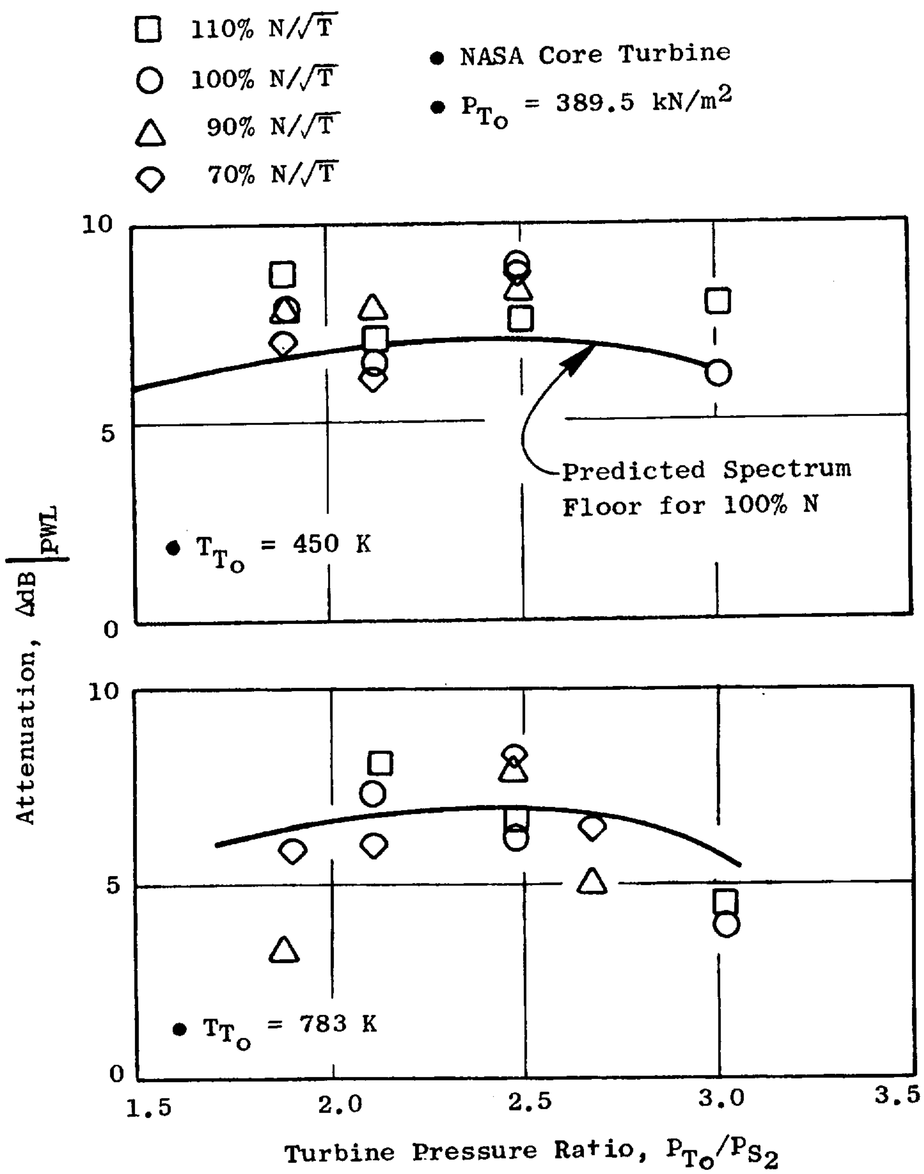

Figure 27. Comparison of Theory and Data for the Single-Stage High Pressure Turbine, Hot and Cold Inlet Flow.

5.0 USE OF THE THEORY AS A WORKING TOOL

5.1 CONCEPTUALIZATION

The basic mechanism behind low frequency noise attenuation by gas turbine blade rows and the governing equations for an actuator-disk modeling were first proposed by R. Mani as part of an unpublished study for the discharge reflection coefficient from a blade row. Bekofske extended the theory to include Mach number changes and flow turning across the blade elements and proposed a solution involving isolated blade rows. His published work (References 3 and 8) included a computer program to effect the solution. This isolated blade-row theory ultimately contributed to the development of General Electric's Unified Line prediction method for gas turbine engine combustor noise (Reference 2). However, comparison with component data revealed some shortcomings in the theory and the limitations of the actuator-disk model were not clear. The finite-chord model of Section 3 demonstrated the correctness of the actuator-disk assumption for the frequency range of interest for combustor noise. The theory/data comparisons of Section 4 provided validation of the refinements proposed in Section 3 to the basic theory. The computer programs of Appendices A and B provide the working tools required to implement the theory. A brief explanation of these multistaging, multimode programs is given below in 5.2. Detailed descriptions and listings can be found in the appendices.

The computer programs are really the only accurate means of defining the low frequency noise transmission through a given turbine. It is recognized, however, that occasionally a need arises to make "quick and dirty" assessments of a given system with only the information available in a preliminary design cycle deck. Section 5.3 suggests some simplifications and approximations that lend themselves to "back of the envelope" type calculations.

Together, Sections 5.2 and 5.3 constitute the working charts that were the second objective in this program.

5.2 COMPUTERIZED PREDICTION

The two computer programs in the Appendices are in FORTRAN and written for time-share usage. The basic flow chart used is shown in Figure 28. The input required is shown in Table VII and consists of the axial flow velocity, absolute flow angle, wheel speed (in the case of a rotating blade row), static pressure, and static temperature upstream and downstream of each blade row. This information is conventionally available for at least the engine "design" operating point from the turbine designer. Off-design information is a little more difficult to arrive at. Fortunately the available evidence suggests very little change in the transmission loss over the normal operating range. Also, the turbine tip radius and hub/tip ratio must be specified, along with the number of stages (up to ten total). The program can be run in

MØDMLT Flow Chart

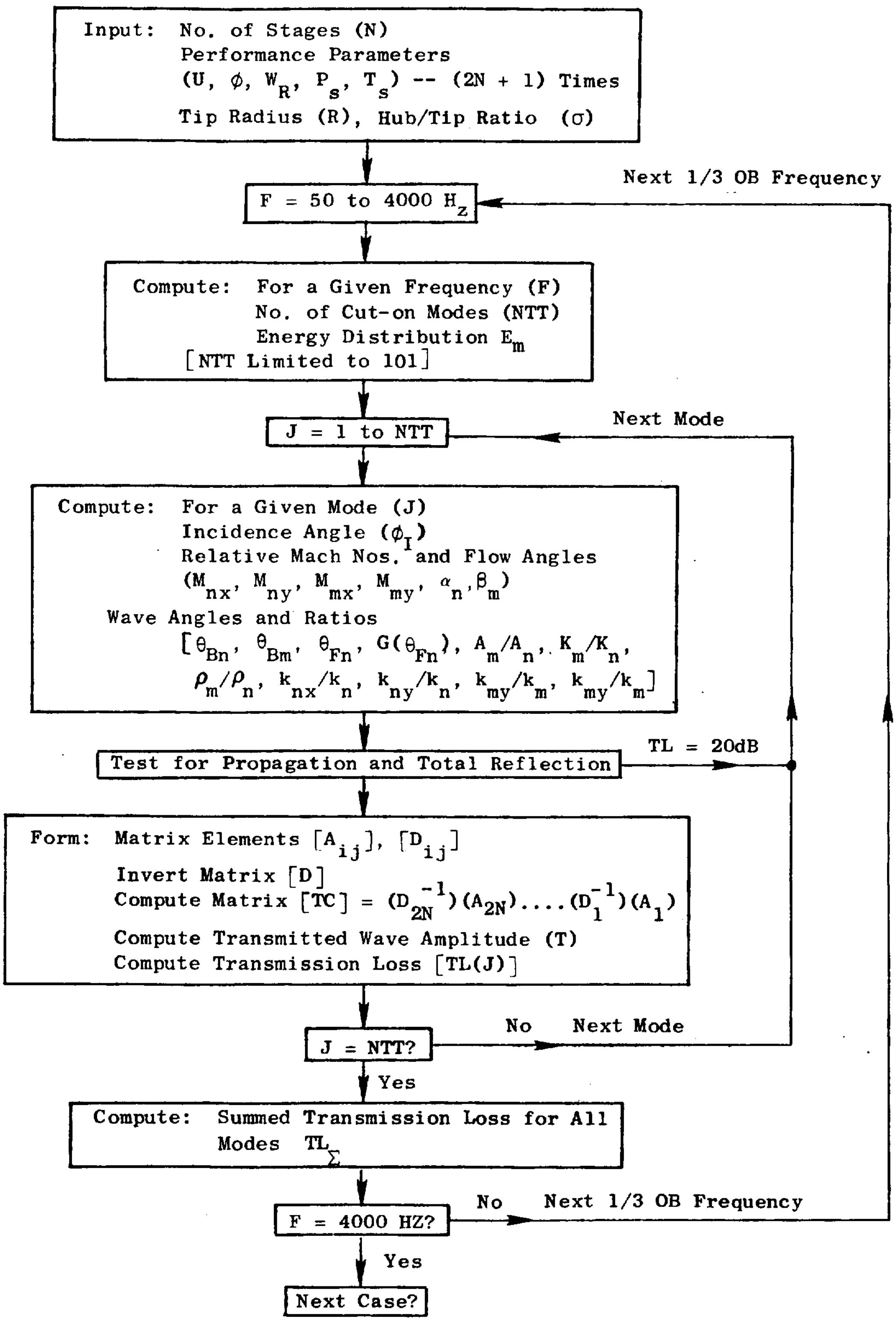

Figure 28. Flow Chart - Multistage, Multimode Computer Program.

Table VII. Typical Input Required for Multistage, Multimode Computer Program.

- Turbine/Power - SLTO at 303 K (546° R)
- Tip Radius (R_o) - 42.7 cm (16.8 in.)
- Hub/Tip Ratio (σ) - 0.889
- Number of Stages (N) - 6(2 + 4)
- Input (2N + 1) Times

Station	Axial Velocity (U) m/sec (ft/sec)	Absolute Flow (ϕ) degrees	Wheel Speed (V_R) m/sec (ft/sec)	Static Pressure (P_s) MN/m^2 ($lb/in.^2$)	Static Temperature (T_s) K (° R)
1	156 (511)	0	0 (0)	2.77 (402.2)	1573 (2832)
2	211 (692)	71.7	434 (1424)	1.66 (240.4)	1404 (2528)
3	282 (926)	-20.8	0 (0)	1.16 (161.8)	1287 (2317)
4	231 (757)	64.6	431 (1415)	0.84 (121.4)	1221 (2197)
5	304 (998)	-5.8	0 (0)	0.56 (81.8)	1113 (2003)
6	173 (568)	59.4	222 (728)	0.53 (77.2)	1087 (1956)
7	178 (585)	-35.5	0 (0)	0.43 (62.5)	1037 (1867)
8	188 (617)	59.8	215 (704)	0.37 (53.0)	1001 (1802)
9	201 (658)	-33.1	0 (0)	0.30 (42.8)	953 (1716)
10	222 (728)	55.6	208 (683)	0.24 (35.3)	914 (1645)
11	247 (809)	-30.8	0 (0)	0.19 (27.1)	860 (1548)
12	264 (865)	45.4	201 (660)	0.16 (23.9)	837 (1506)
13	268 (879)	-5.2	0 (0)	0.15 (21.2)	815 (1467)

an isolated blade-row mode by specifying zero number of stages; the program will then faithfully reproduce the results of the previous published computer programs (References 3 and 8).

The program starts with the lowest specified frequency and computes the number of cut-on modes, the energy distribution, the equivalent plane-wave incidence angle, the transmission loss associated with each spinning mode, and finally the summed transmission loss for that frequency. The frequency distribution specified in the program is the center frequencies for the one-third-octave bands from 50 to 4000 Hz. However, this can be changed very conveniently to any other frequency distribution, for example, the siren tone frequencies from NAS3-19435.

The most important frequency is the first modal cut-on and this is calculated and printed out using the inlet mean radius. The transmission loss at this point exhibits a sharp spike, and the subsequent values of transmission loss register a significant increase as shown in Figure 29, which corresponds to the input of Table VII. The transmission loss below the cut-on frequency corresponds to the axial plane wave only and is 1.5 dB in the example shown. The loss above the cut-on is controlled by the spinning modes and levels off at 9.5 dB.

Equal energy distribution is specified in the two computer programs. This can be changed to any other desired energy distribution, including frequency inverse, as indicated in Appendix A. The differences between equal energy and frequency energy distributions have already been discussed. The latter gives prominent spikes at each cut-on frequency. The height of each spike will depend on the assymmetry of the source: a line source giving equal values for each spike. A symmetric source, such as an annular combustor arrangement, probably will result in rapidly diminishing spikes. Whether these spikes will be discernible in broadband combustor noise spectra remains to be seen. It may be possible to use very high resolution (narrowband) analysis to detect the modal cut-on defects in the transmitted combustor noise spectrum in the exhaust nozzle. Also, the cut-on phenomenon could diffuse over a wide frequency band due to viscous effects, random flow variations, or "soft" duct walls. Cut-on for fan noise has indeed been observed to be a diffuse rather than discrete frequency phenomenon. Some clarification may be provided by the results from CF6-50 tests now proceeding under NASA Lewis funding (ECCP III, NAS3-19736).

It should also be recognized that turbine area, and therefore mean radius, generally will increase proceeding downstream. At the same time the static temperature will decrease. The cut-on frequency is proportional to (a/r^*), and therefore will also decrease. This will not only contribute to the diffusion of the first cut-on spike, but also will mean a sudden shift to a lower frequency in the case of a gooseneck between high and low pressure turbines, as found in the CF6 family of engines. The investigator may prefer to use the radius and hub/tip ratio downstream of the gooseneck in the computer program instead of the high pressure turbine inlet values. These dimensions are used to compute the cut-on frequencies and for no other purpose.

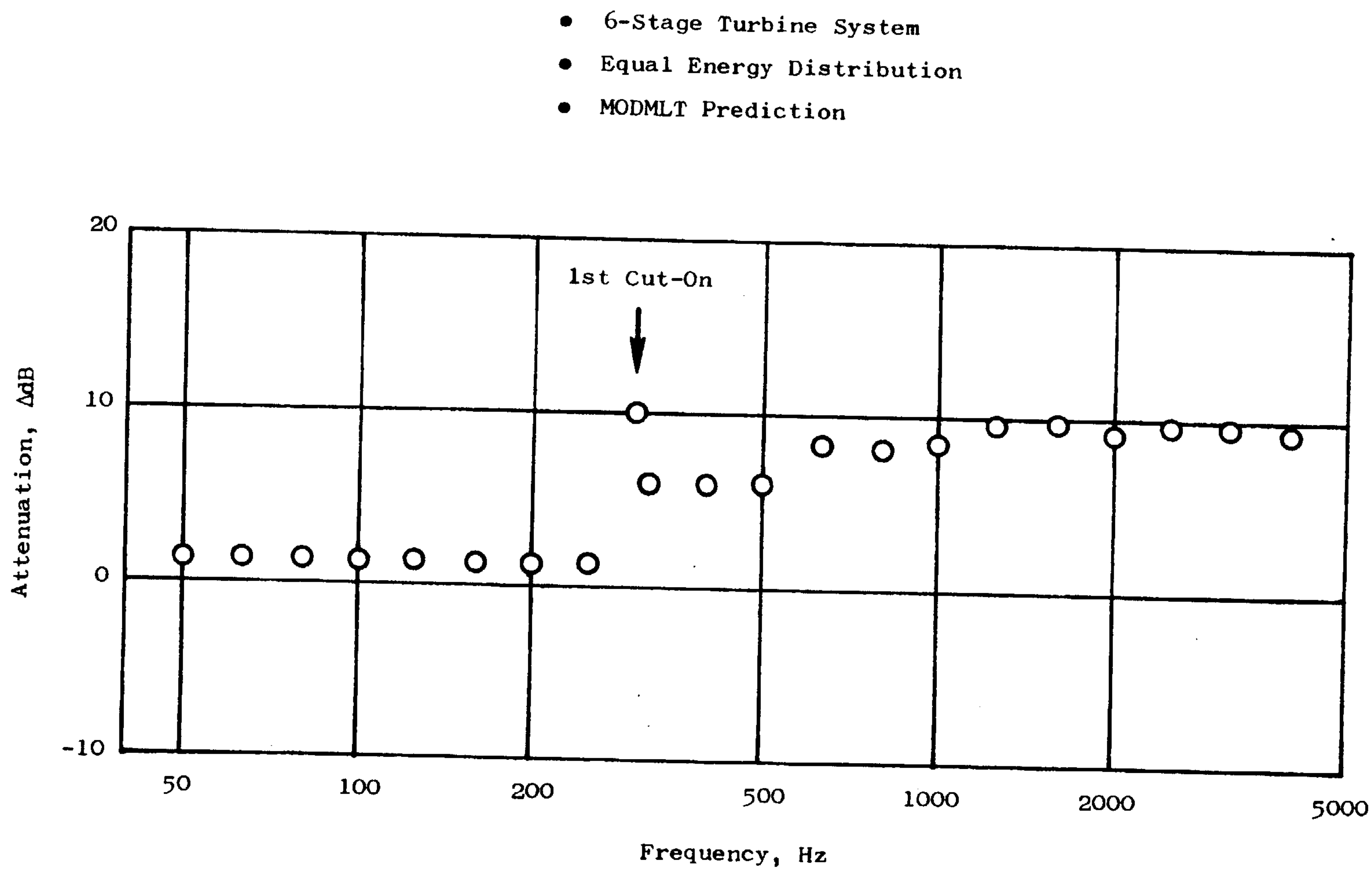

Figure 29. Typical Transmission Loss Spectrum.

5.3 APPROXIMATE ESTIMATION OF THE TRANSMISSION LOSS

The computer prediction methods were parametrically exercised for a number of different aircraft engine turbine systems (Table VIII) in an effort to discern trends and simplifications that could be used in a semiempirical prediction technique. The net outcome was the prediction spectrum shown in Figure 30(a). The transmission loss for frequencies below first cut-on is constant, corresponding to $\theta_I = 0$. Then at $f = f_c$, the loss increases to 10 dB, which represents a mean value obtained using equal energy distribution for multistage turbines. This value will, of course, be higher in the case of an asymmetric source. The maximum value indicated by the test data is 20 dB. For frequencies higher than f_c, the transmission loss decreases to a value somewhat below a final asymptotic value which is attained with a small jump at the second cut-on.

The first cut-on frequency is clearly the most crucial element here because the variation in the flat part of the transmission loss spectrum is fairly small from turbine to turbine. Figure 30(b) provides a convenient method of estimating this frequency given the mean turbine radius and static temperature. The inlet axial Mach number is assumed to be 0.3. The Mach number correction is actually $\sqrt{1 - M_x^2}$; higher Mach numbers result in lower cut-on frequencies.

In general, the transmission loss below the first cut-on is very low (5 dB or less). Therefore, a small turbine would offer little resistance to the transmission of peak combustor noise levels which, it is generally accepted, occur near 400 Hz for current engines. For example, the turboshaft engine turbine system used in the study (Table VIII) will induce only 3.2-dB transmission loss below 1350 Hz because of its size. The predicted transmission loss is shown in Figure 31. It is interesting to note that an engine (core noise) data correlation using combustor source noise parameters collapsed the available data along two lines as shown in Figure 32 (Reference 2). Comparison with the component data line suggests much lower overall transmission loss for the three turboshaft engines than the turbojet and turbofan engines. One of the obvious differences is the exhaust transmission loss due to the nozzle, and flow is much lower for turboshafts. The other difference is that all three of the turboshafts in Figure 32 were very small engines and would have turbine transmission loss spectra similar to that shown in Figure 31.

Table VIII suggests that 9 dB is a good value for the $f > 2f_c$ asymptotic part of the transmission loss spectrum. Keeping in mind that the frequency range of interest for combustor noise is normally below 2000 Hz, a constant value of 9 dB above $2f_c$ would result in less than ±1.5-dB error for the turbines in Table VIII which encompass a very wide range of variables.

The transmission loss below cut-on is defined by Figure 33. The loss actually decreases with pressure ratio and Mach number for multistage turbines. The reason for this, and the constant asymptotic value for $f > 2f_c$, lies in the influence of upstream blade rows on the reflected upstream-propagating

Table VIII. Transmission Loss for Different Turbine Systems.

Total Stages	Turbine P_R	1st Stg P_R	Turbine ΔT (K)	1st Row Inlet	Mach No. Exhaust	Cut-On Freq f_c (Hz)	Average Trans. Loss		
							Below c/o	315-500 Hz	Asymptotic -2000 Hz
1	3.1	3.1	128	0.217	0.775	369	4.8	7.0	6.8
1	2.56	2.56	62	0.520	1.022	229	0.5	6.5	6.6
2	3.62	2.06	447	0.227	0.884	182	4.8	8.4	8.7
3	5.16	2.17	135	0.519	0.977	186	1.9	7.3	8.0
3	4.66	1.78	343	0.212	0.777	310	5.2	9.3	10.1
3	12.7	5.07	640	0.130	1.239	364	3.4	6.5	8.8
4	16.81	2.33	666	0.113	0.828	1350	3.2	3.2	7.8
4	3.05	1.50	219	0.427	0.675	292	5.5	9.5	10.4
5	23.03	4.61	817	0.131	1.265	370	1.5	4.6	7.6
6	15.13	2.30	650	0.128	0.889	519	3.4	3.4	9.3
6	19.5	2.55	735	0.203	0.927	224	1.3	6.8	8.2
7	17.72	2.24	740	0.169	0.933	223	2.4	7.8	9.1
8	18.1	2.26	722	0.167	0.951	219	2.4	7.7	9.2

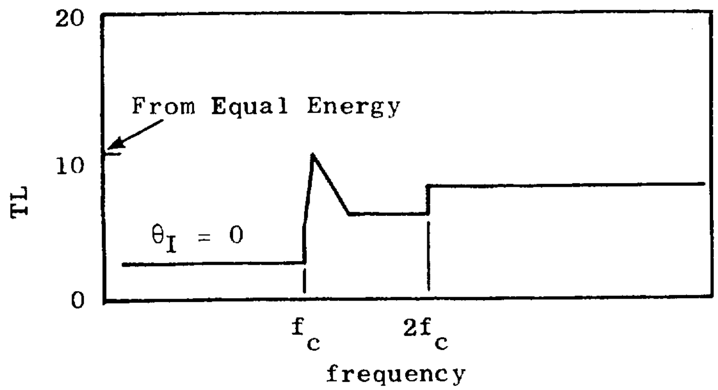

(a) Proposed Spectrum for Transmission Loss

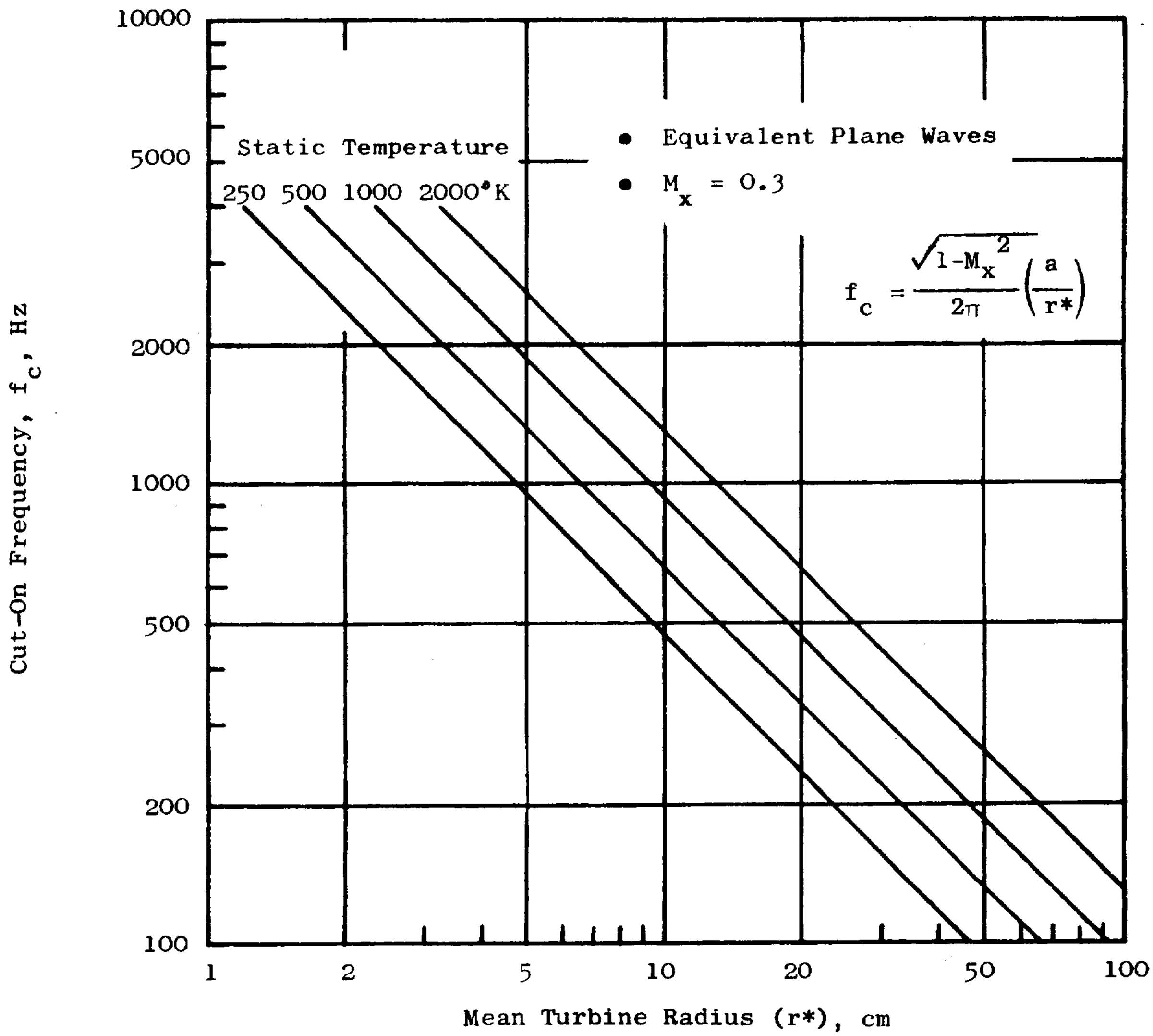

(b) Sample Chart for Computing First Cut-On Frequency

Figure 30. Approximate Prediction of Turbine Transmission Loss.

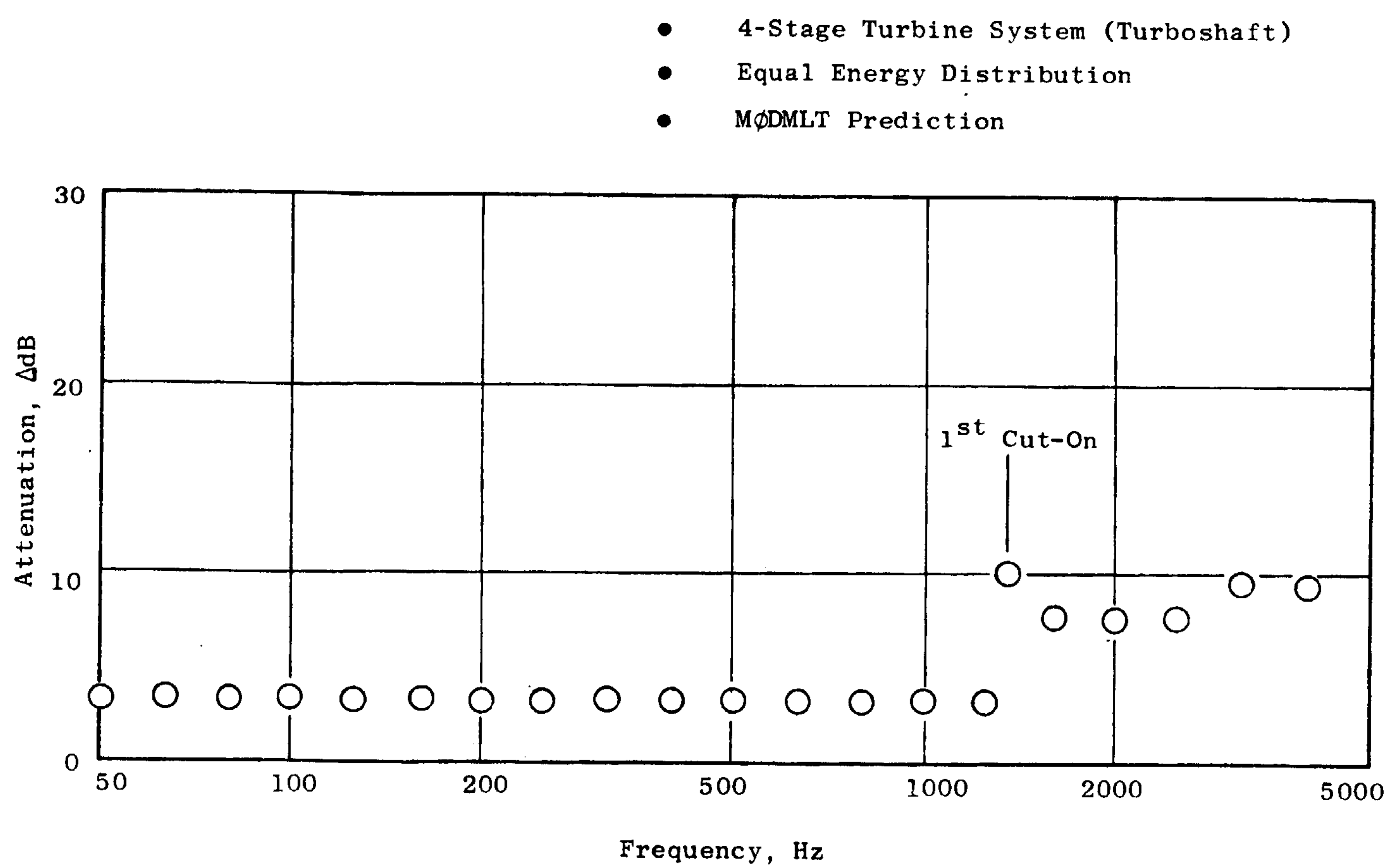

Figure 31. Transmission Loss Spectrum for a Turboshaft Engine Turbine.

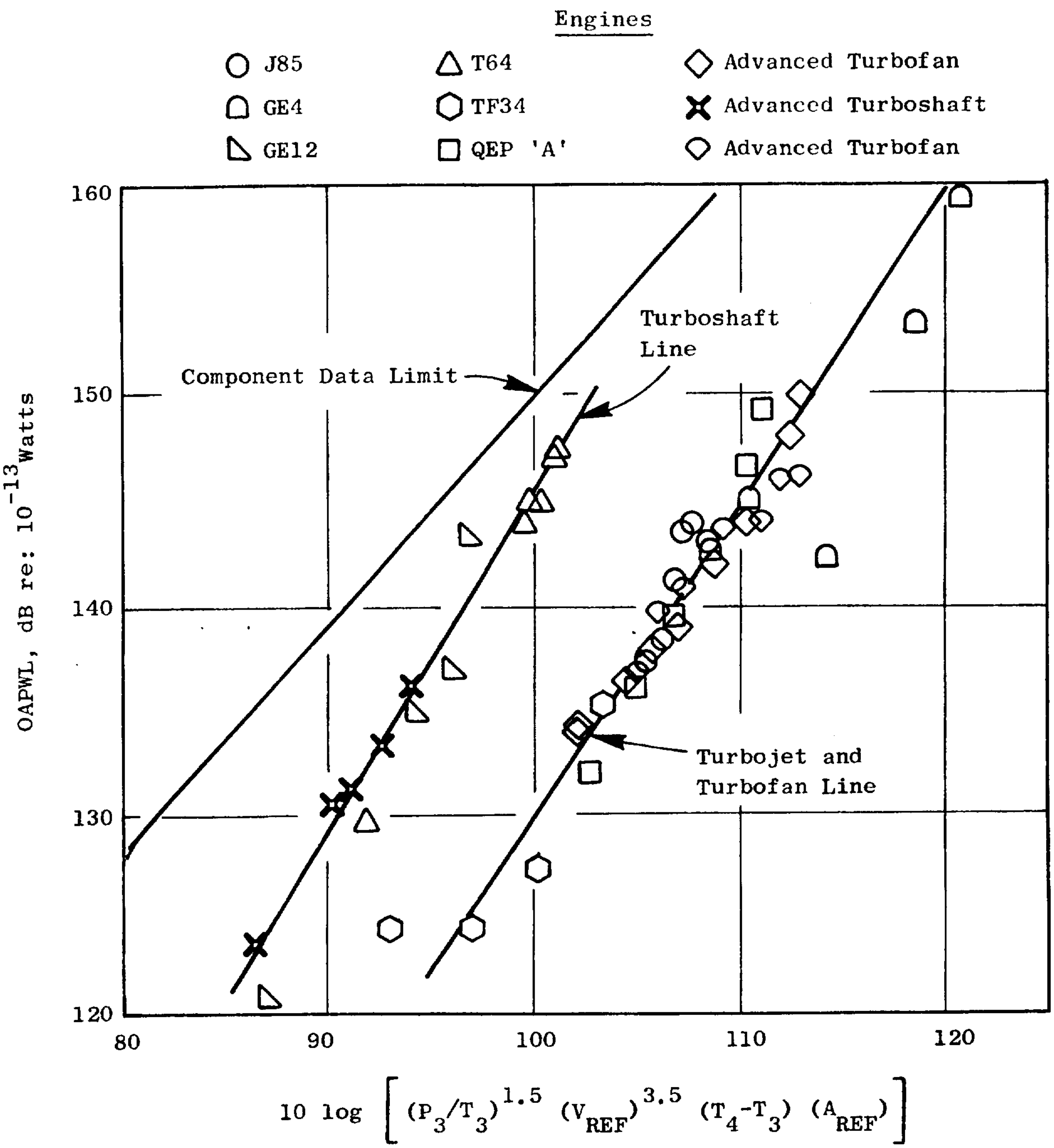

Figure 32. Engine Data Correlation Using Source Noise Parameters.

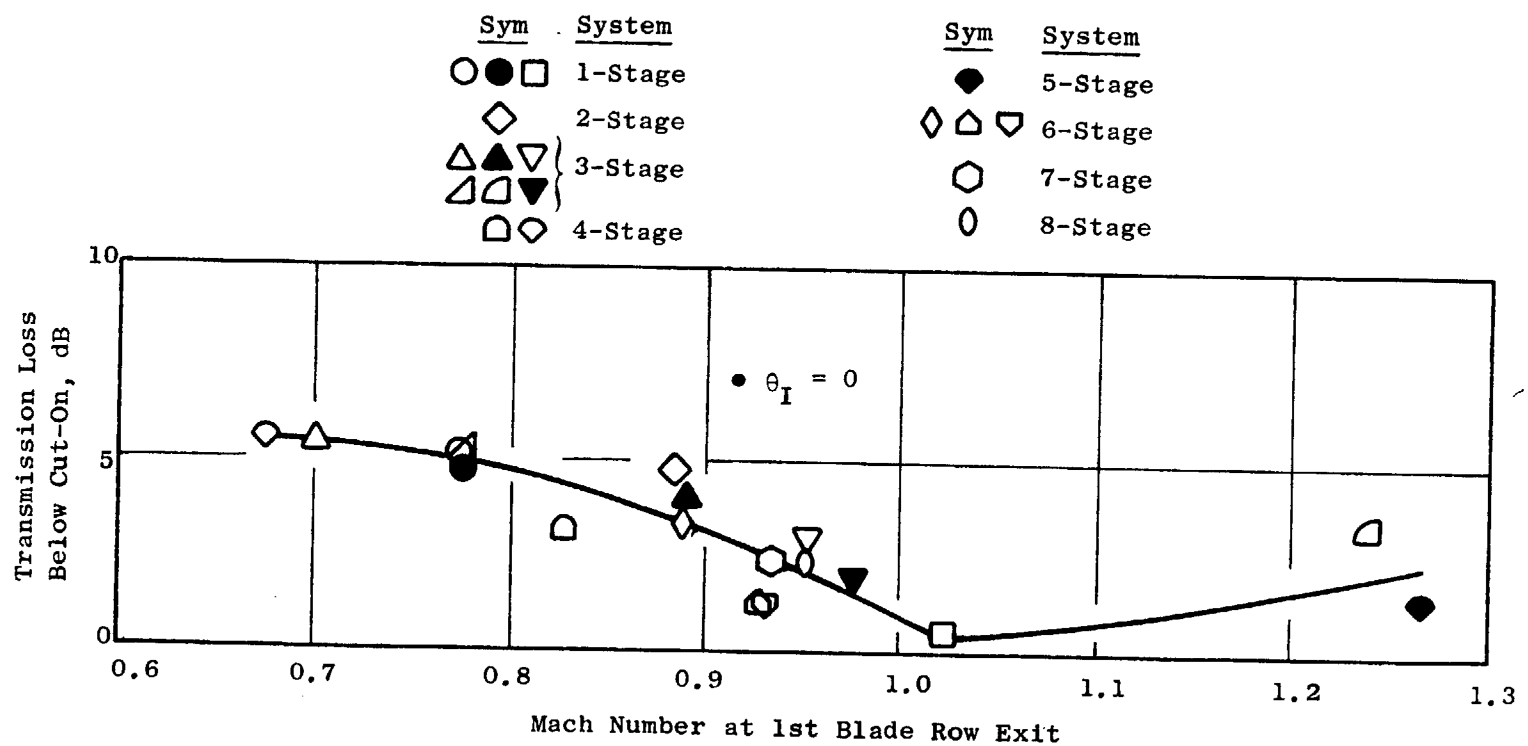

Figure 33. Correlation for Turbine Transmission Loss Below Cut-On.

waves from downstream rows. High pressure ratios cause almost complete reflection at upstream rows and almost total restoration of the upstream-propagating energy to the downstream direction. In fact, there can be no upstream transmission of acoustic energy through a choked blade row. On the other hand, blade rows operating with small pressure drops will permit two-way transmission of the acoustic energy. The net effect for turbines having two or more stages is increased transmission loss at low pressure ratios. Figure 25 is recommended for predicting single-stage turbine transmission loss.

Finally, the data suggest that the value between $f_c < f < 2f_c$ is approximately two-thirds of the difference between the asymptotic and axial plane-wave values. That is, if the asymptotic value of the transmission loss is 9 dB and that for $\theta_I = 0$ is 3 dB, the value between f_c and $2f_c$ should be taken to be 7 dB.

The above described approximate method of estimating turbine transmission loss is summarized below. The intent of the procedure is to generate a transmission loss characteristic such as the one shown in Figure (30a) for a specific turbine design.

Turbine Transfer Loss Approximation Procedure

1. Determine f_c from $f_c = \frac{\sqrt{1 - M_x^2}}{2\pi} \frac{a}{r^*}$

   where f_c = turbine cut-on frequency

   M_x = turbine inlet Mach number

   a = turbine inlet speed of sound based on inlet static temperature

   r^* = turbine mean radius

   (Note that Figure (30b) shows calculated values of f_c for $M_x = 0.3$).

   The value of TL (transmission loss) at f_c will be 10 dB or more, depending on source symmetry as discussed in the first paragraph of Section 5.3. The potential effects of a gooseneck transition between high and low pressure turbines should be considered here, as discussed in Section 5.2.

2. At frequencies above $f = 2f_c$, TL is 9 dB for a multistage turbine, and is determined from Figure 25 for a single stage turbine.

3. At frequencies below $f = f_c$, TL is determined from Figure 33 as a function of the exit Mach number from the first blade row.

4. The constant value of TL in the range above f_c and below $2f_c$ [referring to Figure (30a)] can be estimated to be 2/3 of the way between No. 2 and No. 3 values determined above.

5. A transmission loss spectrum similar to Figure (30a) can now be drawn for the specific turbine design being evaluated.

It is important to remember that this procedure yields only the turbine transmission loss. The transmission loss through the exhaust nozzle can also be an important consideration for gas turbine engines, particularly turbojets and turbofans. A fuller discussion of exhaust nozzle transmission loss can be found in Section 2.4 of Reference 2. Briefly, the loss can be modelled as a transmission loss, due to flow changes at the exhaust nozzle and through the jet(s), and a radiation loss, due to passage of the acoustic wave from a duct into open space. Classical analysis of the latter suggests that this part is negligible except for nozzles with characteristic dimensions very small compared to the acoustic wavelength. This is not usually the case except for very low frequencies. The transmission loss part postulates the same mechanism, specific impedance, and Mach number discontinuities as used in the turbine blade-row transmission modeling. A closed-form solution can be obtained for axial flow and $\theta_I = 0$ and is given in Reference 2. A chart is shown in Figure 34(a) for the total loss proceeding from inside the exhaust nozzle to ambient conditions. The computer prediction programs were used here to generate the convenient chart in Figure 34(b) for the transmission loss due to changes in the flow through the exhaust nozzle. The effect of higher order modes is included. This chart defines the exhaust nozzle transmission loss as a function of the temperature ratio across the nozzle.

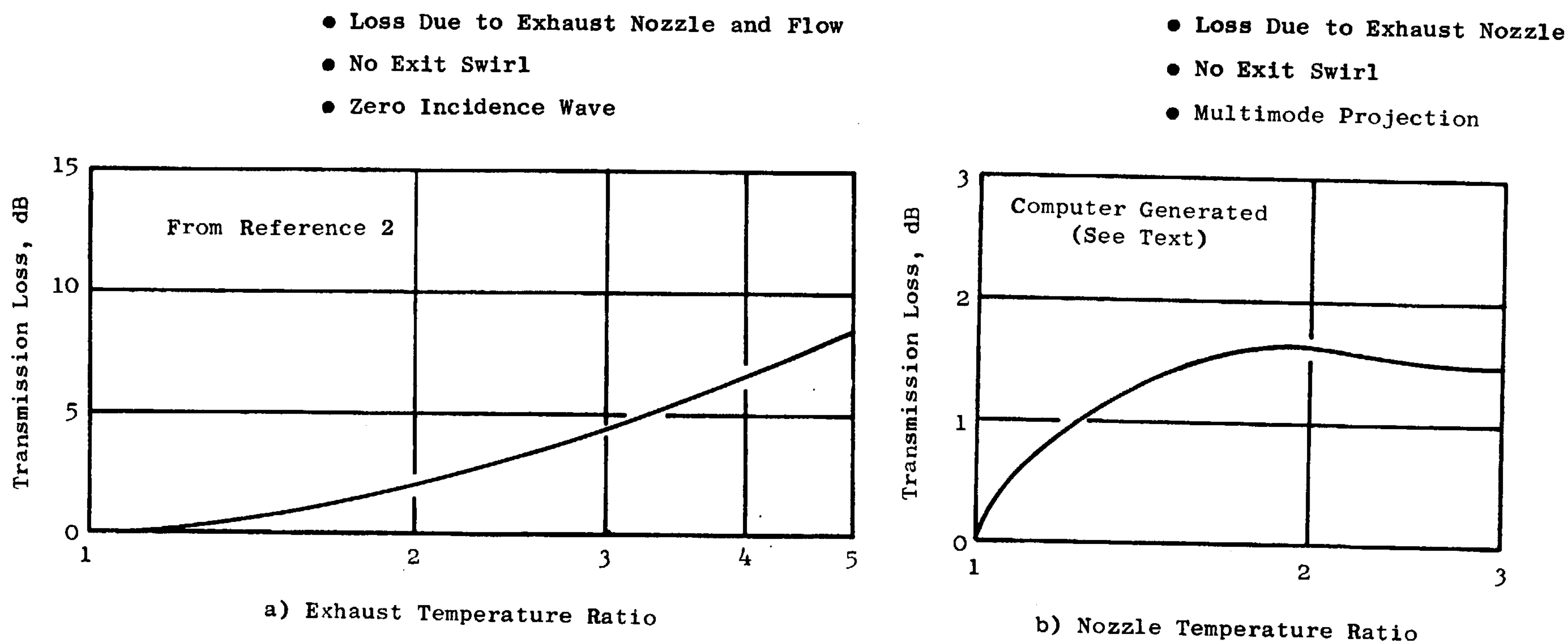

Figure 34. Transmission Loss Through Exhaust Nozzle and Flow.

6.0 CONCLUSIONS

Two theoretical models were presented to describe the transmission of low frequency noise through aircraft engine turbines. The somewhat complex, finite-chord analysis indicated that the simpler actuator-disk analysis was valid for frequencies as high as 0.4 to 0.5 of the blade passing frequency. In essence, it meant that the simpler model was adequate over the entire frequency range of interest for combustor noise. It was shown that multiple blade row and spinning mode considerations also had to be introduced into the analysis in order to fully explain the transmission through the blade rows. Interaction of acoustic waves with turbine blade passage shocks was found to be a very weak, second-order effect.

The improved theory demonstrated that turbine transmission loss spectrum, in the midfrequency range (200-1200 Hz) was indeed flat as postulated by the floor of the bathtub spectral fit to the data of NAS3-19435. The scatter in the data about this floor was found to be due to higher order mode cut-ons and a biased energy assignment because of the assymmetric sound injection. Also, the flat transmission loss apparently extended to 2000-2500 Hz. Diffraction by the turbine blades was probably responsible for increasing the transmission loss at higher frequencies, giving one end of the bathtub spectrum. The other end of the bathtub, the rise at very low frequencies, was shown to be a spurious effect introduced by the location of the downstream sensors at a pressure cancellation point.

The theory suggested a step function type of transmission loss spectrum, with the jump occurring at the first modal cut-on frequency. The attenuation below this frequency was predicted to be constant (with frequency) as would correspond to the transmission loss associated with the axial plane wave alone. This value would vary from about 5 dB to 1 dB, decreasing with pressure ratio for multistage turbines. The transmission loss (prediction) for frequencies greater than the cut-off frequency was found to vary between (9 ± 1.5) dB, independent of the number of stages or turbine pressure ratio.

The first cut-on frequency, which is inversely proportional to size, appeared to be a critical element in the transmission loss since combustor noise generally peaks in the vicinity of 400 Hz. In particular, small turboshaft engine turbines would suffer since the step jump to the 9-dB asymptotic value is delayed to beyond 1000 Hz. Turbojets and turbofans should exhibit higher transmission losses, not only due to earlier cut-on, but also because of higher losses at the exhaust nozzle induced by accelerating flow.

The exhaust nozzle and turbine transmission losses were computed separately and independently. It should be a fairly straightforward matter to link the two wave systems with due consideration being given to the phase change between turbine exhaust and core nozzle exit.

The analysis performed in this contract has provided two of the four modules required for the modular prediction of combustor noise. The work proceeding under another NASA Lewis Contract, NAS3-19736, wherein combustor noise is being measured at the source and various locations in a CF6-50 engine, should further the activity.

PRECEDING PAGE BLANK NOT FILMED

APPENDIX A

MATRIX INVERSION COMPUTER PROGRAM

The transmission loss for an unchoked turbine can be determined exactly using the matrix inversion procedure outlined in Section 3.3. The method has been programmed for time-share usage and a FORTRAN listing is provided in Figure 35.

A flow chart for the computer program is given in Figure 36. The program reads the input parameters and then, for each of the one-third octave band center frequencies from 50 to 4000 Hz, calculates the cut-on modes (the axial plane wave is always cut-on). Equal energy is assigned to each mode. An equivalent plane wave (see Equation 62, and text, page 39) is defined for spinning mode along with a corresponding incidence angle.

The angles for the forward- and backward-travelling waves are calculated at each blade row and, if total reflection occurs or if there is no forward propagation, the transmission loss for that mode is set to 20 dB. Otherwise, the (A) and (D) matrices are formed, (D) inverted, and ($D^{-1}A$) computed. The transfer coefficient matrix is obtained by multiplying the matrix product for all the blade rows and the transmitted wave amplitude T extracted. The transmission loss for that mode is then found. When this computation has been effected for all the modes at any frequency, the transmitted waves are weighted according to the energy distribution and summed to define the transmission loss at that frequency.

The frequency and energy distribution can be redefined as required by the user. The working frequencies are listed in lines 310 through 330 and the energy assignment imposed in line 1570. For example, if frequency inverse energy distribution is desired, line 1570 is changed to: 1570 E(J1) = 1./SQRT (1. - (FRSQ**2)), where FRSQ is the ratio of the cut-on frequency to the working frequency.

The turbine tip radius and hub/tip ratio are input in line 300. Normally, the values at the high pressure turbine inlet are used. However, the values at intermediate stations, such as the low pressure turbine inlet, may be more advisable in case of large variations in tip dimensions.

An input sheet is shown in Figure 37. The performance data are stored in a data file and the name of this file inserted when requested by the program. A typical output is given in Figure 38. The print-out includes the input parameters, the cut-on frequency, and the transmission loss for each frequency. The number of cut-on modes at each frequency is also shown, and the angles for the incident, reflected, and transmitted acoustic waves; the amplitudes of the transmitted and first reflected waves, the energy fraction, and the transmission loss are provided for each mode.

********** MODMLT **********

```
*#RUNH *;
*#LIBRARY/MTINV,R=(ULIB)USERLIB/TDS,R
C     ***** FILENAME MODMLT *****
      COMMON /CANGP / PI,TODEG,TORAD
      COMMON /CINPUT/ NSTAGE,IOPT,IPRINT,PTO,TTO,STAGEX(5,21),
&                          NSTA,TITLE
      CHARACTER TITLE*40
      COMMON /CUTOFA/ THCL,THCH
      COMMON /CAERO / V(21),MX(21),MY(21),AMOAN(21),RHORAT(21),
&                    MACH(21),AS(21)
      REAL  KNQKM(21),MX,MY,MACH
      INTEGER FREQ(20)
      EQUIVALENCE  (KNQKM,AMOAN)
      COMMON /CAEROI/ U(21),PHI(21),VR(21),P(21),T(21),GAM(21)
      COMMON /COUT  / TLOSS(100),THI(100),THR(100),THT(100),
&                        Q(100),B(100),TW(100)
      COMMON /CMATRX/ D(3,3,21),DI(3,3,21),A(3,3,21),PROD(3,3)
      COMMON /CATTCH/ CF1,CF2,CF3,BUF(380)

      DIMENSION  STAGEP(105)
      DIMENSION  E(100)
      EQUIVALENCE (STAGEP(1),STAGEX(1,1))
      CHARACTER CF1*1/"/"/,CF2*8,CF3*1/";"/
      CHARACTER TITLE*40,BLANK*40
      REAL  MACHN,MACHM,KMYKM,KNYKN,KMXKM,KNXKN,KMYSAV,KMXSAV,
&           KNN,KMM
      EQUIVALENCE (IBITS,BITS)

      DATA BITS/037777777777/,OKA/040370000000/,JPO/0040075040007/
      DATA R0,SIGMA/16.8,0.889/
      DATA FREQ/50,63,80,100,125,160,200,
&                250,315,400,500,630,800,1000,
&                1250,1600,2000,2500,3150,4000/
      DATA PI,TODEG,TORAD/3.1415927,57.29578,.01745329253/
      DATA BLANK/"                                        "/

      NAMELIST /TNOISE/ IOPT,PTO,TTO,STAGEP,TITLE,GAM,IAERO
      TAN(X)= SIN(X)/COS(X)

C     SET UP NAMELIST INPUT FILE

      IAERO = 0
      CALL FPARAM(3,JPO)
      PRINT," INPUT FILE NAME "
      READ,CF2
      CALL ATTACH(1,CF1,1,0,STAT,BUF)
      IF( STAT.EQ.0. .OR. STAT.EQ.OKA ) GO TO 5
```

Figure 35. Program Listing - Matrix Inversion Program.

```
      PRINT 1,STAT
    1 FORMAT(" INPUT FILE STATUS=",O12)
      STOP

C     INITIALIZATION ******************

    5 IOPT   = 1
      DO 10 I=1,21
      STAGEX(1,I)= BITS
      GAM(I)= BITS
   10 CONTINUE
      PTO    = 14.696
      TTO    = 518.7
      TITLE = BLANK

C     READ INPUT FILE **** COUNT NP. OF STATIONS

   15 CALL READNA(1,TNOISE,"$TNOISE",JEND)
      IF( JEND.EQ.0 ) GO TO 400
      DO 17 I=1,21
      IF(STAGEX(1,I).EQ.BITS ) GO TO 18
      U(I)    = STAGEX(1,I) * 3.048
      PHI(I) = STAGEX(2,I)
      VR(I)   = STAGEX(3,I) * 3.048
      P(I)    = STAGEX(4,I) / 6.895
      T(I)    = STAGEX(5,I) * 1.8
      IF( GAM(I).NE.BITS ) GO TO 17
      GAM(I)= GAMX(T(I))
   17 CONTINUE
   18 NSTA   = I-1
      IF( NSTA.EQ.20 ) NSTA = 21
      NSTAGE= (NSTA-1)/2
      PRINT 21,TITLE,NSTAGE
   21 FORMAT(//16X,A40//32X,I2,"  STAGES"//)
      PRINT 22
   22 FORMAT(28X,"* AERO-THERMO PARAMETERS *"//
&      2X,"STAGE",3X,"STATION",3X,"U- FPS",3X,"PHI- DEG",
&      3X,"VR- FPS",2X,"PS- PSIA",2X,"TS- DEG R"/)
       NSTG   = 0
      DO 24 I=1,NSTA
      IF(((I/2)*2)/I.EQ.0 ) NSTG=NSTG+1
      IF( I.EQ.NSTA ) NSTG=IBITS
      PRINT 23,NSTG,I,U(I),PHI(I),VR(I),P(I),T(I)
   23 FORMAT(4X,I1,7X,I2,F12.3,4F10.3)
   24 CONTINUE
      IF( IAERO.EQ.0. ) GO TO 27
      PRINT 25
   25 FORMAT(/2X,"STAGE",3X,"STATION",5X,"MX",8X,"MY",
&              7X,"MACH",5X,"KNQKM",7X,"V"/)
      NSTG   = 0
      DO 26 I=1,NSTA
```

Figure 35. Program Listing - Matrix Inversion Program (Continued).

```
      IF(((I/2)*2)/I.EQ.0 ) NSTG=NSTG+1
      IF( I.EQ.1 ) GO TO 26
      PRINT 23,NSTG,I,MX(I),MY(I),MACH(I),KNQKM(I),V(I)
   26 CONTINUE
   27 CONTINUE
   28 FORMAT(//2X,'THETA-I',3X,'THETA-R',3X,'THETA-T',6X,
     &        'T',9X,'B',9X,'E',6X,'T-LOSS'//)

C     CALCULATE AERO-THERMO PARAMETERS

      DO 29 I=1,NSTA
      AS(I) = 41.42*SQRT(GAM(I)*T(I))
      MX(I) = U(I)/AS(I)
      IF( I.EQ.1 ) GO TO 29
      AMQAN(I)= SQRT(GAM(I)*T(I)/(GAM(I-1)*T(I-1)))
      RHORAT(I)= T(I)*P(I-1)/(T(I-1)*P(I))
   29 CONTINUE

      AS1 = AS(1)
      RMEAN= RO*SQRT((1.+SIGMA**2)/2.)
      RMEAN = RMEAN/2.54
      FP1 = 1.
      FREQCO= ((FP1*(AS1*12.))/(2.*PI*RMEAN))*SQRT(1.-XM1**2)
      FREQC1= AINT(FREQCO)
      PRINT 30,FREQC1
      PRINT 28
   30 FORMAT(//10X,'***** FIRST CUT-ON OCCURS AT',1X,F5.0,
     &        1X,'HZ *****'///)
      DO 300 L=1,20
      FP = (2.*PI*FREQ(L)*RMEAN)/(AS1*12.)
      XM1 = MX(1)
       NTH=FP/SQRT(1.-XM1**2)
      IF( NTH.GT.50 ) NTH=50
      NTT = 2*NTH+1
      FRSQ= 0.
      THI(1)= 0.
      DO 32 J=1,NTT
      E(J)= 0.
   32 CONTINUE
      E(1)= 1.
      ESIGMA= 1.
      THI(1)= 0.
      IF( NTH.LT.1 ) GO TO 50
C    **** COMPUTE CUT-ON MODES, ANGLES, AND ENERGY
      DO 40 J=1,NTH
      FJ = J
      F1=FP/FJ
      F2 = SQRT(F1**4-F1**2*(1.-XM1**2))
      F3 = XM1**2+F1**2
      F4 = (F2-XM1)/F3
      J1 = 2*J
```

Figure 35. Program Listing - Matrix Inversion Program (Continued).

ORIGINAL PAGE IS
OF POOR QUALITY

```
      J2 = 2*J+1
      THI(1)= 0.
      THI(J1)= TODEG*ARCOS(F4)
      THI(J2)= -THI(J1)
      FC = (FJ*AS1*12.)/(2.*PI*RMEAN)
      FC = FC*SQRT(1.-XM1**2)
      FRSQ = FC/FREQ(L)
      IF( FRSQ.GT.1.025 ) GO TO 40
      E(J1) = 1.
      E(J2)= E(J1)
      ESIGMA= ESIGMA+2.*E(J1)
   40 CONTINUE
   50 CONTINUE

C     **** COMPUTE ENERGY DISTRIBUTION
      DO 60 K=1,J2
      E(K)= E(K)/ESIGMA
   60 CONTINUE


C     ****** INNER LOOP TO BUILD MATRICES *****

      SUMT= 0.
      DO 185 K=1,NTT
   62 THFN    = THI(K)*TORAD
      KMYSAV= 0.
      KMXSAV= 0.
      M       = 1
   65 M       = M+1
      IF( M.GT.NSTA ) GO TO 100

C     CALCULATE ANGLES AND RATIOS

      N       = M-1
      V(N)    = U(N)*TAN(TORAD*PHI(N))-VR(N)
      V(M)    = U(M)*TAN(TORAD*PHI(M))-VR(N)
      MY(N) = V(N)/AS(N)
      MY(M) = V(M)/AS(M)
      MACH(N)= SQRT(MX(N)**2+MY(N)**2)
      MACH(M)= SQRT(MX(M)**2+MY(M)**2)
      N       = M-1
      GA  = GAM(I)
      GB  = (GA+1.)/(2.*(GA-1.))
      AASTAR  = ((2.+(GA-1.)*MACH(M)**2)/(GA+1.))**GB/MACH(M)
      XMN     = 1.-MX(N)**2
      XPN     = 1.+MX(N)**2
      XMM     = 1.-MX(M)**2
      SINN    = SIN(THFN)
      COSN    = COS(THFN)
C     **** CHECK FOR UPSTREAM PROPAGATION

```

Figure 35. Program Listing - Matrix Inversion Program (Continued).

```
      PHSPD= U(N)+AS(N)*COSN
      IF( PHSPD.LE.0.  ) GO TO 175
      GMN    = KNQKM(M)*SINN/(1.+MX(N)*COSN+MY(N)*SINN)
      TN     = XMN*SINN
      TD     = XPN*COSN+2.*MX(N)
      THBN   = ATAN2( TN,TD )
      TERM   = -GMN*MX(M)*(1.-GMN*MY(M))
C    **** CHECK FOR TOTAL REFLECTION

      RDCL= (1.-GMN*MY(M))**2-XMM*GMN**2
      IF( RDCL.LE.0.  ) GO TO 175
      RADICL= GMN*SQRT(RDCL)
      TN = -TERM+RADICL
      TD     = (1.-GMN*MY(M))**2-GMN**2
      THFM   = ATAN2( TN,TD )
      IF( N.NE.1 ) GO TO 70
      THR(K)= TODEG*THBN
   70 THBM   = ATAN2( TN-2.*TERM , TD )
      MACHM  = MACH(M)
      MACHN  = MACH(N)
      ALFAN  = ATAN2( MY(N),MX(N)  )
      BETAM  = ATAN2( MY(M)  , MX(M)  )
      IF( MACH(M).LT.1.  ) GO TO 71
      DOT    = COS(BETAM)
      BM     = BETAM
      BETAM  = ARCOS(AASTAR*DOT)
      BETAM  = SIGN(1,BM)*BETAM
   71 CONTINUE
      KMYKM  = GMN
      KNYKN  = KMYSAV
      KMXKM  = (1.-GMN*MY(M))/MX(M)
      KNXKN  = KMXSAV
      KMYSAV= KMYKM
      KMXSAV= KMXKM
      QKNN   = 0.
      IF( N.EQ.1 ) GO TO 75
      QKNN    = 1./SQRT(KNXKN**2+KNYKN**2)
   75 QKMM   = 1./SQRT(KMXKM**2+KMYKM**2)
      A(1,1,N)= MX(N)+COS(THFN)
      A(1,2,N)= MX(N)-COS(THBN)
      A(1,3,N)= KNYKN*QKNN
      A(2,1,N)= 1.+MACHN*COS(ALFAN-THFN)
      A(2,2,N)= 1.-MACHN*COS(ALFAN+THBN)
      A(2,3,N)= QKNN*(MX(N)*KNYKN-MY(N)*KNXKN)
      D(1,1,N)= (MX(M)+COS(THFM))/AMQAN(M)
      D(1,2,N)= (MX(M)-COS(THBM))/AMQAN(M)
      D(1,3,N)= KMYKM*QKMM/AMQAN(M)
      D(2,1,N)= RHORAT(M)*(1.+MACHM*COS(BETAM-THFM))
      D(2,2,N)= RHORAT( )*(1.-MACHM*COS(BETAM+THBM))
      D(2,3,N)= RHORAT(M)*(QKMM*(MX(M)*KMYKM-MY(M)*KMXKM))
      A(3,1,N)= 0.
```

Figure 35. Program Listing - Matrix Inversion Program (Continued).

```
      A(3,2,N)= 0.
      A(3,3,N)= 0.
      D(3,1,N)= SIN(BETAM-THFM)
      D(3,2,N)= -SIN(BETAM+THBM)
      D(3,3,N)= QKMM*(KMYKM*SIN(BETAM)+KMXKM*COS(BETAM))
      GO TO 80
   78 FORMAT(5X,'***DOWNSTREAM RELATIVE FLOW AT ROW',I3,
&              1X,'IS SUPERSONIC***'///)
C    ***** COMPUTE INVERSE OF MATRIX AND STORE

   80 CALL DINVER( N )
      THFN   = THFM
      GO TO 65

C    ***** COMPUTE MATRIX PRODUCT

  100 CALL MAPROD( NSTA-1 )

C    ***** STORE AMPLITUDES

  110 THT(K)= THFM*TODEG
      B(K)   = -PROD(2,1)/PROD(2,2)
      TW(K)  = PROD(1,1)+B(K)*PROD(1,2)
      Q(K)  = PROD(3,1)+B(K)*PROD(3,2)

C    ***** COMPUTE TRANSMISSION LOSS

  120 AS1     = AS(1)
      ASN     = AS(NSTA)
      MX(1)  = U(1)/AS1
      MX(NSTA)= U(NSTA)/ASN
      VV1     = U(1)*TAN(TORAD*PHI(1))
      VVN     = U(NSTA)*TAN(TORAD*PHI(NSTA))
      MY(1)  = VV1/AS1
      MY(NSTA)= VVN/ASN
      RHORA  = P(NSTA)*T(1)*ASN/(P(1)*T(NSTA)*AS1)
      TERM2  = (1.+MX(NSTA)*COS(THFM)+
&      (MY(NSTA)+VR(NSTA-1)/ASN)*SIN(THFM))*(COS(THFM)+MX(NSTA))
      THIN    = THI(K)*TORAD
      TERM1  = (1.+MX(1)*COS(THIN)+MY(1)*
&                            SIN(THIN))*(COS(THIN)+MX(1))
      TLOSS(K)= 10.*ALOG10(RHORA*ABS(TERM1/TERM2)/TW(K)**2)
      IF( TW(K).LT.0. ) GO TO 176
      IF( TW(K).GE.1.) GO TO 176
      GO TO 180
  175 TLOSS(K)= 20.
      GO TO 177
  176 TLOSS(K) = 25.
  177 B(K) = 1.
      TW(K)= 0.
  180 CONTINUE
```

Figure 35. Program Listing - Matrix Inversion Program (Continued).

```
      IF( TLOSS(K).LT.0. ) TLOSS(K) = 1.
      SUMI= 1.
      TL = TLOSS(K)/10.
      SUMT= SUMT+E(K)/10.**TL
  185 CONTINUE
      TLSIGMA=10.*ALOG10(SUMI/SUMT)
C    ***** PRINT OUTPUT

  200 KT   =   K
      DO 240 I=1,KT
      PRINT 235,THI(I),THR(I),THT(I),TW(I),B(I),E(I),TLOSS(I)
  235 FORMAT(F9.3,2F10.3,F9.4,3F10.4)
  240 CONTINUE
      PRINT 245,FREQ(L),TLSIGMA
  245 FORMAT(/14X,'FREQUENCY=',I4,1X,'HZ',5X,
&              'TRANSMISSION LOSS=',F6.2////)
  300 CONTINUE

      IF( JEND.NE.-1 ) GO TO 15

  400 STOP
      END
CGAMX           FUNCTION GAMX(T)
      FUNCTION GAMX(T)
      IF( T.LE.800. ) GO TO 10
      IF( T.GE.3600. ) GO TO 12
      GAMX  = 2.23708/T**.070271
      GO TO 15
   10 GAMX  = 1.4
      GO TO 15
   12 GAMX  = 1.254
   15 RETURN
      END

CDINVER           CALCULATE INVERSE OF MATRIX D
      SUBROUTINE  DINVER( N )
      COMMON /CMATRX/ D(3,3,21),DI(3,3,21),A(3,3,21),PROD(3,3)
      DIMENSION DD(9,21),DDI(9,21),LABEL(3)
      EQUIVALENCE (DD(1,1),D(1,1,1)),(DDI(1,1),DI(1,1,1))
      DIMENSION  PPROD(9),TEMP(3,3),TEMP1(3,3),TEMP2(9)
      EQUIVALENCE  (PPROD(1),PROD(1,1)),(TEMP2(1),TEMP1(1,1))

      NN    = N
      DO 10 I=1,9
      DDI(I,N)= DD(I,N)
   10 CONTINUE
      CALL MTINV(DDI(1,N),3,3,3,LABEL)
   20 RETURN

C    **** ENTRY  MAPROD ** COMPUTE PRODUCT OF DI AND A

```

Figure 35. Program Listing - Matrix Inversion Program (Continued).

```
      ENTRY   MAPROD( N )
      NN     = N
      DO 30 I=1,3
      DO 30 J=1,3
      PROD(I,J)= 0.
      IF( I.EQ.J ) PROD(I,J)=1.
   30 CONTINUE

      DO 100 L=1,NN
      DO 60 J=1,3
      DO 50 I=1,3
      TEMP(I,J)= 0.
      DO 40 K=1,3
      TEMP(I,J)= TEMP(I,J)+DI(I,K,L)*A(K,J,L)
   40 CONTINUE
   50 CONTINUE
   60 CONTINUE

      DO 90 J=1,3
      DO 80 I=1,3
      TEMP1(I,J)= 0.
      DO 70 K=1,3
      TEMP1(I,J)= TEMP1(I,J)+TEMP(I,K)*PROD(K,J)
   70 CONTINUE
   80 CONTINUE
   90 CONTINUE

      DO 95 I=1,9
      PPROD(I)= TEMP2(I)
   95 CONTINUE
  100 CONTINUE
  200 RETURN
      END

CCUTOFF          DETERMIN LOWER/UPPER CUTOFF LIMITS
      SUBROUTINE  CUTOFF
      COMMON /CANGP / PI,TODEG,TORAD
      COMMON /CUTOFA/ THCL,THCU
      COMMON /CAERO / V(21),MX(21),MY(21),AMQAN(21),
&                RHORAT(21),MACH(21),AS(21)
      REAL  MX,MY,MACH,KNQKM(21)
      EQUIVALENCE  (KNQKM,AMQAN)
      COMMON /CINPUT/ NSTAGE,IOPT,IPRINT,PTO,TTO,
&                          STAGEX(5,15),NSTA
      COMMON /CAERO1/ U(21),PHI(21),VR(21),PSI(21),T(21),GAM(21)
      DIMENSION THC1(45),THC2(21),THC3(21),ANGFA(2)
      EQUIVALENCE  (THC2,THC1(22)),(THC3,THC1(43))
      DATA BITS/O37777777777/

      TAN(X)= SIN(X)/COS(X)

```


Figure 35. Program Listing - Matrix Inversion Program (Continued).

```
C     ***** CALCULATE THE 3  CUTFF INCIDENCE ANGLES

      DO 5 I=1,45
      THC1(I)= BITS
    5 CONTINUE
      DO 100 I=1,NSTA
      II     = I+1
      THC1(I)= 90.+TODEG*ARSIN(MX(I))
      THC2(I)= -THC1(I)
      IF( I.EQ.NSTA ) GO TO 100
      VV1    = U(I)*TAN(TORAD*PHI(I))-VR(I)
      VV2    = U(II)*TAN(TORAD*PHI(II) )-VR(I)
      MY(I) = VV1/AS(I)
      MY(II)= VV2/AS(II)
      MACH(I)= SQRT(MX(I)**2+MY(I)**2)
      MACH(II)= SQRT(MX(II)**2+MY(II)**2)
      TERM   = SQRT(1.-MX(II)**2)
      ANGFM(1)= ATAN2( TERM,-MX(II))
      ANGFM(2)= ATAN2(-TERM,-MX(II) )
      KGO    = 1
   10 ANG    = ANGFM(KGO)
      GNM    = SIN(ANG)/(KNQKM(II)*(1.+MX(II)*COS(ANG)+
     &          MY(II)*SIN(ANG)))
      X      = (1.-GNM*MY(I))**2-(1.-MX(I)**2)*GNM**2
      IF( X.GE.0. ) GO TO 20
      IF( KGO.EQ.2 ) GO TO 100
      KGO    = 2
      GO TO 10
   20 XNU    = GNM*MX(I)*(1.-GNM*MY(I))+GNM*SQRT(X)
      XDEN   = (1.-GNM*MY(I))**2-GNM**2
      THC3(I)= TODEG*ATAN2( XNU,XDEN )
  100 CONTINUE

C    ***FIND LARGEST - ANGLE AND SMALLEST + ANGLE

      THCL   = -500.
      DO 110 I=1,44
      IF( THC1(I).EQ.BITS .OR. THC1(I).GT.0. ) GO TO 110
      THCL   = AMAX1( THCL,THC1(I) )
  110 CONTINUE
      THCU   = 500.
      DO 115 I=1,44
      IF( THC1(I).EQ.BITS .OR. THC1(I).LE.0. ) GO TO 115
      THCU   = AMIN1( THCU,THC1(I) )
  115 CONTINUE

  120 RETURN
      END
      SUBROUTINE VNA1
      RETURN
      END
```

Figure 35. Program Listing - Matrix Inversion Program (Continued).

******* FILENAME MTINV *******

```
10C    MTINV
30*          *************MATRIX INVERSION************************
40 SUBROUTINE MTINV(A,NRARG,NCARG, IDIM,LABEL)
50 DIMENSION A(IDIM,NCARG),LABEL(NRARG)
60 1 NR=NRARG
70 NC=NCARG
80 DO 21 J1=1,NR
90 21 LABEL(J1)=J1
100 DO 291 J1=1,NR
110*          **************FIND REMAINING ROW CONTAINING LARGEST***
120*          **************ABSOLUTE VALUE IN PIVOTAL COLUMN********
130 101 TEMP=0.0
140 DO 121 J2=J1,NR
150 IF(ABS(A(J2,J1)).LT.TEMP) GO TO 121
160 TEMP=ABS(A(J2,J1))
170 IBIG=J2
180 121 CONTINUE
190 IF(IBIG.EQ.J1)GO TO 201
200*          **************REARRANGE ROWS TO PLACE LARGEST ABSOLUTE
210*          **************VALUE IN PIVOT POSITION*****************
220 DO 141 J2=1,NC
230 TEMP=A(J1,J2)
240 A(J1,J2)=A(IBIG,J2)
250 141 A(IBIG,J2)=TEMP
260 I=LABEL(J1)
270 LABEL(J1)=LABEL(IBIG)
280 LABEL(IBIG)=I
290*        ::::COMPUTE COEFFICIENTS IN PIVOTAL ROW::::
300 201 TEMP=A(J1,J1)
310 A(J1,J1)=1.0
320 DO 221 J2=1,NC
330 221 A(J1,J2)=A(J1,J2)/TEMP
340*          **************COMPUTE COEFFICIENTS IN OTHER ROWS******
350 DO 281 J2=1,NR
360 IF(J2.EQ.J1) GO TO 281
370 TEMP=A(J2,J1)
380 A(J2,J1)=0.0
390 DO 241 J3=1,NC
400 241 A(J2,J3)=A(J2,J3)-TEMP*A(J1,J3)
410 281 CONTINUE
420 291 CONTINUE
430*          **************INTERCHANGE COLUMNS ACCORDING TO********
440*          **************INTERCHANGES OF ROWS OF ORIGINAL MATRIX*
450 301 N1=NR-1
460 DO 391 J1=1,N1
470 DO 321 J2=J1,NR
480 IF(LABEL(J2).NE.J1) GO TO 321
```

Figure 35. Program Listing - Matrix Inversion Program (Continued).

```
IF(J2.EQ.J1) GO TO 391
GO TO 341
321 CONTINUE
341 DO 361 J3=1,NR
TEMP=A(J3,J1)
A(J3,J1)=A(J3,J2)
361 A(J3,J2)=TEMP
LABEL(J2)=LABEL(J1)
391 CONTINUE
5001 RETURN
END
```

Figure 35. Program Listing - Matrix Inversion Program (Concluded).

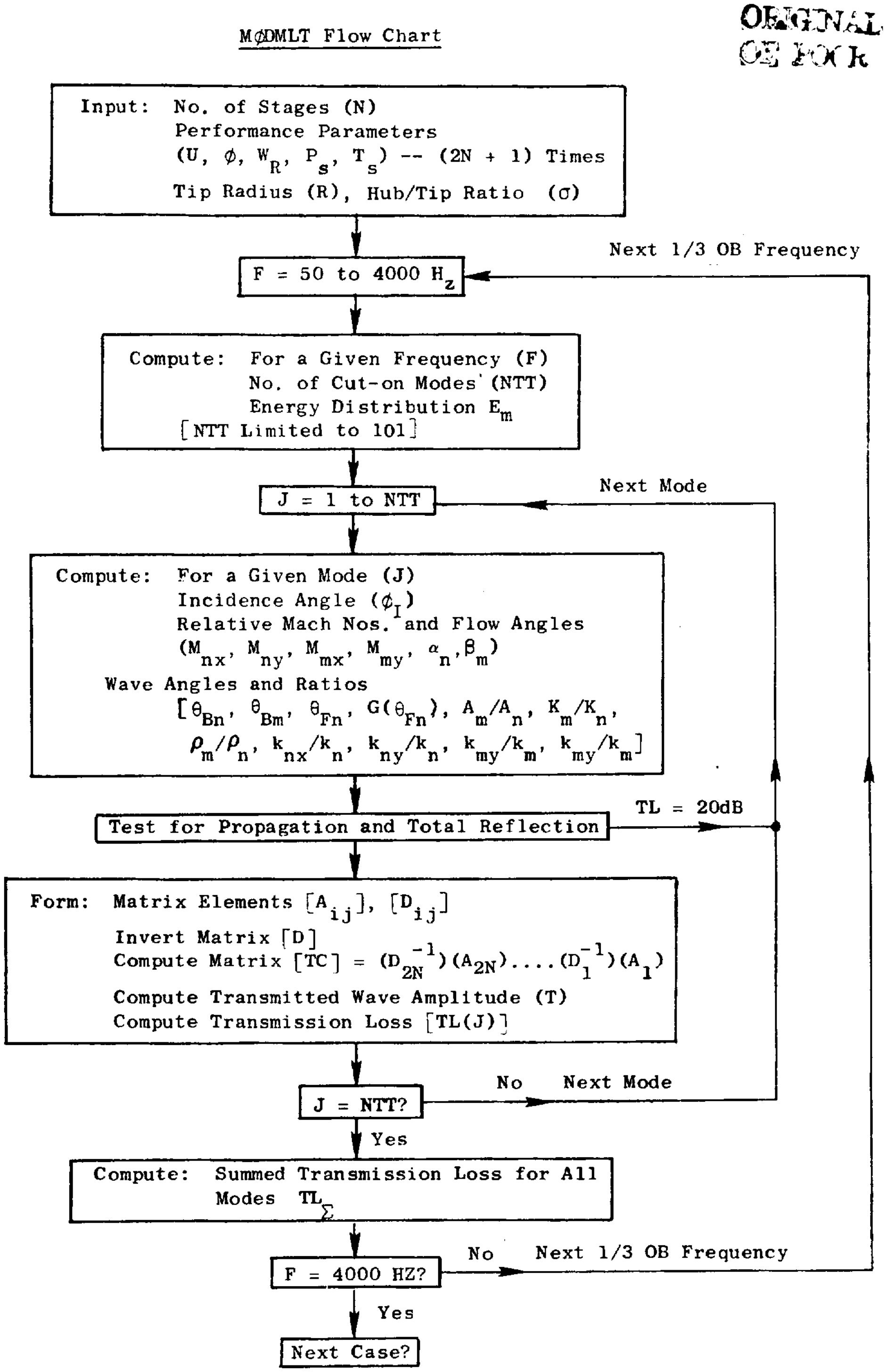

Figure 36. Flow Chart - Multistage, Multimode Computer Program Using Matrix Inversion.

Tip Radius (R_∞) -
Hub/Tip Ratio (σ) -

Data File

Turbine/Power -
No. of Stages (N) -
(use 0 for isolated row)
Input (2N + 1) times:

	Stn	Axial Vel. (U) (m/sec)	Abs. Flow Angle (ϕ) (deg)	Wheel Speed (V_R) (m/sec)	Static Pressure (P_s) (kN/m^2 or kPa)	Static Temp (T_s) (K)
1						
2						
3						
4						
5						
6						
7						
8						
9						
10						
11						
12						
13						
14						
15						
16						
17						

Figure 37. Input Sheet

07/13/77 11.317

INPUT FILE NAME = DFLP11

3-STG LPT: 2.0 PR 100% N

3 STAGES

* AERO-THERMO PARAMETERS *

STAGE	STATION	U- FPS	PHI- DEG	VR- FPS	PS- PSIA	TS- DEG R
1	1	607.000	0.	0.	34.630	730.000
1	2	421.000	62.100	409.000	28.470	693.000
2	3	327.000	-33.600	0.	26.170	679.000
2	4	300.000	62.100	428.000	23.400	660.000
3	5	255.000	-2.300	0.	21.390	648.000
3	6	219.000	55.100	437.000	20.280	641.000
	7	213.000	45.630	0.	19.560	639.000

***** FIRST CUT-ON OCCURS AT 219. HZ *****

THETA-I	THETA-R	THETA-T	T	B	E	T-LOSS
0.	0.	0.	0.5267	1.5109	1.0000	5.3529

FREQUENCY= 50 HZ TRANSMISSION LOSS= 5.35

0.	0.	0.	0.5267	1.5109	1.0000	5.3529

FREQUENCY= 63 HZ TRANSMISSION LOSS= 5.35

0.	0.	0.	0.5267	1.5109	1.0000	5.3529

FREQUENCY= 80 HZ TRANSMISSION LOSS= 5.35

0.	0.	0.	0.5267	1.5109	1.0000	5.3529

FREQUENCY= 100 HZ TRANSMISSION LOSS= 5.35

0.	0.	0.	0.5267	1.5109	1.0000	5.3529

FREQUENCY= 125 HZ TRANSMISSION LOSS= 5.35

0.	0.	0.	0.5267	1.5109	1.0000	5.3529

FREQUENCY= 160 HZ TRANSMISSION LOSS= 5.35

Figure 38. Typical Output.

0.	0.	0.	0.5267	1.5109	0.3333	5.3529
105.152	0.	0.	0.	1.0000	0.3333	20.0000
-105.152	-51.205	0.	0.	1.0000	0.3333	20.0000

FREQUENCY= 200 HZ TRANSMISSION LOSS= 9.84

0.	0.	0.	0.5267	1.5109	0.3333	5.3529
76.617	0.	0.	0.	1.0000	0.3333	20.0000
-76.617	-32.310	-53.120	0.2976	0.4328	0.3333	10.0400

FREQUENCY= 250 HZ TRANSMISSION LOSS= 8.74

0.	0.	0.	0.5267	1.5109	0.3333	5.3529
59.477	0.	0.	0.	1.0000	0.3333	20.0000
-59.477	-23.662	-41.815	0.3052	0.7204	0.3333	10.4325

FREQUENCY= 315 HZ TRANSMISSION LOSS= 8.84

0.	0.	0.	0.5267	1.5109	0.2000	5.3529
46.429	17.875	40.278	0.2935	0.9117	0.2000	8.9339
-46.429	-17.875	-32.994	0.3463	0.9371	0.2000	9.5133
105.152	0.	0.	0.	1.0000	0.2000	20.0000
-105.152	-51.205	0.	0.	1.0000	0.2000	20.0000

FREQUENCY= 400 HZ TRANSMISSION LOSS= 9.58

0.	0.	0.	0.5267	1.5109	0.2000	5.3529
37.004	13.991	30.951	0.3139	1.0457	0.2000	8.6506
-37.004	-13.991	-26.537	0.3872	1.0872	0.2000	8.5684
76.617	0.	0.	0.	1.0000	0.2000	20.0000
-76.617	-32.310	-53.120	0.2976	0.4328	0.2000	10.0400

FREQUENCY= 500 HZ TRANSMISSION LOSS= 8.69

0.	0.	0.	0.5267	1.5109	0.1429	5.3529
29.310	10.955	23.895	0.3529	1.1762	0.1429	7.9020
-29.310	-10.955	-21.202	0.4261	1.2054	0.1429	7.7004
59.477	0.	0.	0.	1.0000	0.1429	20.0000
-59.477	-23.662	-41.815	0.3052	0.7204	0.1429	10.4325
96.118	0.	0.	0.	1.0000	0.1429	20.0000
-96.118	-44.399	0.	0.	1.0000	0.1429	20.0000

FREQUENCY= 630 HZ TRANSMISSION LOSS= 9.74

0.	0.	0.	0.5267	1.5109	0.1111	5.3529
23.056	8.554	18.450	0.3954	1.2860	0.1111	7.1333
-23.056	-8.554	-16.811	0.4594	1.2969	0.1111	6.9859
46.429	17.875	40.278	0.2935	0.9117	0.1111	8.9339
-46.429	-17.875	-32.994	0.3463	0.9371	0.1111	9.5133
71.205	0.	0.	0.	1.0000	0.1111	20.0000
-71.205	-29.421	-49.603	0.2878	0.5184	0.1111	10.5856

Figure 38. Typical Output (Continued).

105.152	0.	0.	0.	1.0000	0.1111	20.0000
-105.152	-51.205	0.	0.	1.0000	0.1111	20.0000

FREQUENCY= 800 HZ TRANSMISSION LOSS= 9.36

0.	0.	0.	0.5267	1.5109	0.0909	5.3529
18.434	6.810	14.566	0.4300	1.3624	0.0909	6.5610
-18.434	-6.810	-13.529	0.4830	1.3598	0.0909	6.4870
37.004	13.991	30.951	0.3139	1.0457	0.0909	8.6506
-37.004	-13.991	-26.537	0.3872	1.0872	0.0909	8.5684
56.048	0.	0.	0.	1.0000	0.0909	20.0000
-56.048	-22.086	-39.510	0.3142	0.7784	0.0909	10.2468
76.617	0.	0.	0.	1.0000	0.0909	20.0000
-76.617	-32.310	-53.120	0.2976	0.4328	0.0909	10.0400
105.152	0.	0.	0.	1.0000	0.0909	20.0000
-105.152	-51.205	0.	0.	1.0000	0.0909	20.0000

FREQUENCY=1000 HZ TRANSMISSION LOSS= 9.46

0.	0.	0.	0.5267	1.5109	0.0769	5.3529
14.742	5.432	11.539	0.4574	1.4160	0.0769	6.1467
-14.742	-5.432	-10.879	0.5000	1.4055	0.0769	6.1268
29.546	11.046	24.105	0.3515	1.1721	0.0769	7.9292
-29.546	-11.046	-21.366	0.4249	1.2019	0.0769	7.7276
44.532	17.076	38.329	0.2946	0.9351	0.0769	8.9583
-44.532	-17.076	-31.700	0.3538	0.9677	0.0769	9.3381
59.979	0.	0.	0.	1.0000	0.0769	20.0000
-59.979	-23.897	-42.152	0.3040	0.7118	0.0769	10.4557
76.617	0.	0.	0.	1.0000	0.0769	20.0000
-76.617	-32.310	-53.120	0.2976	0.4328	0.0769	10.0400
97.357	0.	0.	0.	1.0000	0.0769	20.0000
-97.357	-45.279	0.	0.	1.0000	0.0769	20.0000

FREQUENCY=1250 HZ TRANSMISSION LOSS= 9.15

0.	0.	0.	0.5267	1.5109	0.0588	5.3529
11.515	4.235	8.942	0.4795	1.4548	0.0588	5.8398
-11.515	-4.235	-8.542	0.5125	1.4409	0.0588	5.8530
23.056	8.554	18.450	0.3954	1.2860	0.0588	7.1333
-23.056	-8.554	-16.811	0.4594	1.2969	0.0588	6.9859
34.668	13.058	28.762	0.3239	1.0841	0.0588	8.4587
-34.668	-13.058	-24.923	0.3986	1.1236	0.0588	8.3105
46.429	17.875	40.278	0.2935	0.9117	0.0588	8.9339
-46.429	-17.875	-32.994	0.3463	0.9371	0.0588	9.5133
58.498	0.	0.	0.	1.0000	0.0588	20.0000
-58.498	-23.208	-41.158	0.3076	0.7370	0.0588	10.3843
71.205	0.	0.	0.	1.0000	0.0588	20.0000
-71.205	-29.421	-49.603	0.2878	0.5184	0.0588	10.5856
85.390	0.	0.	0.	1.0000	0.0588	20.0000
-85.390	-37.382	0.	0.	1.0000	0.0588	20.0000
105.152	0.	0.	0.	1.0000	0.0588	20.0000
-105.152	-51.205	0.	0.	1.0000	0.0588	20.0000

FREQUENCY=1600 HZ TRANSMISSION LOSS= 9.35

0.	0.	0.	0.5267	1.5109	0.0476	5.3529
9.211	3.384	7.115	0.4934	1.4769	0.0476	5.6613
-9.211	-3.384	-6.859	0.5196	1.4627	0.0476	5.6873

Figure 38. Typical Output (Continued).

18.434	6.810	14.566	0.4300	1.3624	0.0476	6.5610
-18.434	-6.810	-13.529	0.4830	1.3598	0.0476	6.4870
27.689	10.327	22.461	0.3631	1.2048	0.0476	7.7103
-27.689	-10.327	-20.069	0.4347	1.2296	0.0476	7.5136
37.004	13.991	30.951	0.3139	1.0457	0.0476	8.6506
-37.004	-13.991	-26.537	0.3872	1.0872	0.0476	8.5684
46.429	17.875	40.278	0.2935	0.9117	0.0476	8.9339
-46.429	-17.875	-32.994	0.3463	0.9371	0.0476	9.5133
56.048	0.	0.	0.	1.0000	0.0476	20.0000
-56.048	-22.086	-39.510	0.3142	0.7784	0.0476	10.2468
66.011	0.	0.	0.	1.0000	0.0476	20.0000
-66.011	-26.793	-46.176	0.2923	0.6081	0.0476	10.6358
76.617	0.	0.	0.	1.0000	0.0476	20.0000
-76.617	-32.310	-53.120	0.2976	0.4328	0.0476	10.0400
88.591	0.	0.	0.	1.0000	0.0476	20.0000
-88.591	-39.371	0.	0.	1.0000	0.0476	20.0000
105.152	0.	0.	0.	1.0000	0.0476	20.0000
-105.152	-51.205	0.	0.	1.0000	0.0476	20.0000

FREQUENCY=2000 HZ TRANSMISSION LOSS= 9.26

0.	0.	0.	0.5267	1.5109	0.0400	5.3529
7.368	2.705	5.668	0.5032	1.4908	0.0400	5.5462
-7.368	-2.705	-5.504	0.5239	1.4778	0.0400	5.5756
14.742	5.432	11.539	0.4574	1.4160	0.0400	6.1467
-14.742	-5.432	-10.879	0.5000	1.4055	0.0400	6.1268
22.131	8.203	17.664	0.4022	1.3019	0.0400	7.0165
-22.131	-8.203	-16.157	0.4642	1.3099	0.0400	6.8830
29.546	11.046	24.105	0.3515	1.1721	0.0400	7.9292
-29.546	-11.046	-21.366	0.4249	1.2019	0.0400	7.7276
37.004	13.991	30.951	0.3139	1.0457	0.0400	8.6506
-37.004	-13.991	-26.537	0.3872	1.0872	0.0400	8.5684
44.532	17.076	38.329	0.2946	0.9351	0.0400	8.9583
-44.532	-17.076	-31.700	0.3538	0.9677	0.0400	9.3381
52.169	20.354	46.443	0.3079	0.8687	0.0400	8.3781
-52.169	-20.354	-36.891	0.3259	0.8430	0.0400	9.9852
59.979	0.	0.	0.	1.0000	0.0400	20.0000
-59.979	-23.897	-42.152	0.3040	0.7118	0.0400	10.4557
68.067	0.	0.	0.	1.0000	0.0400	20.0000
-68.067	-27.318	-47.537	0.2897	0.5725	0.0400	10.6455
76.617	0.	0.	0.	1.0000	0.0400	20.0000
-76.617	-32.310	-53.120	0.2976	0.4328	0.0400	10.0400
86.016	0.	0.	0.	1.0000	0.0400	20.0000
-86.016	-37.765	0.	0.	1.0000	0.0400	20.0000
97.357	0.	0.	0.	1.0000	0.0400	20.0000
-97.357	-45.279	0.	0.	1.0000	0.0400	20.0000

FREQUENCY=2500 HZ TRANSMISSION LOSS= 8.96

0.	0.	0.	0.5267	1.5109	0.0303	5.3529
5.847	2.146	4.483	0.5101	1.4997	0.0303	5.4708
-5.847	-2.146	-4.380	0.5265	1.4884	0.0303	5.4990
11.698	4.302	9.088	0.4783	1.4529	0.0303	5.8555
-11.698	-4.302	-8.675	0.5119	1.4390	0.0303	5.8673
17.555	6.481	13.839	0.4367	1.3759	0.0303	6.4575
-17.555	-6.481	-12.900	0.4873	1.3711	0.0303	6.3975
23.424	8.694	18.763	0.3927	1.2797	0.0303	7.1797
-23.424	-8.694	-17.071	0.4574	1.2917	0.0303	7.0270
29.310	10.955	23.895	0.3529	1.1762	0.0303	7.9020
-29.310	-10.955	-21.202	0.4261	1.2054	0.0303	7.7004
35.223	13.279	29.279	0.3214	1.0748	0.0303	8.5076
-35.223	-13.279	-25.308	0.3958	1.1150	0.0303	8.3725

Figure 38. Typical Output (Continued).

41.176	15.685	34.974	0.3005	0.9815	0.0303	8.8893
-41.176	-15.685	-29.404	0.3680	1.0214	0.0303	9.0083
47.184	18.196	41.065	0.2937	0.9032	0.0303	8.9084
-47.184	-18.196	-33.508	0.3435	0.9248	0.0303	9.5805
53.273	20.842	47.680	0.3173	0.8729	0.0303	8.0982
-53.273	-20.842	-37.637	0.3224	0.8247	0.0303	10.0647
59.477	0.	0.	0.	1.0000	0.0303	20.0000
-59.477	-23.662	-41.815	0.3052	0.7204	0.0303	10.4325
65.849	0.	0.	0.	1.0000	0.0303	20.0000
-65.849	-26.714	-46.068	0.2926	0.6109	0.0303	10.6337
72.470	0.	0.	0.	1.0000	0.0303	20.0000
-72.470	-30.082	-50.431	0.2880	0.4970	0.0303	10.5258
79.481	0.	0.	0.	1.0000	0.0303	20.0000
-79.481	-33.909	-54.950	0.3527	0.4328	0.0303	8.3979
87.146	0.	0.	0.	1.0000	0.0303	20.0000
-87.146	-38.463	0.	0.	1.0000	0.0303	20.0000
96.118	0.	0.	0.	1.0000	0.0303	20.0000
-96.118	-44.399	0.	0.	1.0000	0.0303	20.0000
109.677	0.	0.	0.	1.0000	0.0303	20.0000
-109.677	-54.998	0.	0.	1.0000	0.0303	20.0000

FREQUENCY=3150 HZ TRANSMISSION LOSS= 9.06

0.	0.	0.	0.5267	1.5109	0.0244	5.3529
4.605	1.689	3.521	0.5151	1.5051	0.0244	5.4228
-4.605	-1.689	-3.457	0.5279	1.4957	0.0244	5.4475
9.211	3.384	7.115	0.4934	1.4769	0.0244	5.6613
-9.211	-3.384	-6.859	0.5196	1.4627	0.0244	5.6873
13.820	5.089	10.792	0.4639	1.4279	0.0244	6.0529
-13.820	-5.089	-10.213	0.5038	1.4161	0.0244	6.0441
18.434	6.810	14.566	0.4300	1.3624	0.0244	6.5610
-18.434	-6.810	-13.529	0.4830	1.3598	0.0244	6.4870
23.056	8.554	18.450	0.3954	1.2860	0.0244	7.1333
-23.056	-8.554	-16.811	0.4594	1.2969	0.0244	6.9859
27.689	10.327	22.461	0.3631	1.2048	0.0244	7.7103
-27.689	-10.327	-20.069	0.4347	1.2296	0.0244	7.5136
32.337	12.137	26.619	0.3355	1.1236	0.0244	8.2338
-32.337	-12.137	-23.308	0.4103	1.1595	0.0244	8.0474
37.004	13.991	30.951	0.3139	1.0457	0.0244	8.6506
-37.004	-13.991	-26.537	0.3872	1.0872	0.0244	8.5684
41.699	15.900	35.489	0.2993	0.9739	0.0244	8.9082
-41.699	-15.900	-29.763	0.3657	1.0131	0.0244	9.0613
46.429	17.875	40.278	0.2935	0.9117	0.0244	8.9339
-46.429	-17.875	-32.994	0.3463	0.9371	0.0244	9.5133
51.207	19.931	45.378	0.3026	0.8706	0.0244	8.5509
-51.207	-19.931	-36.239	0.3291	0.8590	0.0244	9.9127
56.048	0.	0.	0.	1.0000	0.0244	20.0000
-56.048	-22.086	-39.510	0.3142	0.7784	0.0244	10.2468
60.972	0.	0.	0.	1.0000	0.0244	20.0000
-60.972	-24.363	-42.817	0.3017	0.6949	0.0244	10.4982
66.011	0.	0.	0.	1.0000	0.0244	20.0000
-66.011	-26.793	-46.176	0.2923	0.6081	0.0244	10.6358
71.205	0.	0.	0.	1.0000	0.0244	20.0000
-71.205	-29.421	-49.603	0.2878	0.5184	0.0244	10.5855
76.617	0.	0.	0.	1.0000	0.0244	20.0000
-76.617	-32.310	-53.120	0.2976	0.4328	0.0244	10.0400
82.351	0.	0.	0.	1.0000	0.0244	20.0000
-82.351	-35.565	0.	0.	1.0000	0.0244	20.0000
88.591	0.	0.	0.	1.0000	0.0244	20.0000
-88.591	-39.371	0.	0.	1.0000	0.0244	20.0000
95.741	0.	0.	0.	1.0000	0.0244	20.0000
-95.741	-44.134	0.	0.	1.0000	0.0244	20.0000
105.152	0.	0.	0.	1.0000	0.0244	20.0000
-105.152	-51.205	0.	0.	1.0000	0.0244	20.0000

FREQUENCY=4000 HZ TRANSMISSION LOSS= 9.15

Figure 38. Typical Output (Continued).

3-STG LPT: 3.0 PR 100% N

3 STAGES

* AERO-THERMO PARAMETERS *

STAGE	STATION	U- FPS	PHI- DEG	VR- FPS	PS- PSIA	TS- DEG R
1	1	673.000	0.	0.	33.480	723.000
1	2	523.000	62.100	409.000	23.410	657.000
2	3	413.000	-42.900	0.	21.060	641.000
2	4	407.000	62.000	423.000	16.910	608.000
3	5	349.000	-26.500	0.	15.080	591.000
3	6	317.000	55.100	437.000	13.770	579.000
	7	322.000	18.260	0.	12.830	569.000

***** FIRST CUT-ON OCCURS AT 193. HZ *****

THETA-I	THETA-R	THETA-T	T	B	E	T-LOSS
0.	0.	0.	0.4913	1.6899	1.0000	4.0764

FREQUENCY= 50 HZ TRANSMISSION LOSS= 4.08

0.	0.	0.	0.4913	1.6899	1.0000	4.0764

FREQUENCY= 63 HZ TRANSMISSION LOSS= 4.08

0.	0.	0.	0.4913	1.6899	1.0000	4.0764

FREQUENCY= 80 HZ TRANSMISSION LOSS= 4.08

0.	0.	0.	0.4913	1.6899	1.0000	4.0764

FREQUENCY= 100 HZ TRANSMISSION LOSS= 4.08

0.	0.	0.	0.4913	1.6899	1.0000	4.0764

FREQUENCY= 125 HZ TRANSMISSION LOSS= 4.08

0.	0.	0.	0.4913	1.6899	1.0000	4.0764

FREQUENCY= 160 HZ TRANSMISSION LOSS= 4.08

0.	0.	0.	0.4913	1.6899	0.3333	4.0764

Figure 38. Typical Output (Continued).

101.591	1.689	3.521	0.	1.0000	0.3333	20.0000
-101.591	-42.721	-3.457	0.	1.0000	0.3333	20.0000

FREQUENCY= 200 HZ TRANSMISSION LOSS= 8.63

0.	0.	0.	0.4913	1.6899	0.3333	4.0764
77.135	1.689	3.521	0.	1.0000	0.3333	20.0000
-77.135	-28.544	-3.457	0.	1.0000	0.3333	20.0000

FREQUENCY= 250 HZ TRANSMISSION LOSS= 8.63

0.	0.	0.	0.4913	1.6899	0.3333	4.0764
60.501	1.689	3.521	0.	1.0000	0.3333	20.0000
-60.501	-21.080	-44.766	0.2306	0.8926	0.3333	10.8433

FREQUENCY= 315 HZ TRANSMISSION LOSS= 7.93

0.	0.	0.	0.4913	1.6899	0.2000	4.0764
47.488	15.977	38.565	0.2034	1.1035	0.2000	10.2793
-47.488	-15.977	-35.095	0.2575	1.1111	0.2000	10.0447
101.591	3.384	7.115	0.	1.0000	0.2000	20.0000
-101.591	-42.721	-6.859	0.	1.0000	0.2000	20.0000

FREQUENCY= 400 HZ TRANSMISSION LOSS= 9.18

0.	0.	0.	0.4913	1.6899	0.2000	4.0764
37.962	12.524	30.220	0.2087	1.2347	0.2000	10.4037
-37.962	-12.524	-28.073	0.2932	1.2554	0.2000	8.9554
77.135	3.384	7.115	0.	1.0000	0.2000	20.0000
-77.135	-28.544	-6.859	0.	1.0000	0.2000	20.0000

FREQUENCY= 500 HZ TRANSMISSION LOSS= 9.00

0.	0.	0.	0.4913	1.6899	0.1429	4.0764
30.127	9.815	23.642	0.2371	1.3525	0.1429	9.5699
-30.127	-9.815	-22.316	0.3344	1.3659	0.1429	7.8009
60.501	3.384	7.115	0.	1.0000	0.1429	20.0000
-60.501	-21.080	-44.766	0.2306	0.8926	0.1429	10.8433
94.733	5.089	10.792	0.	1.0000	0.1429	20.0000
-94.733	-38.226	-10.213	0.	1.0000	0.1429	20.0000

FREQUENCY= 630 HZ TRANSMISSION LOSS= 9.53

0.	0.	0.	0.4913	1.6899	0.1111	4.0764
23.728	7.668	18.428	0.2796	1.4558	0.1111	8.3457
-23.728	-7.668	-17.616	0.3759	1.4517	0.1111	6.7459
47.488	15.977	38.565	0.2034	1.1035	0.1111	10.2793
-47.488	-15.977	-35.095	0.2575	1.1111	0.1111	10.0447
71.956	5.089	10.792	0.	1.0000	0.1111	20.0000
-71.956	-26.080	-53.357	0.2378	0.6830	0.1111	10.3005
101.591	6.310	14.566	0.	1.0000	0.1111	20.0000
-101.591	-42.721	-13.529	0.	1.0000	0.1111	20.0000

FREQUENCY= 800 HZ TRANSMISSION LOSS= 9.27

Figure 38. Typical Output (Continued).

0.	0.	0.	0.4913	1.6899	0.0909	4.0764
18.984	6.107	14.642	0.3239	1.5338	0.0909	7.2129
-18.984	-6.107	-14.126	0.4098	1.5127	0.0909	5.9530
37.962	12.524	30.220	0.2087	1.2347	0.0909	10.4037
-37.962	-12.524	-28.073	0.2932	1.2554	0.0909	8.9554
57.105	5.089	10.792	0.	1.0000	0.0909	20.0000
-57.105	-19.696	-42.231	0.2353	0.9521	0.0909	10.7237
77.135	6.810	14.566	0.	1.0000	0.0909	20.0000
-77.135	-28.544	-13.529	0.	1.0000	0.0909	20.0000
101.591	8.554	18.450	0.	1.0000	0.0909	20.0000
-101.591	-42.721	-16.811	0.	1.0000	0.0909	20.0000

FREQUENCY=1000 HZ TRANSMISSION LOSS= 9.67

0.	0.	0.	0.4913	1.6899	0.0769	4.0764
15.189	4.871	11.655	0.3655	1.5923	0.0769	6.2727
-15.189	-4.871	-11.326	0.4369	1.5593	0.0769	5.3515
30.368	9.897	23.841	0.2358	1.3488	0.0769	9.6069
-30.368	-9.897	-22.493	0.3330	1.3626	0.0769	7.8392
45.578	15.268	36.857	0.2016	1.1283	0.0769	10.4281
-45.578	-15.268	-33.683	0.2635	1.1410	0.0769	9.8574
60.998	6.810	14.566	0.	1.0000	0.0769	20.0000
-60.998	-21.285	-45.137	0.2300	0.8838	0.0769	10.8544
77.135	8.554	18.450	0.	1.0000	0.0769	20.0000
-77.135	-28.544	-16.811	0.	1.0000	0.0769	20.0000
95.753	10.327	22.461	0.	1.0000	0.0769	20.0000
-95.753	-38.864	-20.069	0.	1.0000	0.0769	20.0000

FREQUENCY=1250 HZ TRANSMISSION LOSS= 9.32

0.	0.	0.	0.4913	1.6899	0.0588	4.0764
11.867	3.798	9.068	0.4033	1.6361	0.0588	5.5097
-11.867	-3.798	-8.867	0.4589	1.5976	0.0588	4.8796
23.728	7.668	18.428	0.2796	1.4558	0.0588	8.3457
-23.728	-7.668	-17.616	0.3759	1.4517	0.0588	6.7459
35.588	11.692	28.202	0.2149	1.2695	0.0588	10.2328
-35.588	-11.692	-26.327	0.3045	1.2896	0.0588	9.6271
47.488	15.977	38.565	0.2034	1.1035	0.0588	10.2793
-47.488	-15.977	-35.095	0.2575	1.1111	0.0588	10.0447
59.534	8.554	18.450	0.	1.0000	0.0588	20.0000
-59.534	-20.681	-44.043	0.2317	0.9098	0.0588	10.8167
71.956	10.327	22.461	0.	1.0000	0.0588	20.0000
-71.956	-26.080	-53.357	0.2378	0.6830	0.0588	10.3005
85.318	12.137	26.619	0.	1.0000	0.0588	20.0000
-85.318	-32.763	-23.308	0.	1.0000	0.0588	20.0000
101.591	13.991	30.951	0.	1.0000	0.0588	20.0000
-101.591	-42.721	-26.537	0.	1.0000	0.0588	20.0000

FREQUENCY=1600 HZ TRANSMISSION LOSS= 9.26

0.	0.	0.	0.4913	1.6899	0.0476	4.0764
9.494	3.035	7.234	0.4289	1.6610	0.0476	5.0376
-9.494	-3.035	-7.106	0.4725	1.6229	0.0476	4.5900
18.984	6.107	14.642	0.3239	1.5338	0.0476	7.2129
-18.984	-6.107	-14.126	0.4098	1.5127	0.0476	5.9530
28.470	9.254	22.280	0.2462	1.3787	0.0476	9.2965
-28.470	-9.254	-21.100	0.3445	1.3885	0.0476	7.5343

Figure 38. Typical Output (Continued).

37.962	12.524	30.220	0.2087	1.2347	0.0476	10.4037
-37.962	-12.524	-28.073	0.2932	1.2554	0.0476	8.9554
47.488	15.977	38.565	0.2034	1.1035	0.0476	10.2793
-47.488	-15.977	-35.095	0.2575	1.1111	0.0476	10.0447
57.105	10.327	22.461	0.	1.0000	0.0476	20.0000
-57.105	-19.696	-42.231	0.2353	0.9521	0.0476	10.7237
66.918	12.137	26.619	0.	1.0000	0.0476	20.0000
-66.918	-23.811	-49.571	0.2276	0.7760	0.0476	10.8199
77.135	13.991	30.951	0.	1.0000	0.0476	20.0000
-77.135	-28.544	-26.537	0.	1.0000	0.0476	20.0000
88.214	15.900	35.489	0.	1.0000	0.0476	20.0000
-88.214	-34.367	-29.763	0.	1.0000	0.0476	20.0000
101.591	17.875	40.278	0.	1.0000	0.0476	20.0000
-101.591	-42.721	-32.994	0.	1.0000	0.0476	20.0000

FREQUENCY=2000 HZ TRANSMISSION LOSS= 9.33

0.	0.	0.	0.4913	1.6899	0.0370	4.0764
7.596	2.426	5.775	0.4473	1.6761	0.0370	4.7190
-7.596	-2.426	-5.693	0.4815	1.6413	0.0370	4.3956
15.189	4.871	11.655	0.3655	1.5923	0.0370	6.2727
-15.189	-4.871	-11.326	0.4369	1.5593	0.0370	5.3515
22.779	7.354	17.666	0.2876	1.4715	0.0370	8.1300
-22.779	-7.354	-16.918	0.3826	1.4641	0.0370	6.5862
30.368	9.897	23.841	0.2358	1.3488	0.0370	9.6069
-30.368	-9.897	-22.493	0.3330	1.3626	0.0370	7.8392
37.962	12.524	30.220	0.2087	1.2347	0.0370	10.4037
-37.962	-12.524	-28.073	0.2932	1.2554	0.0370	8.9554
45.578	15.268	35.857	0.2016	1.1283	0.0370	10.4281
-45.578	-15.268	-33.683	0.2635	1.1410	0.0370	9.8574
53.242	18.170	43.829	0.2364	1.0594	0.0370	8.7630
-53.242	-18.170	-39.358	0.2427	1.0177	0.0370	10.5067
60.998	13.991	30.951	0.	1.0000	0.0370	20.0000
-60.998	-21.285	-45.137	0.2300	0.8833	0.0370	10.8544
68.919	15.900	35.489	0.	1.0000	0.0370	20.0000
-68.919	-24.698	-51.075	0.2293	0.7388	0.0370	10.7057
77.135	17.875	40.278	0.	1.0000	0.0370	20.0000
-77.135	-28.544	-32.994	0.	1.0000	0.0370	20.0000
85.888	19.931	45.378	0.	1.0000	0.0370	20.0000
-85.888	-33.074	-36.239	0.	1.0000	0.0370	20.0000
95.753	0.	0.	0.	1.0000	0.0370	20.0000
-95.753	-38.864	-39.510	0.	1.0000	0.0370	20.0000
109.031	0.	0.	0.	1.0000	0.0370	20.0000
-109.031	-48.219	-42.817	0.	1.0000	0.0370	20.0000

FREQUENCY=2500 HZ TRANSMISSION LOSS= 9.31

0.	0.	0.	0.4913	1.6899	0.0303	4.0764
6.029	1.925	4.575	0.4607	1.6851	0.0303	4.5012
-6.029	-1.925	-4.524	0.4873	1.6550	0.0303	4.2643
12.056	3.859	9.214	0.4012	1.6339	0.0303	5.5502
-12.056	-3.859	-9.007	0.4578	1.5955	0.0303	4.9045
18.081	5.812	13.928	0.3334	1.5483	0.0303	6.9876
-18.081	-5.812	-13.460	0.4163	1.5240	0.0303	5.8056
24.104	7.793	18.731	0.2765	1.4496	0.0303	8.4293
-24.104	-7.793	-17.893	0.3733	1.4467	0.0303	6.8093
30.127	9.815	23.642	0.2371	1.3525	0.0303	9.5699
-30.127	-9.815	-22.316	0.3344	1.3659	0.0303	7.8009
36.153	11.889	28.680	0.2133	1.2611	0.0303	10.2300
-36.153	-11.889	-26.742	0.3017	1.2815	0.0303	8.7071
42.190	14.032	33.871	0.2022	1.1746	0.0303	10.5237
-42.190	-14.032	-31.184	0.2755	1.1929	0.0303	9.4359

Figure 38. Typical Output (Continued).

48.247	16.261	39.249	0.2047	1.0940	0.0303	10.1955
-48.247	-16.261	-35.656	0.2553	1.0991	0.0303	10.1145
54.343	15.900	35.489	0.	1.0000	0.0303	20.0000
-54.343	-18.600	-40.176	0.2403	0.9992	0.0303	10.5767
60.501	17.875	40.278	0.	1.0000	0.0303	20.0000
-60.501	-21.080	-44.766	0.2306	0.8926	0.0303	10.8433
66.760	19.931	45.378	0.	1.0000	0.0303	20.0000
-66.760	-23.741	-49.453	0.2276	0.7789	0.0303	10.8261
73.175	0.	0.	0.	1.0000	0.0303	20.0000
-73.175	-26.647	-54.274	0.2470	0.6624	0.0303	9.9323
79.838	0.	0.	0.	1.0000	0.0303	20.0000
-79.838	-29.891	-42.817	0.	1.0000	0.0303	20.0000
86.913	0.	0.	0.	1.0000	0.0303	20.0000
-86.913	-33.639	-46.176	0.	1.0000	0.0303	20.0000
94.733	0.	0.	0.	1.0000	0.0303	20.0000
-94.733	-38.226	-49.603	0.	1.0000	0.0303	20.0000
104.250	0.	0.	0.	1.0000	0.0303	20.0000
-104.250	-44.604	-53.120	0.	1.0000	0.0303	20.0000
	FREQUENCY=3150 HZ		TRANSMISSION LOSS= 9.26			
0.	0.	0.	0.4913	1.6899	0.0233	4.0764
4.748	1.515	3.598	0.4701	1.6901	0.0233	4.3556
-4.748	-1.515	-3.566	0.4907	1.6650	0.0233	4.1805
9.494	3.035	7.234	0.4289	1.6610	0.0233	5.0376
-9.494	-3.035	-7.106	0.4725	1.6229	0.0233	4.5900
14.240	4.564	10.913	0.3764	1.6057	0.0233	6.0456
-14.240	-4.564	-10.624	0.4435	1.5705	0.0233	5.2102
18.984	6.107	14.642	0.3239	1.5338	0.0233	7.2129
-18.984	-6.107	-14.126	0.4098	1.5127	0.0233	5.9530
23.728	7.668	18.428	0.2796	1.4558	0.0233	8.3457
-23.728	-7.668	-17.616	0.3759	1.4517	0.0233	6.7459
28.470	9.254	22.280	0.2462	1.3787	0.0233	9.2965
-28.470	-9.254	-21.100	0.3445	1.3885	0.0233	7.5343
33.214	10.871	26.207	0.2231	1.3050	0.0233	9.9905
-33.214	-10.871	-24.583	0.3168	1.3232	0.0233	8.2793
37.962	12.524	30.220	0.2087	1.2347	0.0233	10.4037
-37.962	-12.524	-28.073	0.2932	1.2554	0.0233	8.9554
42.719	14.223	34.334	0.2018	1.1673	0.0233	10.5210
-42.719	-14.223	-31.574	0.2735	1.1849	0.0233	9.5471
47.488	15.977	38.565	0.2034	1.1035	0.0233	10.2793
-47.488	-15.977	-35.095	0.2575	1.1111	0.0233	10.0447
52.280	17.797	42.936	0.2227	1.0553	0.0233	9.3149
-52.280	-17.797	-38.644	0.2448	1.0336	0.0233	10.4406
57.105	0.	0.	0.	1.0000	0.0233	20.0000
-57.105	-19.696	-42.231	0.2353	0.9521	0.0233	10.7237
61.977	0.	0.	0.	1.0000	0.0233	20.0000
-61.977	-21.693	-45.869	0.2291	0.8663	0.0233	10.8710
66.918	0.	0.	0.	1.0000	0.0233	20.0000
-66.918	-23.811	-49.571	0.2276	0.7760	0.0233	10.8199
71.956	0.	0.	0.	1.0000	0.0233	20.0000
-71.956	-26.080	-53.357	0.2378	0.6830	0.0233	10.3005
77.135	0.	0.	0.	1.0000	0.0233	20.0000
-77.135	-28.544	-53.120	0.	1.0000	0.0233	20.0000
82.518	0.	0.	0.	1.0000	0.0233	20.0000
-82.518	-31.271	0.	0.	1.0000	0.0233	20.0000
88.214	0.	0.	0.	1.0000	0.0233	20.0000
-88.214	-34.367	0.	0.	1.0000	0.0233	20.0000
94.419	0.	0.	0.	1.0000	0.0233	20.0000
-94.419	-38.031	0.	0.	1.0000	0.0233	20.0000
101.591	0.	0.	0.	1.0000	0.0233	20.0000
-101.591	-42.721	0.	0.	1.0000	0.0233	20.0000
111.521	0.	0.	0.	1.0000	0.0233	20.0000
-111.521	-50.228	0.	0.	1.0000	0.0233	20.0000
	FREQUENCY=4000 HZ		TRANSMISSION LOSS= 9.33			

Figure 38. Typical Output (Continued).

3-STG LPT: 4.0 PR 100% N

3 STAGES

* AERO-THERMO PARAMETERS *

STAGE	STATION	U- FPS	PHI- DEG	VR- FPS	PS- PSIA	TS- DEG R
1	1	681.000	0.	0.	33.340	722.000
1	2	554.000	62.100	409.000	21.820	645.000
2	3	445.000	-45.100	0.	19.260	626.000
2	4	462.000	62.000	428.000	14.320	581.000
3	5	403.000	-33.700	0.	12.430	562.000
3	6	377.000	55.100	437.000	11.040	546.000
	7	386.000	5.900	0.	10.030	534.000

***** FIRST CUT-ON OCCURS AT 187. HZ *****

THETA-I	THETA-R	THETA-T	T	B	E	T-LOSS
0.	0.	0.	0.4803	1.6387	1.0000	2.9605

FREQUENCY= 50 HZ TRANSMISSION LOSS= 2.96

0.	0.	0.	0.4803	1.6387	1.0000	2.9605

FREQUENCY= 63 HZ TRANSMISSION LOSS= 2.96

0.	0.	0.	0.4803	1.6387	1.0000	2.9605

FREQUENCY= 80 HZ TRANSMISSION LOSS= 2.96

0.	0.	0.	0.4803	1.6387	1.0000	2.9605

FREQUENCY= 100 HZ TRANSMISSION LOSS= 2.96

0.	0.	0.	0.4803	1.6387	1.0000	2.9605

FREQUENCY= 125 HZ TRANSMISSION LOSS= 2.96

0.	0.	0.	0.4803	1.6387	1.0000	2.9605

FREQUENCY= 160 HZ TRANSMISSION LOSS= 2.96

0.	0.	0.	0.4803	1.6387	0.3333	2.9605

Figure 38. Typical Output (Continued).

101.257	1.515	3.598	0.	1.0000	0.3333	20.0000
-101.257	-41.807	-3.566	0.	1.0000	0.3333	20.0000

FREQUENCY= 200 HZ TRANSMISSION LOSS= 7.56

0.	0.	0.	0.4803	1.6387	0.3333	2.9605
77.185	1.515	3.598	0.	1.0000	0.3333	20.0000
-77.185	-28.085	-3.566	0.	1.0000	0.3333	20.0000

FREQUENCY= 250 HZ TRANSMISSION LOSS= 7.56

0.	0.	0.	0.4803	1.6387	0.3333	2.9605
60.616	1.515	3.598	0.	1.0000	0.3333	20.0000
-60.616	-20.762	-46.740	0.1900	0.9404	0.3333	11.1783

FREQUENCY= 315 HZ TRANSMISSION LOSS= 7.05

0.	0.	0.	0.4803	1.6387	0.2000	2.9605
47.611	15.744	37.799	0.1593	1.1509	0.2000	11.1567
-47.611	-15.744	-36.505	0.2101	1.1540	0.2000	10.4406
101.257	3.035	7.234	0.	1.0000	0.2000	20.0000
-101.257	-41.807	-7.106	0.	1.0000	0.2000	20.0000

FREQUENCY= 400 HZ TRANSMISSION LOSS= 8.58

0.	0.	0.	0.4803	1.6387	0.2000	2.9605
38.074	12.344	29.914	0.1599	1.2793	0.2000	11.4833
-38.074	-12.344	-29.106	0.2415	1.2381	0.2000	9.2664
77.185	3.035	7.234	0.	1.0000	0.2000	20.0000
-77.185	-28.085	-7.106	0.	1.0000	0.2000	20.0000

FREQUENCY= 500 HZ TRANSMISSION LOSS= 8.45

0.	0.	0.	0.4803	1.6387	0.1429	2.9605
30.223	9.675	23.570	0.1813	1.3795	0.1429	10.6591
-30.223	-9.675	-23.067	0.2816	1.3847	0.1429	7.9244
60.616	3.035	7.234	0.	1.0000	0.1429	20.0000
-60.616	-20.762	-46.740	0.1900	0.9404	0.1429	11.1783
94.578	4.564	10.913	0.	1.0000	0.1429	20.0000
-94.578	-37.504	-10.624	0.	1.0000	0.1429	20.0000

FREQUENCY= 630 HZ TRANSMISSION LOSS= 9.11

0.	0.	0.	0.4803	1.6387	0.1111	2.9605
23.807	7.559	18.468	0.2194	1.4602	0.1111	9.1967
-23.807	-7.559	-18.159	0.3258	1.4551	0.1111	6.6254
47.611	15.744	37.799	0.1593	1.1509	0.1111	11.1567
-47.611	-15.744	-36.505	0.2101	1.1540	0.1111	10.4406
72.036	4.564	10.913	0.	1.0000	0.1111	20.0000
-72.036	-25.671	-55.857	0.2089	0.7270	0.1111	10.1223
101.257	6.107	14.642	0.	1.0000	0.1111	20.0000
-101.257	-41.807	-14.126	0.	1.0000	0.1111	20.0000

FREQUENCY= 800 HZ TRANSMISSION LOSS= 8.98

Figure 38. Typical Output (Continued).

0.	0.	0.	0.4803	1.6387	0.0909	2.9605
19.050	6.020	14.727	0.2656	1.5197	0.0909	7.6710
-19.050	-6.020	-14.530	0.3649	1.5027	0.0909	5.6051
38.074	12.344	29.914	0.1599	1.2793	0.0909	11.4833
-38.074	-12.344	-29.106	0.2415	1.2881	0.0909	9.2661
57.224	4.564	10.913	0.	1.0000	0.0909	20.0000
-57.224	-19.403	-44.054	0.1929	0.9995	0.0909	11.0919
77.185	6.107	14.642	0.	1.0000	0.0909	20.0000
-77.185	-28.085	-14.126	0.	1.0000	0.0909	20.0000
101.257	7.668	18.428	0.	1.0000	0.0909	20.0000
-101.257	-41.807	-17.616	0.	1.0000	0.0909	20.0000

FREQUENCY=1000 HZ TRANSMISSION LOSS= 9.38

0.	0.	0.	0.4803	1.6387	0.0769	2.9605
15.242	4.802	11.754	0.3145	1.5647	0.0769	6.3041
-15.242	-4.802	-11.629	0.3985	1.5331	0.0769	4.8039
30.464	9.755	23.763	0.1802	1.3765	0.0769	10.6997
-30.464	-9.755	-23.252	0.2801	1.3819	0.0769	7.9703
45.699	15.046	36.201	0.1570	1.1771	0.0769	11.3538
-45.699	-15.046	-35.016	0.2151	1.1824	0.0769	10.2467
61.112	6.107	14.642	0.	1.0000	0.0769	20.0000
-61.112	-20.964	-47.133	0.1896	0.9316	0.0769	11.1855
77.185	7.668	18.428	0.	1.0000	0.0769	20.0000
-77.185	-28.085	-17.616	0.	1.0000	0.0769	20.0000
95.577	9.254	22.280	0.	1.0000	0.0769	20.0000
-95.577	-38.119	-21.100	0.	1.0000	0.0769	20.0000

FREQUENCY=1250 HZ TRANSMISSION LOSS= 9.07

0.	0.	0.	0.4803	1.6387	0.0588	2.9605
11.909	3.745	9.166	0.3628	1.5989	0.0588	5.1452
-11.909	-3.745	-9.090	0.4275	1.5669	0.0588	4.1552
23.807	7.559	18.468	0.2194	1.4602	0.0588	9.1967
-23.807	-7.559	-18.159	0.3258	1.4551	0.0588	6.6254
35.695	11.524	27.979	0.1642	1.3100	0.0588	11.3372
-35.695	-11.524	-27.272	0.2521	1.3187	0.0588	8.8938
47.611	15.744	37.799	0.1593	1.1509	0.0588	11.1567
-47.611	-15.744	-36.505	0.2101	1.1540	0.0588	10.4406
59.650	7.668	18.428	0.	1.0000	0.0588	20.0000
-59.650	-20.371	-45.973	0.1906	0.9575	0.0588	11.1637
72.036	9.254	22.280	0.	1.0000	0.0588	20.0000
-72.036	-25.671	-55.857	0.2089	0.7270	0.0588	10.1223
85.300	10.871	26.207	0.	1.0000	0.0588	20.0000
-85.300	-32.206	-24.583	0.	1.0000	0.0588	20.0000
101.257	12.524	30.220	0.	1.0000	0.0588	20.0000
-101.257	-41.807	-28.073	0.	1.0000	0.0588	20.0000

FREQUENCY=1600 HZ TRANSMISSION LOSS= 9.01

0.	0.	0.	0.4803	1.6387	0.0476	2.9605
9.528	2.992	7.324	0.3972	1.6184	0.0476	4.4157
-9.528	-2.992	-7.275	0.4465	1.5858	0.0476	3.7456
19.050	6.020	14.727	0.2656	1.5197	0.0476	7.6710
-19.050	-6.020	-14.530	0.3649	1.5027	0.0476	5.6051
28.562	9.122	22.243	0.1889	1.4004	0.0475	10.3529
-28.562	-9.122	-21.797	0.2920	1.4036	0.0476	7.6021

Figure 38. Typical Output (Continued).

38.074	12.344	29.914	0.1599	1.2793	0.0476	11.4833
-38.074	-12.344	-29.106	0.2415	1.2881	0.0476	9.2664
47.611	15.744	37.799	0.1593	1.1509	0.0476	11.1567
-47.611	-15.744	-36.505	0.2101	1.1540	[illegible]	10.4406
57.224	9.254	22.280	0.	1.0000	0.0476	20.0000
-57.224	-19.403	-44.054	0.1929	0.9995	0.0475	11.0919
67.017	10.871	26.207	0.	1.0000	0.0476	20.0000
-67.017	-23.445	-51.837	0.1903	0.8228	0.0476	11.0489
77.185	12.524	30.220	0.	1.0000	0.0476	20.0000
-77.185	-28.085	-28.073	0.	1.0000	0.0476	20.0000
88.162	14.223	34.334	0.	1.0000	0.0476	20.0000
-88.162	-33.766	-31.574	0.	1.0000	0.0476	20.0000
101.257	15.977	38.565	0.	1.0000	0.0476	20.0000
-101.257	-41.807	-35.095	0.	1.0000	0.0476	20.0000

FREQUENCY=2000 HZ TRANSMISSION LOSS= 9.08

0.	0.	0.	0.4803	1.6387	0.0370	2.9605
7.623	2.392	5.854	0.4225	1.6300	0.0370	3.9217
-7.623	-2.392	-5.823	0.4598	1.5998	0.0370	3.4636
15.242	4.802	11.754	0.3145	1.5647	0.0370	6.3041
-15.242	-4.802	-11.629	0.3985	1.5381	0.0370	4.8039
22.856	7.250	17.718	0.2273	1.4722	0.0370	8.9178
-22.856	-7.250	-17.433	0.3333	1.4649	0.0370	6.4229
30.464	9.755	23.763	0.1802	1.3765	0.0370	10.6997
-30.464	-9.755	-23.252	0.2801	1.3819	0.0370	7.9703
38.074	12.344	29.914	0.1599	1.2793	0.0370	11.4833
-38.074	-12.344	-29.106	0.2415	1.2881	0.0370	9.2664
45.699	15.046	36.291	0.1570	1.1771	0.0370	11.3588
-45.699	-15.046	-35.016	0.2151	1.1824	0.0370	10.2467
53.364	10.871	26.207	0.	1.0000	0.0370	20.0000
-53.364	-17.901	-41.012	0.1983	1.0639	0.0370	10.8972
61.112	12.524	30.220	0.	1.0000	0.0370	20.0000
-61.112	-20.964	-47.133	0.1896	0.9316	0.0370	11.1865
69.011	14.223	34.334	0.	1.0000	0.0370	20.0000
-69.011	-24.316	-53.433	0.1934	0.7847	0.0370	10.8684
77.185	15.977	38.565	0.	1.0000	0.0370	20.0000
-77.185	-28.085	-35.095	0.	1.0000	0.0370	20.0000
85.864	17.797	42.936	0.	1.0000	0.0370	20.0000
-85.864	-32.509	-38.644	0.	1.0000	0.0370	20.0000
95.577	0.	0.	0.	1.0000	0.0370	20.0000
-95.577	-38.119	-42.231	0.	1.0000	0.0370	20.0000
108.308	0.	0.	0.	1.0000	0.0370	20.0000
-108.308	-46.903	-45.869	0.	1.0000	0.0370	20.0000

FREQUENCY=2500 HZ TRANSMISSION LOSS= 9.22

0.	0.	0.	0.4803	1.6387	0.0303	2.9605
6.050	1.898	4.643	0.4408	1.6368	0.0303	3.5867
-6.050	-1.898	-4.623	0.4690	1.6104	0.0303	3.2692
12.098	3.804	9.31[illegible]	0.3601	1.5972	0.0303	5.2075
-12.098	-3.804	-9.2[illegible]4	0.4259	1.5653	0.0303	4.1900
18.143	5.729	14.01[illegible]	0.2764	1.5308	0.0303	7.3508
-18.143	-5.729	-13.839	0.3728	1.5114	0.0303	5.4112
24.184	7.682	18.767	0.2165	1.4555	0.0303	9.3031
-24.184	-7.682	-18.448	0.3229	1.4511	0.0303	6.7053
30.223	9.675	23.570	0.1813	1.3795	0.0303	10.6591
-30.223	-9.675	-23.067	0.2816	1.3847	0.0303	7.9244
36.262	11.719	28.438	0.1630	1.3027	0.0303	11.3797
-36.262	-11.719	-27.708	0.2495	1.3115	0.0303	8.9854
42.307	13.829	33.388	0.1562	1.2232	0.0303	11.5306
-42.307	-13.829	-32.380	0.2255	1.2310	0.0303	9.8513

Figure 38. Typical Output (Continued).

48.370	16.023	38.436	0.1608	1.1406	0.0303	11.0481
-48.370	-16.023	-37.098	0.2083	1.1425	0.0303	10.5119
54.465	14.223	34.334	0.	1.0000	0.0303	20.0000
-54.465	-18.325	-41.878	0.1965	1.0458	0.0303	10.9622
60.616	15.977	38.565	0.	1.0000	0.0303	20.0000
-60.616	-20.762	-46.740	0.1900	0.9404	0.0303	11.1783
66.859	17.797	42.936	0.	1.0000	0.0303	20.0000
-66.859	-23.377	-51.711	0.1902	0.8258	0.0303	11.0552
73.248	0.	0.	0.	1.0000	0.0303	20.0000
-73.248	-26.227	-42.231	0.	1.0000	0.0303	20.0000
79.870	0.	0.	0.	1.0000	0.0303	20.0000
-79.870	-29.402	-45.869	0.	1.0000	0.0303	20.0000
86.877	0.	0.	0.	1.0000	0.0303	20.0000
-86.877	-33.058	-49.571	0.	1.0000	0.0303	20.0000
94.578	0.	0.	0.	1.0000	0.0303	20.0000
-94.578	-37.504	-53.357	0.	1.0000	0.0303	20.0000
103.812	0.	0.	0.	1.0000	0.0303	20.0000
-103.812	-43.581	-53.120	0.	1.0000	0.0303	20.0000

FREQUENCY=3150 HZ TRANSMISSION LOSS= 9.11

0.	0.	0.	0.4803	1.6387	0.0233	2.9605
4.765	1.494	3.654	0.4536	1.6403	0.0233	3.3651
-4.765	-1.494	-3.642	0.4749	1.6182	0.0233	3.1405
9.528	2.992	7.324	0.3972	1.6184	0.0233	4.4152
-9.528	-2.992	-7.275	0.4465	1.5858	0.0233	3.7456
14.290	4.500	11.014	0.3280	1.5752	0.0233	5.9630
-14.290	-4.500	-10.903	0.4069	1.5466	0.0233	4.6117
19.050	6.020	14.727	0.2656	1.5197	0.0233	7.6710
-19.050	-6.020	-14.530	0.3649	1.5027	0.0233	5.6051
23.807	7.559	18.468	0.2194	1.4602	0.0233	9.1967
-23.807	-7.559	-18.159	0.3258	1.4551	0.0233	6.6254
28.562	9.122	22.243	0.1889	1.4004	0.0233	10.3520
-28.562	-9.122	-21.795	0.2920	1.4036	0.0233	7.6024
33.317	10.715	26.056	0.1702	1.3404	0.0233	11.1031
-33.317	-10.715	-25.442	0.2640	1.3481	0.0233	8.4911
38.074	12.344	29.914	0.1599	1.2793	0.0233	11.4833
-38.074	-12.344	-29.106	0.2415	1.2881	0.0233	9.2664
42.837	14.017	33.825	0.1561	1.2161	0.0233	11.5167
-42.837	-14.017	-32.791	0.2238	1.2235	0.0233	9.9173
47.611	15.744	37.799	0.1593	1.1509	0.0233	11.1567
-47.611	-15.744	-36.505	0.2101	1.1540	0.0233	10.4406
52.403	17.534	41.846	0.1800	1.0908	0.0233	9.9079
-52.403	-17.534	-40.256	0.1999	1.0794	0.0233	10.8344
57.224	0.	0.	0.	1.0000	0.0233	20.0000
-57.224	-19.403	-44.054	0.1929	0.9995	0.0233	11.0919
62.089	0.	0.	0.	1.0000	0.0233	20.0000
-62.089	-21.366	-47.909	0.1892	0.9141	0.0233	11.1893
67.017	0.	0.	0.	1.0000	0.0233	20.0000
-67.017	-23.445	-51.837	0.1903	0.8228	0.0233	11.0489
72.036	0.	0.	0.	1.0000	0.0233	20.0000
-72.036	-25.671	-55.857	0.2089	0.7270	0.0233	10.1223
77.185	0.	0.	0.	1.0000	0.0233	20.0000
-77.185	-28.085	-53.120	0.	1.0000	0.0233	20.0000
82.528	0.	0.	0.	1.0000	0.0233	20.0000
-82.528	-30.750	0.	0.	1.0000	0.0233	20.0000
88.162	0.	0.	0.	1.0000	0.0233	20.0000
-88.162	-33.766	0.	0.	1.0000	0.0233	20.0000
94.270	0.	0.	0.	1.0000	0.0233	20.0000
-94.270	-37.317	0.	0.	1.0000	0.0233	20.0000
101.257	0.	0.	0.	1.0000	0.0233	20.0000
-101.257	-41.807	0.	0.	1.0000	0.0233	20.0000
110.556	0.	0.	0.	1.0000	0.0233	20.0000
-110.556	-48.668	0.	0.	1.0000	0.0233	20.0000

FREQUENCY=4000 HZ TRANSMISSION LOSS= 9.09

Figure 38. Typical Output (Continued).

```
                    3-STG LPT: 5.2 PR  100% N

                                  3  STAGES

                          * AERO-THERMO PARAMETERS *

STAGE   STATION    U- FPS    PHI- DEG    VR- FPS   PS- PSIA   TS- DEG R
  1        1      682.000     0.          0.        33.310    722.000
  1        2      567.000    62.100     409.000     21.180    639.000
  2        3      460.000   -46.000       0.        18.440    619.000
  2        4      508.000    62.000     428.000     12.550    561.000
  3        5      461.000   -38.800       0.        10.340    535.000
  3        6      444.000    55.000     437.000      8.840    516.000
           7      464.000    -4.700       0.         7.750    498.000

          ***** FIRST CUT-ON OCCURS AT  186. HZ *****

THETA-I    THETA-R    THETA-T      T          B          E        T-LOSS
  0.         0.         0.       0.4585     1.5652     1.0000     1.8801

           FREQUENCY=  50 HZ      TRANSMISSION LOSS=  1.88


  0.         0.         0.       0.4585     1.5652     1.0000     1.8801

           FREQUENCY=  63 HZ      TRANSMISSION LOSS=  1.88


  0.         0.         0.       0.4585     1.5652     1.0000     1.8801

           FREQUENCY=  80 HZ      TRANSMISSION LOSS=  1.88


  0.         0.         0.       0.4585     1.5652     1.0000     1.8801

           FREQUENCY= 100 HZ      TRANSMISSION LOSS=  1.88


  0.         0.         0.       0.4585     1.5652     1.0000     1.8801

           FREQUENCY= 125 HZ      TRANSMISSION LOSS=  1.88


  0.                    0.       0.4585     1.5652     1.0000     1.8801

           FREQUENCY= 160 HZ      TRANSMISSION LOSS=  1.88


  0.         0.         0.       0.4585     1.565[illegible]     0.3[illegible]33     1.8801
```

Figure 38. Typical Output (Continued).

101.232	1.494	3.654	0.	1.0000	0.3333	20.0000
-101.232	-41.708	-3.642	0.	1.0000	0.3333	20.0000

FREQUENCY= 200 HZ   TRANSMISSION LOSS= 6.52

0.	0.	0.	0.4585	1.5652	0.3333	1.8801
77.198	1.494	3.654	0.	1.0000	0.3333	20.0000
-77.198	-28.034	-3.642	0.	1.0000	0.3333	20.0000

FREQUENCY= 250 HZ   TRANSMISSION LOSS= 6.52

0.	0.	0.	0.4585	1.5652	0.3333	1.8801
60.635	1.494	3.654	0.	1.0000	0.3333	20.0000
-60.635	-20.727	-49.338	0.1522	0.9530	0.3333	11.6097

FREQUENCY= 315 HZ   TRANSMISSION LOSS= 6.15

0.	0.	0.	0.4585	1.5652	0.2000	1.8801
47.629	15.717	37.148	0.1192	1.1619	0.2000	12.2968
-47.629	-15.717	-38.382	0.1674	1.1630	0.2000	10.8807
101.232	2.992	7.324	0.	1.0000	0.2000	20.0000
-101.232	-41.708	-7.275	0.	1.0000	0.2000	20.0000

FREQUENCY= 400 HZ   TRANSMISSION LOSS= 7.91

0.	0.	0.	0.4585	1.5652	0.2000	1.8801
38.091	12.324	29.710	0.1188	1.2882	0.2000	12.6840
-38.091	-12.324	-30.490	0.1947	1.2910	0.2000	9.5948
77.198	2.992	7.324	0.	1.0000	0.2000	20.0000
-77.198	-28.034	-7.275	0.	1.0000	0.2000	20.0000

FREQUENCY= 500 HZ   TRANSMISSION LOSS= 7.79

0.	0.	0.	0.4585	1.5652	0.1429	1.8801
30.237	9.659	23.592	0.1351	1.3775	0.1429	11.8156
-30.237	-9.659	-24.080	0.2324	1.3791	0.1429	8.0492
60.635	2.992	7.324	0.	1.0000	0.1429	20.0000
-60.635	-20.727	-49.338	0.1522	0.9530	0.1429	11.6097
94.570	4.500	11.014	0.	1.0000	0.1429	20.0000
-94.570	-37.426	-10.903	0.	1.0000	0.1429	20.0000

FREQUENCY= 630 HZ   TRANSMISSION LOSS= 8.58

0.	0.	0.	0.4585	1.5652	0.1111	1.8801
23.818	7.547	18.595	0.1686	1.4415	0.1111	10.0769
-23.818	-7.547	-18.896	0.2769	1.4392	0.1111	6.5020
47.629	15.717	37.148	0.1192	1.1619	0.1111	12.2968
-47.629	-15.717	-38.382	0.1674	1.1630	0.1111	10.8807
72.051	4.500	11.014	0.	1.0000	0.1111	20.0000
-72.051	-25.626	-10.903	0.	1.0000	0.1111	20.0000
101.232	6.020	14.727	0.	1.0000	0.1111	20.0000
-101.232	-41.708	-14.530	0.	1.0000	0.1111	20.0000

FREQUENCY= 800 HZ   TRANSMISSION LOSS= 8.93

Figure 38. Typical Output (Continued).

0.	0.	0.	0.4585	1.5652	0.0909	1.8801
19.059	6.010	14.889	0.2137	1.4840	0.0909	8.1364
-19.059	-6.010	-15.081	0.3183	1.4770	0.0909	5.2606
38.091	12.324	29.710	0.1188	1.2882	0.0909	12.6840
-38.091	-12.324	-30.490	0.1947	1.2910	0.0909	9.5943
57.243	4.500	11.014	0.	1.0000	0.0909	20.0000
-57.243	-19.370	-46.460	0.1538	1.0115	0.0909	11.5525
77.198	6.020	14.727	0.	1.0000	0.0909	20.0000
-77.198	-28.034	-14.530	0.	1.0000	0.0909	20.0000
101.232	7.559	18.468	0.	1.0000	0.0909	20.0000
-101.232	-41.708	-18.159	0.	1.0000	0.0909	20.0000

FREQUENCY=1000 HZ TRANSMISSION LOSS= 9.00

0.	0.	0.	0.4585	1.5652	0.0769	1.8801
15.250	4.795	11.921	0.2658	1.5143	0.0769	6.3283
-15.250	-4.795	-12.044	0.3555	1.5031	0.0769	4.2709
30.478	9.739	23.780	0.1343	1.3749	0.0769	11.8613
-30.478	-9.739	-24.276	0.2310	1.3766	0.0769	8.1028
45.717	15.021	35.657	0.1176	1.1887	0.0769	12.4894
-45.717	-15.021	-36.791	0.1716	1.1905	0.0769	10.6750
61.130	6.020	14.727	0.	1.0000	0.0769	20.0000
-61.130	-20.929	-49.759	0.1514	0.9442	0.0769	11.6474
77.198	7.559	18.468	0.	1.0000	0.0769	20.0000
-77.198	-28.034	-18.159	0.	1.0000	0.0769	20.0000
95.567	9.122	22.243	0.	1.0000	0.0769	20.0000
-95.567	-38.038	-21.795	0.	1.0000	0.0769	20.0000

FREQUENCY=1250 HZ TRANSMISSION LOSS= 8.74

0.	0.	0.	0.4585	1.5652	0.0588	1.8801
11.915	3.739	9.321	0.3209	1.5367	0.0588	4.7660
-11.915	-3.739	-9.396	0.3890	1.5228	0.0588	3.4586
23.818	7.547	18.595	0.1686	1.4415	0.0588	10.0769
-23.818	-7.547	-18.896	0.2769	1.4392	0.0588	6.5020
35.711	11.505	27.856	0.1218	1.3166	0.0588	12.5478
-35.711	-11.505	-28.539	0.2044	1.3194	0.0588	9.1726
47.629	15.717	37.148	0.1192	1.1619	0.0588	12.2968
-47.629	-15.717	-38.382	0.1674	1.1630	0.0588	10.8807
59.669	7.559	18.468	0.	1.0000	0.0588	20.0000
-59.669	-20.336	-48.517	0.1526	0.9699	0.0588	11.5977
72.051	9.122	22.243	0.	1.0000	0.0588	20.0000
-72.051	-25.626	-21.795	0.	1.0000	0.0588	20.0000
85.306	10.715	26.056	0.	1.0000	0.0588	20.0000
-85.306	-32.144	-25.442	0.	1.0000	0.0588	20.0000
101.232	12.344	29.914	0.	1.0000	0.0588	20.0000
-101.232	-41.708	-29.106	0.	1.0000	0.0588	20.0000

FREQUENCY=1600 HZ TRANSMISSION LOSS= 8.86

0.	0.	0.	0.4585	1.5652	0.0476	1.8801
9.533	2.988	7.461	0.3615	1.5495	0.0476	3.7791
-9.533	-2.988	-7.509	0.4118	1.5350	0.0476	2.9379
19.059	6.010	14.889	0.2137	1.4840	0.0476	8.1364
-19.059	-6.010	-15.081	0.3183	1.4770	0.0476	5.2606
28.576	9.107	22.299	0.1415	1.3948	0.0476	11.4644
-28.576	-9.107	-22.734	0.2426	1.3957	0.0476	7.6696

Figure 38. Typical Output (Continued).

38.091	12.324	29.710	0.1188	1.2882	0.0476	12.6840
-38.091	-12.324	-30.490	0.1947	1.2910	0.0476	9.5948
47.629	15.717	37.148	0.1195	1.1619	0.0476	12.2724
-47.629	-15.717	-38.382	0.1674	1.1630	0.0476	10.8822
57.243	9.122	22.243	0.	1.0000	0.0476	20.0000
-57.243	-19.370	-46.460	0.1538	1.0115	0.0476	11.5526
67.034	10.715	26.056	0.	1.0000	0.0476	20.0000
-67.034	-23.404	-54.801	0.1547	0.8355	0.0476	11.3803
77.198	12.344	29.914	0.	1.0000	0.0476	20.0000
-77.198	-28.034	-29.106	0.	1.0000	0.0476	20.0000
88.164	14.017	33.825	0.	1.0000	0.0476	20.0000
-88.164	-33.701	-32.791	0.	1.0000	0.0476	20.0000
101.232	15.744	37.799	0.	1.0000	0.0476	20.0000
-101.232	-41.708	-36.505	0.	1.0000	0.0476	20.0000

FREQUENCY=2000 HZ TRANSMISSION LOSS= 8.76

0.	0.	0.	0.4585	1.5652	0.0370	1.8801
7.627	2.388	5.972	0.3918	1.5572	0.0370	3.1164
-7.627	-2.388	-6.003	0.4283	1.5436	0.0370	2.5741
15.250	4.795	11.921	0.2658	1.5143	0.0370	6.3283
-15.250	-4.795	-12.044	0.3555	1.5031	0.0370	4.2709
22.867	7.238	17.854	0.1759	1.4503	0.0370	9.7300
-22.867	-7.238	-18.131	0.2846	1.4472	0.0370	6.2573
30.478	9.739	23.780	0.1343	1.3749	0.0370	11.8613
-30.478	-9.739	-24.276	0.2310	1.3766	0.0370	8.1028
38.091	12.324	29.710	0.1187	1.2882	0.0370	12.6880
-38.091	-12.324	-30.490	0.1947	1.2910	0.0370	9.5949
45.717	15.021	35.657	0.1176	1.1887	0.0370	12.4894
-45.717	-15.021	-36.791	0.1716	1.1905	0.0370	10.6750
53.383	10.715	26.056	0.	1.0000	0.0370	20.0000
-53.383	-17.871	-43.203	0.1578	1.0750	0.0370	11.3592
61.130	12.344	29.914	0.	1.0000	0.0370	20.0000
-61.130	-20.929	-49.759	0.1514	0.9442	0.0370	11.6474
69.028	14.017	33.825	0.	1.0000	0.0370	20.0000
-69.028	-24.273	-56.511	0.1588	0.7971	0.0370	11.1200
77.198	15.744	37.799	0.	1.0000	0.0370	20.0000
-77.198	-28.034	-36.505	0.	1.0000	0.0370	20.0000
85.870	17.534	41.846	0.	1.0000	0.0370	20.0000
-85.870	-32.446	-40.256	0.	1.0000	0.0370	20.0000
95.567	0.	0.	0.	1.0000	0.0370	20.0000
-95.567	-38.038	-44.054	0.	1.0000	0.0370	20.0000
108.245	0.	0.	0.	1.0000	0.0370	20.0000
-108.245	-46.766	-47.909	0.	1.0000	0.0370	20.0000

FREQUENCY=2500 HZ TRANSMISSION LOSS= 8.88

0.	0.	0.	0.4585	1.5652	0.0303	1.8801
6.053	1.895	4.742	0.4137	1.5619	0.0303	2.6714
-6.053	-1.895	-4.761	0.4401	1.5499	0.0303	2.3192
12.104	3.798	9.468	0.3176	1.5356	0.0303	4.8503
-12.104	-3.798	-9.546	0.3871	1.5217	0.0303	3.5023
18.152	5.720	14.183	0.2248	1.4916	0.0303	7.7179
-18.152	-5.720	-14.357	0.3269	1.4835	0.0303	5.0223
24.196	7.670	18.889	0.1658	1.4379	0.0303	10.2081
-24.196	-7.670	-19.200	0.2739	1.4360	0.0303	6.5984
30.237	9.659	23.592	0.1351	1.3775	0.0303	11.8156
-30.237	-9.659	-24.080	0.2324	1.3791	0.0303	8.0492
36.277	11.699	28.297	0.1209	1.3100	0.0303	12.5894
-36.277	-11.699	-29.003	0.2019	1.3128	0.0303	9.2768
42.325	13.806	33.011	0.1165	1.2345	0.0303	12.6987
-42.325	-13.806	-33.978	0.1805	1.2370	0.0303	10.2453

Figure 38. Typical Output (Continued).

48.388	15.997	37.741	0.1223	1.1511	0.0303	12.0433
-48.388	-15.997	-39.016	0.1659	1.1519	0.0303	10.9557
54.484	14.017	33.825	0.	1.0000	0.0303	20.0000
-54.484	-18.294	-44.129	0.1568	1.0572	0.0303	11.4078
60.635	15.744	37.799	0.	1.0000	0.0303	20.0000
-60.635	-20.727	-49.338	0.1522	0.9530	0.0303	11.6088
66.877	17.534	41.846	0.	1.0000	0.0303	20.0000
-66.877	-23.336	-54.666	0.1542	0.8385	0.0303	11.4140
73.263	0.	0.	0.	1.0000	0.0303	20.0000
-73.263	-26.180	-44.054	0.	1.0000	0.0303	20.0000
79.881	0.	0.	0.	1.0000	0.0303	20.0000
-79.881	-29.348	-47.909	0.	1.0000	0.0303	20.0000
86.881	0.	0.	0.	1.0000	0.0303	20.0000
-86.881	-32.995	-51.837	0.	1.0000	0.0303	20.0000
94.570	0.	0.	0.	1.0000	0.0303	20.0000
-94.570	-37.426	-55.857	0.	1.0000	0.0303	20.0000
103.776	0.	0.	0.	1.0000	0.0303	20.0000
-103.776	-43.472	-53.120	0.	1.0000	0.0303	20.0000

FREQUENCY=3150 HZ TRANSMISSION LOSS= 8.77

0.	0.	0.	0.4585	1.5652	0.0233	1.8801
4.767	1.492	3.736	0.4289	1.5645	0.0233	2.3815
-4.767	-1.492	-3.748	0.4481	1.5544	0.0233	2.1472
9.533	2.988	7.461	0.3615	1.5495	0.0233	3.7791
-9.533	-2.988	-7.509	0.4118	1.5350	0.0233	2.9379
14.297	4.492	11.178	0.2809	1.5212	0.0233	5.8703
-14.297	-4.492	-11.286	0.3651	1.5090	0.0233	4.0316
[illegible]	6.010	14.889	0.2137	1.4840	0.0233	8.1364
[illegible]	-6.010	-15.081	0.3183	1.4770	0.0233	5.2606
[illegible]	7.547	18.595	0.1685	1.4415	0.0233	10.0769
-23.818	-7.547	-18.896	0.2769	1.4392	0.0233	6.5020
28.576	9.107	22.299	0.1415	1.3948	0.0233	11.4644
-28.576	-9.107	-22.734	0.2426	1.3957	0.0233	7.6696
33.332	10.697	26.003	0.1263	1.3438	0.0233	12.3053
-33.332	-10.697	-26.597	0.21[illegible]	1.3463	0.0233	8.7093

Figure 38. Typical Output (Continued).

38.091	12.324	29.710	0.1188	1.2882	0.0233	12.6840
-38.091	-12.324	-30.490	0.1947	1.2910	0.0233	9.5948
42.854	13.994	33.424	0.1168	1.2275	0.0233	12.6581
-42.854	-13.994	-34.416	0.1790	1.2299	0.0233	10.3182
47.629	15.717	37.148	0.1195	1.1619	0.0233	12.2724
-47.629	-15.717	-38.382	0.1674	1.1630	0.0233	10.8822
52.422	17.505	40.888	0.1380	1.0939	0.0233	10.8213
-52.422	-17.505	-42.394	0.1592	1.0902	0.0233	11.2929
57.243	0.	0.	0.	1.0000	0.0233	20.0000
-57.243	-19.370	-46.460	0.1538	1.0115	0.0233	11.5526
62.107	0.	0.	0.	1.0000	0.0233	20.0000
-62.107	-21.329	-50.592	0.1521	0.9267	0.0233	11.5943
67.034	0.	0.	0.	1.0000	0.0233	20.0000
-67.034	-23.404	-54.801	0.1547	0.8355	0.0233	11.3808
72.051	0.	0.	0.	1.0000	0.0233	20.0000
-72.051	-25.626	-55.857	0.	1.[illegible]	0.0233	20.0000
77.198	0.	0.	0.	1.0000	0.0233	20.0000
-77.198	-28.034	-53.120	0.	1.0000	0.0233	20.0000
82.536	0.	0.	0.	1.0000	0.0233	20.0000
-82.536	-30.693	0.	0.	1.0000	0.0233	20.0000
88.164	0.	0.	0.	1.0000	0.0233	20.0000
-88.164	-33.701	0.	0.	1.0000	0.0233	20.0000
94.263	0.	0.	0.	1.0000	0.0233	20.0000
-94.263	-37.239	0.	0.	1.0000	0.0233	20.0000
101.232	0.	0.	0.	1.0000	0.0233	20.0000
-101.232	-41.708	0.	0.	1.0000	0.0233	20.0000
110.472	0.	0.	0.	1.0000	0.0233	20.0000
-110.472	-48.510	0.	0.	1.0000	0.0233	20.0000

FREQUENCY=4000 HZ   TRANSMISSION LOSS= 8.84

Figure 38. Typical Output (Concluded).

APPENDIX B

GENERALIZED ITERATIVE PROCEDURE COMPUTER PROGRAM

The matrix inversion procedure cannot be used for turbines containing choked blade rows because the matrices decouple at these rows. The problem is really that it becomes impossible to determine the three downstream amplitudes (F_m, B_m, Q_m) because one of the three available equations is independent of the downstream amplitudes for a choked row. However, it remains possible to calculate F_m, B_n, and Q_m in terms of F_n, B_m, and Q_n. The solution procedure utilized here exploits this fact. The value of B_m is guessed at each choked blade row. The amplitudes F_n and Q_n from the computations for the preceding row are used in the choked flow equation to calculate a B_n*. If B_n* is not the same as the B_n from the immediately preceding computations, the program returns to the last blade row where B was guessed, and a new guess is made. If B_n* agrees with B_n, then F_m and Q_m are calculated using the other two equations available at that blade row, and the program continues to the next row. The final verification of a correct guess is made at the last blade row where the assumption of an anechoic termination requires $B_m = 0$.

This procedure is summarized in the flow chart of Figure 39. Each choked blade row entails verification of the last guess in the form of $B_n = B_n*$? Once this is achieved, a new guess (B_m) follows. The final verification is $(B_m)_{last\ stage} = 0$. The one deviation is at the first blade row; if this is unchoked, the program guesses at B_1. Since $F_1 = 1$, $Q_1 = 0$, F_2, B_2, and Q_2 can be calculated.

A listing of the program can be found in Figure 40, and a sample output is provided in Figure 41. Both input and output frequency distribution and energy assignment are the same as in the matrix inversion program.

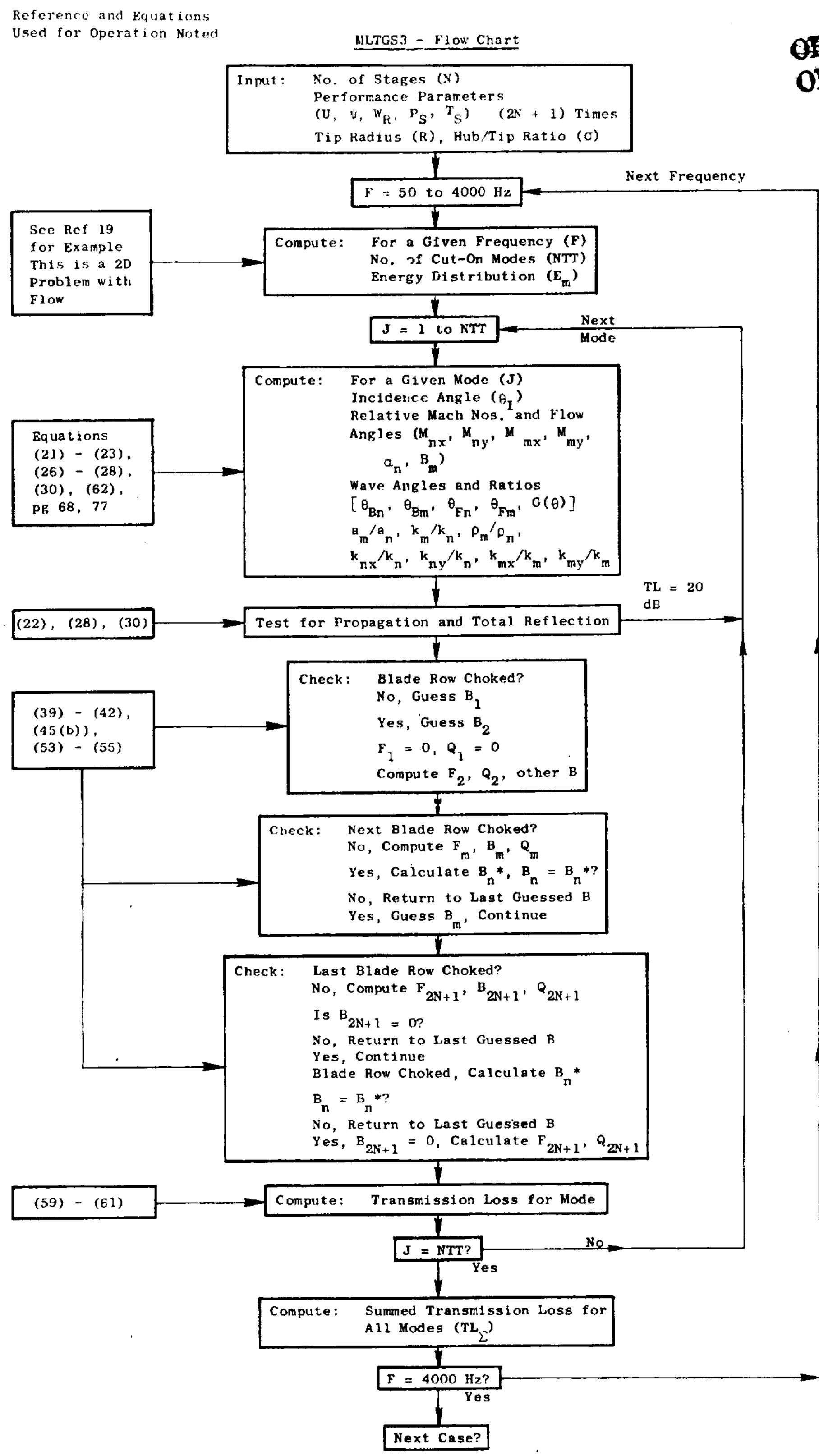

Figure 39. Flow Chart - Mutistage, Multimode Computer Program Using Iterative Solution.

********** MLTGS3 **********

```
*#RUNH *;
*#LIBRARY/MTINV,R=(ULIB)USERLIB/TDS,R
C      ******* FILENAME MLTGS3 *******
        COMMON /CANGP / PI,TODEG,TORAD
        COMMON /CINPUT/ NSTAGE,IOPT,IPRINT,PTO,TTO,STAGEX(5,15),
&                        NSTA,TITLE
        CHARACTER TITLE*40
        COMMON /CUTOFA/ THCL,THCU
        COMMON /CAERO / V(15),MX(15),MY(15),AMQAN(15),RHORAT(15),
&                    MACH(15),AS(15)
 REAL KNQKM(15),MX,MY,MACH,MABS
        INTEGER FREQ(20)
        EQUIVALENCE  (KNQKM,AMQAN)
        COMMON /CAEROI/ U(15),PHI(15),VR(15),P(15),T(15),GAM(15)
        COMMON /COUT   / TLOSS(100),THI(100),THR(100),THT(100),
&                        Q(100),B(100),B1(100),TW(100),F(100)
        COMMON /CMATRX/ D(3,3,15),DI(3,3,15),A(3,3,15),PROD(3,3,15)
        COMMON /CATTCH/ CF1,CF2,CF3,BUF(380)

        DIMENSION  STAGEP(75)
        DIMENSION  SMACH(15)
        DIMENSION  E(100)
        EQUIVALENCE (STAGEP(1),STAGEX(1,1))
        CHARACTER CF1*1/"/"/,CF2*8,CF3*1/";"/
        CHARACTER TITLE*40,BLANK*40
        REAL  MACHN,MACHM,KMYKM,KNYKN,KMXKM,KNXKN,KMYSAV,KMXSAV,
&             KNN,KMM
        EQUIVALENCE (IBITS,BITS)

        DATA BITS/03777777777777/,OKA/0403700000000/,JPO/0040075040007/
        DATA RO,SIGMA/11.5,0.882/
        DATA FREQ/50,63,80,100,125,160,200,250,315,400,500,
&                630,800,1000,1250,1600,2000,2500,3150,4000/
        DATA PI,TODEG,TORAD/3.1415927,57.29578,.0174532925/
        DATA BLANK/"                                        "/

        NAMELIST /TNOISE/ IOPT,PTO,TTO,STAGEP,TITLE,GAM,IAERO
        TAN(X)= SIN(X)/COS(X)

C      SET UP NAMELIST INPUT FILE

        IAERO = 0
        CALL FPARAM(3,JPO)
        PRINT," INPUT FILE NAME "
        READ,CF2
        CALL ATTACH(1,CF1,1,0,STAT,BUF)
        IF( STAT.EQ.0. .OR. STAT.EQ.OKA ) GO TO 5
```

Figure 40. Program Listing - Generalized Iterative Procedure.

```
        PRINT 1,STAT
      1 FORMAT(" INPUT FILE STATUS=",O12)
        STOP

C     INITIALIZATION *********************

      5 IOPT   = 1
        DO 10 I=1,15
        STAGEX(1,I)= BITS
        GAM(I)= BITS
     10 CONTINUE
        PTO    = 14.696
        TTO    = 518.7
        TITLE = BLANK

C     READ INPUT FILE **** COUNT NP. OF STATIONS

     15 (I, TNOISE, END = 400)

        DO 17 I=1,15
        IF(STAGEX(1,I).EQ.BITS ) GO TO 18
        U(I)    = STAGEX(1,I) * 3.048
        PHI(I)  = STAGEX(2,I)
        VR(I)   = STAGEX(3,I) * 3.048
        P(I)    = STAGEX(4,I) / 6.895
        T(I)    = STAGEX(5,I) * 1.8
        IF( GAM(I).NE.BITS ) GO TO 17
        GAM(I)= GAMX(T(I))
     17 CONTINUE
     18 NSTA   = I-1
        IF( NSTA.EQ.14 ) NSTA=15
        NSTAGE= (NSTA-1)/2
        PRINT 21,TITLE,NSTAGE
     21 FORMAT(//16X,A40//32X,I2,"  STAGES"//)
        PRINT 22
     22 FORMAT(28X,"* AERO-THERMO PARAMETERS *"//
     &   2X,"STAGE",3X,"STATION",3X,"U- FPS",3X,"PHI- DEG",
     &   3X,"VR- FPS",2X,"PS- PSIA",2X,"TS- DEG R"/)
         NSTG   = 0
        DO 24 I=1,NSTA
        IF(((I/2)*2)/I.EQ.0 ) NSTG=NSTG+1
        IF( I.EQ.NSTA ) NSTG=IBITS
        PRINT 23,NSTG,I,U(I),PHI(I),VR(I),P(I),T(I)
     23 FORMAT(4X,I1,7X,I2,F12.3,4F10.3)
     24 CONTINUE
        IF( IAERO.EQ.0. ) GO TO 27
        PRINT 25
     25 FORMAT(/2X,"STAGE",3X,"STATION",5X,"MX",8X,"MY",
     &             7X,"MACH",5X,"KNOKM",7X,"V"/)
        NSTG   = 0
        DO 26 I=1,NSTA
```

Figure 40. Program Listing - Generalized Iterative Procedure (Continued).

```
      IF(((I/2)*2)/I.EQ.0 ) NSTG=NSTG+1
      IF( I.EQ.1 ) GO TO 26
      PRINT 23,NSTG,I,MX(I),MY(I),MACH(I),KNOKM(I),V(I)
   26 CONTINUE
   27 CONTINUE
   28 FORMAT(//2X,'THETA-I',3X,'THETA-R',3X,'THETA-T',6X,
&            'T',9X,'B',9X,'E',6X,'T-LOSS'/)

C     CALCULATE AERO-THERMO PARAMETERS

      DO 29 I=1,NSTA
      AS(I) = 41.42*SQRT(GAM(I)*T(I))
      MX(I) = U(I)/AS(I)
      IF( I.EQ.1 ) GO TO 29
      AMQAN(I)= SQRT(GAM(I)*T(I)/(GAM(I-1)*T(I-1)))
      RHORAT(I)= T(I)*P(I-1)/(T(I-1)*P(I))
   29 CONTINUE

      AS1 = AS(1)
      RMEAN= RO*SQRT((1.+SIGMA**2)/2.)
      RMEAN = RMEAN/2.54
      FP1 = 1.
      FREQCO= ((FP1*(AS1*12.))/(2.*PI*RMEAN))*SQRT(1.-XM1**2)
      FREQC1= AINT(FREQCO)
      PRINT 30,FREQC1
      PRINT 28
   30 FORMAT(//10X,'**** FIRST CUT-ON OCCURS AT',1X,F4.0,1X,
&           'HZ ****'///)
      DO 300 L=1,20
      FP = (2.*PI*FREQ(L)*RMEAN)/(AS1*12.)
      XM1 = MX(1)
       NTH=FP/SQRT(1.-XM1**2)
      IF( NTH.GT.50 ) NTH=50
      NTT = 2*NTH+1
      FRSQ= 0.
      THI(1)= 0.
      DO 32 J=1,NTT
      E(J)= 0.
   32 CONTINUE
      E(1)= 1.
      ESIGMA= 1.
      THI(1)= 0.
      IF( NTH.LT.1 ) GO TO 50
C    **** COMPUTE CUT-ON MODES, ANGLES, AND ENERGY
      DO 40 J=1,NTH
      FJ = J
      F1=FP/FJ
      F2 = SQRT(F1**4-F1**2*(1.-XM1**2))
      F3 = XM1**2+F1**2
      F4 = (F2-XM1)/F3
      J1 = 2*J
```

Figure 40. Program Listing - Generalized Iterative Procedure (Continued).

```
      J2 = 2*J+1
      THI(1)= 0.
      THI(J1)= TODEG*ARCOS(F4)
      THI(J2)= -THI(J1)
      FC = (FJ*AS1*12.)/(2.*PI*RMEAN)
      FC = FC*SQRT(1.-XM1**2)
      FRSQ = FC/FREQ(L)
      IF( FRSQ.GT.1.025 ) GO TO 40
      E(J1) = 1.
      E(J2)= E(J1)
      ESIGMA= ESIGMA+2.*E(J1)
   40 CONTINUE
   50 CONTINUE
C    **** COMPUTE ENERGY DISTRIBUTION
      DO 60 K=1,J2
      E(K)= E(K)/ESIGMA
   60 CONTINUE
C    ****** INNER LOOP TO BUILD MATRICES *****
      SUMT= 0.
      DO 240 K=1,NTT
   62 THFN    = THI(K)*TORAD
      KMYSAV= 0.
      KMXSAV= 0.
      NGS    = 1
      MISTAK = 1
      F(1) = 1.0
      B(1) = -30.
      Q(1) = 0.
      M      = 1
   65 M      = M+1
      IF( M.GT.NSTA ) GO TO 95
C    CALCULATE ANGLES AND RATIOS
   66 N      = M - 1
      V(N)   = U(N)*TAN(TORAD*PHI(N))-VR(N)
      V(M)   = U(M)*TAN(TORAD*PHI(M))-VR(N)
      MY(N)  = V(N)/AS(N)
      MY(M)  = V(M)/AS(M)
      MACH(N)= SQRT(MX(N)**2+MY(N)**2)
      MACH(M)= SQRT(MX(M)**2+MY(M)**2)
      N      = M-1
      PHIN= PHI(N)*TORAD
      GA = GAM(I)
      GB = (GA+1.)/(2.*(GA-1.))
      AASTAR = ((2.+(GA-1.)*MACH(M)**2)/(GA+1.))**GB/MACH(M)
      XMN    = 1.-MX(N)**2
```


Figure 40. Program Listing - Generalized Iterative Procedure (Continued).

```
      XPN    = 1.+MX(N)**2
      XMM    = 1.-MX(M)**2
      SINN   = SIN(THFN)
      COSN   = COS(THFN)
C**** CHECK FOR UPSTREAM PROPAGATION

      PHSPD= U(N)+AS(N)*COSN
      IF( PHSPD.LE.0. ) GO TO 175
      GMN    = KNQKM(M)*SINN/(1.+MX(N)*COSN+MY(N)*SINN)
      TN     = XMN*SINN
      TD     = XPN*COSN+2.*MX(N)
      THBN   = ATAN2( TN,TD )
      TERM   = -GMN*MX(M)*(1.-GMN*MY(M))
C**** CHECK FOR TOTAL REFLECTION

      RDCL= (1.-GMN*MY(M))**2-XMM*GMN**2
      IF( RDCL.LE.0. ) GO TO 175
      RADICL= GMN*SQRT(RDCL)
      TN = -TERM+RADICL
      TD     = (1.-GMN*MY(M))**2-GMN**2
      THFM   = ATAN2( TN,TD )
      IF( N.NE.1 ) GO TO 70
      THR(K)= TODEG*THBN
   70 THBM   = ATAN2( TN-2.*TERM , TD )
      MACHM = MACH(M)
      MACHN = MACH(N)
      ALFAN = ATAN2( MY(N),MX(N) )
      BETAM = ATAN2( MY(M) , MX(M) )
      IF( MACH(M).LT.1. ) GO TO 71
      DOT    = COS(BETAM)
      BM     = BETAM
      BETAM = ARCOS(AASTAR*DOT)
      BETAM = SIGN(1,BM)*BETAM
   71 CONTINUE
      KMYKM = GMN
      KNYKN = KMYSAV
      KMXKM = (1.-GMN*MY(M))/MX(M)
      KNXKN = KMXSAV
      KMYSAV= KMYKM
      KMXSAV= KMXKM
      QKNN   = 0.
      IF( N.EQ.1 ) GO TO 75
      QKNN    = 1./SQRT(KNXKN**2+KNYKN**2)
   75 QKMM   = 1./SQRT(KMXKM**2+KMYKM**2)
      A(1,1,N)= MX(N)+COS(THFN)
      A(1,2,N)= MX(N)-COS(THBN)
      A(1,3,N)= KNYKN*QKNN
      A(2,1,N)= 1.+MACHN*COS(ALFAN-THFN)
      A(2,2,N)= 1.-MACHN*COS(ALFAN+THBN)
      A(2,3,N)= QKNN*(MX(N)*KNYKN-MY(N)*KNXKN)
      D(1,1,N)= (MX(M)+COS(THFM))/AMQAN(M)
```

Figure 40. Program Listing - Generalized Iterative Procedure (Continued).

```
      D(1,2,N)= (MX(M)-COS(THBM))/AMQAN(M)
      D(1,3,N)= KMYKM*QKMM/AMQAN(M)
      D(2,1,N)= RHORAT(M)*(1.+MACHM*COS(BETAM-THFM))
      D(2,2,N)= RHORAT(M)*(1.-MACHM*COS(BETAM+THBM))
      D(2,3,N)= RHORAT(M)*(QKMM*(MX(M)*KMYKM-MY(M)*KMXKM))
      A(3,1,N)= 0.
      A(3,2,N)= 0.
      A(3,3,N)= 0.
      D(3,1,N)= SIN(BETAM-THFM)
      D(3,2,N)= -SIN(BETAM+THBM)
      D(3,3,N)= QKMM*(KMYKM*SIN(BETAM)+KMXKM*COS(BETAM))
      SMACH(M)=0.
      IF( MACH(M).GT.1. ) GO TO 90
      GO TO 80
   78 FORMAT(5X,'***DOWNSTREAM RELATIVE FLOW AT ROW',I3,
&              1X,'IS SUPERSONIC***'///)
C    ***** COMPUTE INVERSE OF MATRIX AND STORE

   80 CALL DINVER( N )
C    ***** COMPUTE MATRIX PRODUCT *****
      GO TO 155

   90 SMACH(M)=1.
   92 MABS= SQRT(MX(N)**2+(MY(N)+VR(N)/AS(N))**2)
      F5= (GAM(N)+1.)*MABS
      F6= 2.*(1.+MABS**2*(GAM(N)-1.)/2.)/MX(N)
      F7= (GAM(N)-1.)*(MABS**2-1.)
      A(3,1,N)= F7+F6*COS(THFN)-F5*COS(PHIN-THFN)
      A(3,2,N)= F7-F6*COS(THBN)+F5*COS(PHIN+THBN)
      A(3,3,N)= F6*KNYKN-F5*(KNYKN*COS(PHIN)-KNXKN*SIN(PHIN))
      D(3,1,N)=0. ; D(3,2,N)=0. ; D(3,3,N)=0.
      GO TO 65
   95 M    = 1
      BAG=0.
  100 M = M + 1
      IF( M.GT.NSTA ) GO TO 150
      N    = M - 1
      IF( SMACH(M).EQ.1. ) GO TO 110
      IF( MISTAK.EQ.0 ) B(N) = B(N) + 0.01
      BGN1=B(1)
      B1(K)= BGN1
      GO TO 160
  110 CONTINUE

      BGS = B(N)
      B(N) = -(A(3,1,N)*F(N) + A(3,3,N)*Q(N))/A(3,2,N)
      B1(K) = B(1)
      IF( N.GT.1 ) GO TO 123
      B(N+1) = -30.
      IF( FREQ(L).EQ.1600 ) B(N+1)= -85.
      GO TO 130
```

Figure 40. Program Listing - Generalized Iterative Procedure (Continued).

```
  123 GNB = ABS(BGS-B(N))
      B(N+1) = -40.
      IF( M.EQ.NSTA ) B(N+1)= 0.
      IF( GNB.LT.0.05 ) GO TO 130
      IF( NGS.GT.1 ) GO TO 125
      MISTAK = 0
      M = NGS
      GO TO 100
  125 B(NGS) = BGS+.01
      M = NGS
      N  = NGS - 1
  130 NGS= N + 1
      C1= A(1,1,N)*F(N) + A(1,2,N)*B(N) + A(1,3,N)*Q(N)
&         D(1,2,N)*B(N+1)
      C2= A(2,1,N)*F(N) + A(2,2,N)*B(N) + A(2,3,N)*Q(N)
&         D(2,2,N)*B(N+1)
      F(N+1)= (D(2,3,N)*C1 - D(1,3,N)*C2)/
&              ((D(1,1,N)*D(2,3,N)) - (D(2,1,N)*D(1,3,N)))
      IF( THI(K).GT.0. ) GO TO 135
      IF( THI(K).LT.0. ) GO TO 135
      Q(N+1)= (C2-D(2,1,N)*F(N+1))/D(2,3,N)
      GO TO 140
  135 Q(N+1)= (C1-D(1,1,N)*F(N+1))/D(1,3,N)
  140 CONTINUE
      GO TO 100
  150 CONTINUE
      IF(B(N+1).EQ.0.) GO TO 152
      IF(BAG.EQ.0.) BAG=B(N+1)
      BAT= B(N+1)/BAG
      IF(BAT.LT.0.) GO TO 152
      BAG = B(N+1)
      GO TO 165
  152 FN(K)= F(N+1)
      Q(K) = Q(N+1)
      B(K)= B1(K)
      THT(K)= THFM*TODEG
      GO TO 170

  155 CALL  MAPROD ( N )
      THFN = THFM
      GO TO 65

C     ***** STORE AMPLITUDES


  160 F(N+1)= F(N)*PROD(1,1,N)+B(N)*PROD(1,2,N)+Q(N)*PROD(1,3,N)
      B(N+1)= F(N)*PROD(2,1,N)+B(N)*PROD(2,2,N)+Q(N)*PROD(2,3,N)
      Q(N+1)= F(N)*PROD(3,1,N)+B(N)*PROD(3,2,N)+Q(N)*PROD(3,3,N)
      GO TO 100
  165 CONTINUE
      IF( NGS.GT.1 ) BGS=B(NGS)
```

Figure 40. Program Listing - Generalized Iterative Procedure (Continued).

```
      IF( NGS.EQ.1 ) GO TO 167
      GO TO 125
 167  B(1) = B(1) + .0001
      M = 2
      N  = 1
      GO TO 160
C    ***** COMPUTE TRANSMISSION LOSS
 170  AS1    = AS(1)
      ASN    = AS(NSTA)
      MX(1) = U(1)/AS1
      MX(NSTA)= U(NSTA)/ASN
      VV1    = U(1)*TAN(TORAD*PHI(1))
      VVN    = U(NSTA)*TAN(TORAD*PHI(NSTA))
      MY(1) = VV1/AS1
      MY(NSTA)= VVN/ASN
      RHORA = P(NSTA)*T(1)*ASN/(P(1)*T(NSTA)*AS1)
      TERM2 = (1.+MX(NSTA)*COS(THFM)+
&      (MY(NSTA)+VR(NSTA-1)/ASN)*SIN(THFM))*(COS(THFM)+MX(NSTA))
      THIN   = THI(K)*TORAD
      TERM1 = (1.+MX(1)*COS(THIN)+MY(1)*
&                      SIN(THIN))*(COS(THIN)+MX(1))
      TLOSS(K)= 10.*ALOG10(RHORA*ABS(TERM1/TERM2)/TW(K)**2)
      IF( TW(K).LT.0. ) GO TO 177
      IF( TW(K).GE.1. ) GO TO 177
      IF( TLOSS(K).LT.0. ) TLOSS(K) = 1.
      GO TO 180
 175  TLOSS(K)= 20.
      B1(K) = 1.
      GO TO 178
 177  TLOSS(K) = 25.
 178  TW(K) = 0.
 180  CONTINUE
      SUMI= 1.
      TL = TLOSS(K)/10.
      SUMT= SUMT+E(K)/10.**TL
C    ***** PRINT OUTPUT
      PRINT 235,THI(K),THR(K),THT(K),TW(K),B1(K),E(K),TLOSS(K)
 235  FORMAT(F9.3,2F10.3,F9.4,3F10.4)
 240  CONTINUE
      TLSIGMA = 10.*ALOG10(SUMI/SUMT)
      PRINT 245,FREQ(L),TLSIGMA
 245  FORMAT(/14X,'FREQUENCY=',I4,1X,'HZ',5X,
&            'TRANSMISSION LOSS=',F6.2////)
 300  CONTINUE
      GO TO 15
 400  STOP
      END
```

Figure 40. Program Listing - Generalized Iterative Procedure (Continued).

```
CGAMX        FUNCTION GAMX(T)
      FUNCTION GAMX(T)
      IF( T.LE.800. ) GO TO 10
      IF( T.GE.3600. ) GO TO 12
      GAMX  = 2.23708/T**.070271
      GO TO 15
   10 GAMX  = 1.4
      GO TO 15
   12 GAMX  = 1.254
   15 RETURN
      END
CDINVER        CALCULATE INVERSE OF MATRIX D
      SUBROUTINE  DINVER( N )
      COMMON /CMATRX/ D(3,3,15),DI(3,3,15),A(3,3,15),PROD(3,3,15)
      DIMENSION DD(9,15),DDI(9,15),LABEL(3)
      EQUIVALENCE (DD(1,1),D(1,1,1)),(DDI(1,1),DI(1,1,1))
      DIMENSION  TEMP(3,3)
      DIMENSION  AA(9,15)
      EQUIVALENCE (AA(1,1),A(1,1,1))
      NN    = N
      DO 10 I=1,9
      DDI(I,N)= DD(I,N)
   10 CONTINUE
      CALL MTINV(DDI(1,N),3,3,3,LABEL)
   20 RETURN
C     **** ENTRY  MAPROD ** COMPUTE PRODUCT OF DI AND A
      ENTRY  MAPROD( N )
      NN    = N
      L = NN
      DO 60 J=1,3
      DO 50 I=1,3
      TEMP(I,J)= 0.
      DO 40 K=1,3
      TEMP(I,J)= TEMP(I,J)+DI(I,K,L)*A(K,J,L)
   40 CONTINUE
   50 CONTINUE
   60 CONTINUE
      DO 100 J=1,3
      DO 100 I=1,3
  100 PROD(I,J,L) = TEMP(I,J)
  200 RETURN
      END
      STOP
```

Figure 40. Program Listing - Generalized Iterative Procedure (Concluded).

```
07/13/77    09.031

LOADER DIAGNOSTICS
<W> ...... LOADED PREVIOUSLY

 INPUT FILE NAME = DFLP39

                NASA CORE HOT HPT: 3.0 PR  100% N

                           1  STAGES

                     * AERO-THERMO PARAMETERS *

STAGE   STATION   U- FPS    PHI- DEG    VR- FPS   PS- PSIA  TS- DEG R
  1        1     388.000     0.           0.       54.730   1375.000
  1        2     512.000    67.300      819.000    36.490   1251.000
           3     857.000   -38.300        0.       18.230   1050.000

      **** FIRST CUT-ON OCCURS AT 369. HZ ****

THETA-I   THETA-R   THETA-T     T         B         E       T-LOSS
  0.        0.        0.      0.2808    0.9600    1.0000    4.7659

        FREQUENCY=  50 HZ     TRANSMISSION LOSS=  4.77


  0.        0.        0.      0.2808    0.9600    1.0000    4.7659

        FREQUENCY=  63 HZ     TRANSMISSION LOSS=  4.77


  0.        0.        0.      0.2808    0.9600    1.0000    4.7659

        FREQUENCY=  80 HZ     TRANSMISSION LOSS=  4.77


  0.        0.        0.      0.2808    0.9600    1.0000    4.7659

        FREQUENCY= 100 HZ     TRANSMISSION LOSS=  4.77


  0.        0.        0.      0.2808    0.9600    1.0000    4.7659

        FREQUENCY= 125 HZ     TRANSMISSION LOSS=  4.77


  0.        0.        0.      0.2808    0.9600    1.0000    4.7659

        FREQUENCY= 160 HZ     TRANSMISSION LOSS=  4.77


  0.        0.        0.      0.2808    0.9600    1.0000    4.7659
```

Figure 41. Sample Output.

FREQUENCY= 200 HZ   TRANSMISSION LOSS= 4.77

0.	0.	0.	0.2808	0.9600	1.0000	4.7659

FREQUENCY= 250 HZ   TRANSMISSION LOSS= 4.77

0.	0.	0.	0.2808	0.9600	1.0000	4.7659

FREQUENCY= 315 HZ   TRANSMISSION LOSS= 4.77

0.	0.	0.	0.2808	0.9600	0.3333	4.7659
76.385	0.	0.	0.	1.0000	0.3333	20.0000
-76.385	-53.807	0.	0.	1.0000	0.3333	20.0000

FREQUENCY= 400 HZ   TRANSMISSION LOSS= 9.28

0.	0.	0.	0.2808	0.9600	0.3333	4.7659
56.016	0.	0.	0.	1.0000	0.3333	20.0000
-56.016	-37.869	-79.743	0.3443	0.1700	0.3333	5.8353

FREQUENCY= 500 HZ   TRANSMISSION LOSS= 6.96

0.	0.	0.	0.2808	0.9600	0.3333	4.7659
42.856	28.409	37.114	0.	0.7300	0.3333	25.0000
-42.856	-28.409	-58.120	0.4122	0.1200	0.3333	2.7835

FREQUENCY= 630 HZ   TRANSMISSION LOSS= 5.41

0.	0.	0.	0.2808	0.9600	0.2000	4.7659
33.098	21.698	30.422	0.2810	0.7300	0.2000	4.4967
-33.098	-21.698	-43.183	0.5850	-0.3500	0.2000	1.0000
76.385	0.	0.	0.	1.0000	0.2000	20.0000
-76.385	-53.807	0.	0.	1.0000	0.2000	20.0000

FREQUENCY= 800 HZ   TRANSMISSION LOSS= 5.22

0.	0.	0.	0.2808	0.9600	0.2000	4.7659
26.206	17.076	25.098	0.2811	0.7800	0.2000	4.6035
-26.206	-17.076	-33.188	0.	-8.8000	0.2000	[illegible]
56.016	0.	0.	0.	1.0000	0.2000	20.0000
-56.016	-37.869	-79.743	0.3443	0.1700	0.2000	5.8353

FREQUENCY=1000 HZ   TRANSMISSION LOSS= 7.19

0.	0.	0.	0.2808	0.9600	0.1429	4.7659
20.835	13.525	20.593	0.2729	0.8200	0.1429	4.9128
-20.835	-13.525	-25.742	0.	2.0000	0.1429	25.0000
43.237	23.676	37.355	0.	0.7200	0.1429	25.0000
-43.237	-23.676	-58.721	0.4092	0.1300	0.1429	2.8780
71.545	0.	0.	0.	1.0000	0.1429	20.0000

Figure 41. Sample Output (Continued).

-71.545	-49.848	-112.284	0.3437	0.0300	0.1429	11.9307

FREQUENCY=1250 HZ TRANSMISSION LOSS= 7.47

0.	0.	0.	0.2808	0.9600	0.1111	4.7659
16.209	10.495	16.455	0.2766	0.8500	0.1111	4.8281
-16.209	-10.495	-19.588	0.1495	1.3600	0.1111	10.4055
33.098	21.698	30.422	0.281[illegible]	0.7300	0.1111	4.4967
-33.098	-21.698	-43.183	0.5850	-0.3500	0.1111	1.0000
51.832	0.	0.	0.	1.0000	0.1111	20.0000
-51.832	-34.802	-72.654	0.3594	0.1800	0.1111	4.8793
76.385	0.	0.	0.	1.0000	0.1111	20.0000
-76.385	-53.807	0.	0.	1.0000	0.1111	20.0000

FREQUENCY=1600 HZ TRANSMISSION LOSS= 6.00

0.	0.	0.	0.2808	0.9600	0.0909	4.7659
12.938	8.365	13.382	0.2809	0.8700	0.0909	4.7115
-12.938	-8.365	-15.383	0.2073	1.1900	0.0909	7.5142
26.206	17.076	25.098	0.2811	0.7800	0.0909	4.6035
-26.206	-17.076	-33.188	0.	-8.8000	0.0909	25.0000
40.266	26.606	35.433	0.	1.0200	0.0909	25.0000
-40.266	-26.606	-54.069	0.4374	0.0700	0.0909	2.0704
56.016	0.	0.	0.	1.0000	0.0909	20.0000
-56.016	-37.869	-79.743	0.3443	0.1700	0.0909	5.8353
76.385	0.	0.	0.	1.0000	0.0909	20.0000
-76.385	-53.807	0.	0.	1.0000	0.0909	20.0000

FREQUENCY=2000 HZ TRANSMISSION LOSS= 7.16

0.	0.	0.	0.2808	0.9600	0.0769	4.7659
10.335	6.676	10.849	0.2752	0.8900	0.0769	4.8978
-10.335	-6.676	-12.128	0.2271	1.1200	0.0769	6.6908
20.835	13.525	20.593	0.2729	0.8200	0.0769	4.9128
-20.835	-13.525	-25.742	0.	2.0000	0.0769	25.0000
31.700	20.754	29.384	0.2822	0.7400	0.0769	4.4865
-31.700	-20.754	-41.118	0.6498	-0.5500	0.0769	1.0000
43.237	28.676	37.355	0.	0.7200	0.0769	25.0000
-43.237	-28.676	-58.721	0.4092	0.1300	0.0769	2.8780
56.016	0.	0.	0.	1.0000	0.0769	20.0000
-56.016	-37.869	-79.743	0.3443	0.1700	0.0769	5.8353
71.545	0.	0.	0.	1.0000	0.0769	20.0000
-71.545	-49.848	-112.284	0.3437	0.0300	0.0769	11.9307

FREQUENCY=2500 HZ TRANSMISSION LOSS= 6.07

0.	0.	0.	0.2808	0.9600	0.0588	4.7659
8.195	5.291	8.706	0.2840	0.9000	0.0588	4.6343
-8.195	-5.291	-9.511	0.2454	1.0700	0.0588	5.9928
16.470	10.666	16.695	0.2721	0.8500	0.0588	4.9678
-16.470	-10.666	-19.928	0.1427	1.3800	0.0588	10.8168
24.918	16.220	24.046	0.2780	0.7900	0.0588	4.7129
-24.918	-16.220	-31.373	0.	12.5800	0.0588	25.0000
33.655	22.076	30.831	0.3049	0.7200	0.0588	3.7790
-33.655	-22.076	-44.012	0.5640	-0.2800	0.0588	1.0000
42.856	28.409	37.114	0.	0.7300	0.0588	25.0000
-42.856	-28.409	-58.120	0.4122	0.1200	0.0588	2.7835
52.809	0.	0.	0.	1.0000	0.0588	20.0000

Figure 41. Sample Output (Continued).

-52.809	-35.513	-74.288	0.3556	0.1800	0.0588	5.0964
64.109	0.	0.	0.	1.0000	0.0588	20.0000
-64.109	-43.985	-94.481	0.3290	0.1200	0.0588	7.9328
78.514	0.	0.	0.	1.0000	0.0588	20.0000
-78.514	-55.586	0.	0.	1.0000	0.0588	20.0000

FREQUENCY=3150 HZ TRANSMISSION LOSS= 6.37

0.	0.	0.	0.2808	0.9600	0.0435	4.7659
6.449	4.162	6.919	0.2871	0.9100	0.0435	4.5451
-6.449	-4.162	-7.418	0.2551	1.0400	0.0435	5.6418
12.938	8.365	13.382	0.2809	0.8700	0.0435	4.7115
-12.938	-8.365	-15.383	0.2073	1.1900	0.0435	7.5142
19.507	12.653	19.430	0.2704	0.8300	0.0435	5.0045
-19.507	-12.653	-23.951	0.0402	1.7100	0.0435	21.8824
26.206	17.076	25.098	0.2811	0.7800	0.0435	4.6035
-26.206	-17.076	-33.188	0.	-8.8000	0.0435	25.0000
33.098	21.698	30.422	0.2810	0.7300	0.0435	4.4967
-33.098	-21.698	-43.183	0.5850	-0.3500	0.0435	1.0000
40.266	26.606	35.433	0.	1.0200	0.0435	25.0000
-40.266	-26.606	-54.069	0.4374	0.0700	0.0435	2.0704
47.837	0.	0.	0.	1.0000	0.0435	20.0000
-47.837	-31.927	-66.084	0.378	0.1700	0.0435	3.9821
56.016	0.	0.	0.	1.0000	0.0435	20.0000
-56.016	-37.869	-79.743	0.3443	0.1700	0.0435	5.8353
65.200	0.	0.	0.	1.0000	0.0435	20.0000
-65.200	-44.830	-96.655	0.3285	0.1100	0.0435	8.2839
76.385	0.	0.	0.	1.0000	0.0435	20.0000
-76.385	-53.807	0.	0.	1.0000	0.0435	20.0000
95.962	0.	0.	0.	1.0000	0.0435	20.0000
-95.962	-71.192	0.	0.	1.0000	0.0435	20.0000

FREQUENCY=4000 HZ TRANSMISSION LOSS= 6.81

Figure 41. Sample Output (Concluded).

APPENDIX C

COUPLING OF LINE SOURCE TO DUCT MODES

To understand the coupling of the sound source with the various duct modes possible in an annulus, we consider an idealized problem in which the annulus is unwrapped into a rectangular duct and the siren source is modeled as a line source (see Figure 42); "r" is the mean radius of the annulus.

We have to solve an equation for the pressure (denoted by "p"):

$$\nabla^2 p + k^2 p = \delta(x)\delta(y)$$

where $k = \omega/a$, $\delta(x)$, $\delta(y)$ are delta functions. The solution is for $-\pi r \leq y \leq \pi r$ and has to be periodic with wavelength "$2\pi r$". Also, at $x \to \pm\infty$, the radiation condition is to be satisfied. Let

$$p = \sum_{m=0}^{\infty} A_m(x) \cos\left(\frac{my}{r}\right).$$

Note that $\delta(y)$ can be expanded in the even Fourier series as:

$$\left\{\frac{1}{2\pi r} + \frac{1}{\pi r} \sum_{1}^{\infty} \cos\left(\frac{my}{r}\right)\right\}.$$ Then $A_0''(x) + k^2 A_0(x) = \delta(x)/2\pi r$ and

$A_m''(x) + [k^2 - (\frac{m}{r})^2] A_m(x) = \delta(x)/\pi r$ for $m \geq 1$. The solution for p can be finally written down as:

$$p = \frac{e^{j k |x|}}{4\pi j k r} + \sum_{1}^{N} \frac{e^{j k_m |x|} \cos\left(\frac{my}{r}\right)}{2j k_m \pi r}$$

$$+ \sum_{N+1}^{\infty} \frac{e^{-\kappa_m |x|} \cos\left(\frac{my}{r}\right)}{2\kappa_m \pi r}$$

where $k_m = \sqrt{k^2 - (\frac{m}{r})^2}$ and N is the largest value of m for which $kr > m$ and $\kappa_m = \sqrt{(\frac{m}{r})^2 - k^2}$ for $m > N$. We are not interested in the terms of the series involving κ_m in the above since they represented nonpropagating terms.

$$E_m \propto (f^2 - f_c^2)^{-\frac{1}{2}}$$

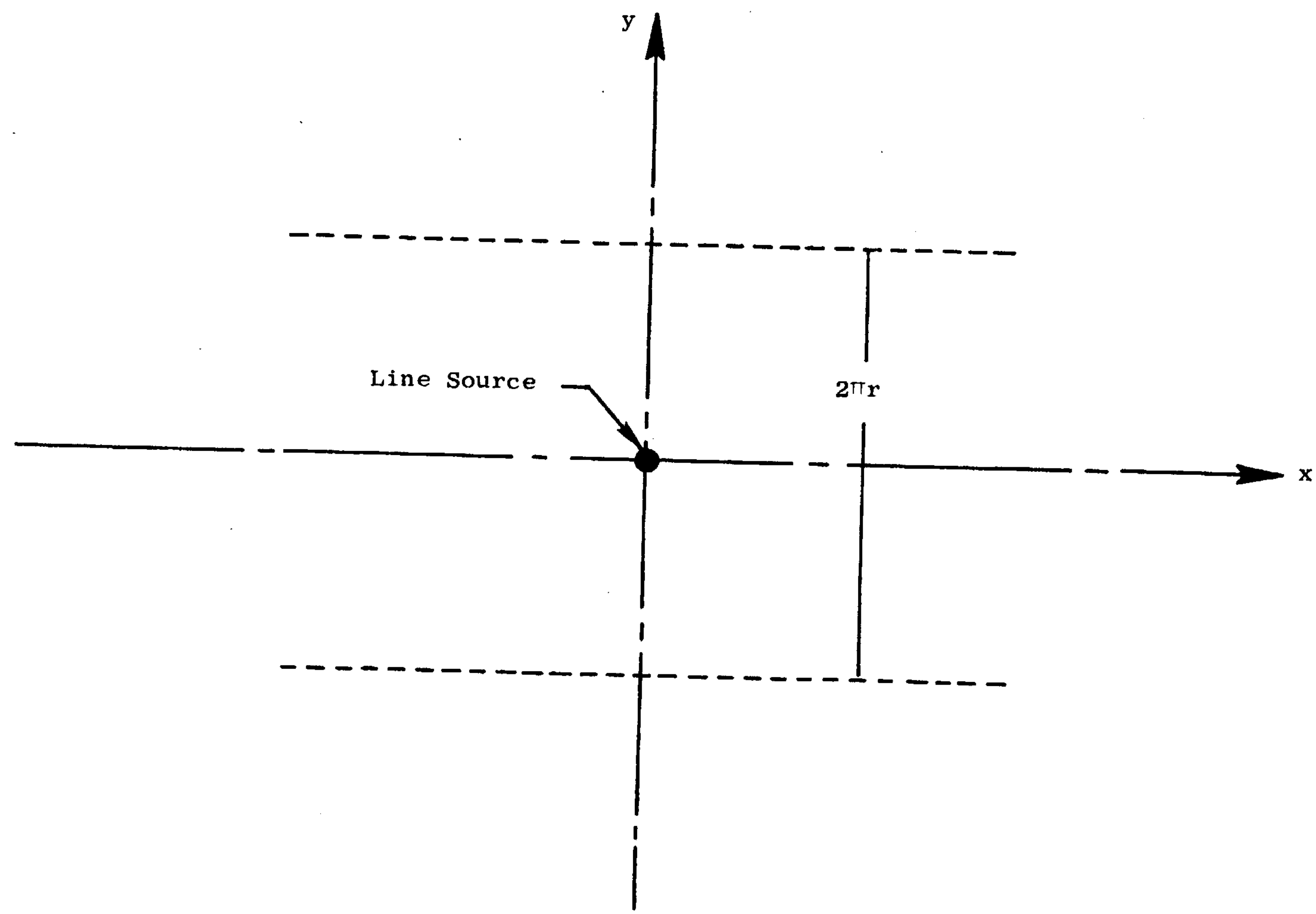

Figure 42. Coupling of Line Source to Duct Modes.

The energy flux associated with each of the propagating terms can be deduced by first writing

$$\cos\left(\frac{my}{r}\right) = \left[\frac{e^{j\,(my/r)} + e^{-j\,(my/r)}}{2}\right]$$

and considering each cos (my/r) term to involve two plane waves (one for +y and other for -y and then noting that the energy flux will be proportional to $\cos^2(my/r) \times (km/k)$. The square of the cosine term is proportional to the power in the wave direction and it is the axial power component that is of interest. Hence the product of the cosine squared and the direction cosine is considered. Since the cut-off frequency for each mode is $\omega_m = (am/r)$, the net result is that the line source will excite energy levels in each propagating mode proportional to $\{f^2 - f_c^2\}^{-1/2}$ where f is the frequency of excitation and f_c the cut-off frequency of the relevant mode.

NOMENCLATURE

a	Speed of sound, m/sec
A/A*	Isentropic area ratio
A_{ij}	Matrix element
(A_n)	Upstream coefficient matrix for n-th blade row
$B_{(\ )}$	Amplitude of backward-travelling wave
BPF	Blade passing frequency, Hz
D_{ij}	Matrix elements
(D_n)	Downstream coefficient matrix for n-th blade row
$\hat{e}$	Unit vector
E_m	Energy assignment to m-th mode
f	Frequency, Hz
$F_{(\ )}$	Amplitude of forward-travelling wave
G	Aeroacoustic flow function
H	Height, cm
$\vec{I}$	Intensity vector
j	$\sqrt{-1}$
k	Wavenumber, ω/a
K	$(k_x^2 + k_y^2)^{1/2}$
ℓ	Axial spacing, cm
L	Length, cm
m	Circumferential lobe number
$\dot{m}$	Mass flow rate, kg/sec
M	Mach number
N	Newtons
$P_{(\ )}$	Pressure, N/m^2
$Q_{(\ )}$	Amplitude of vorticity wave
r	Radius, cm
R_o	Real component of impedance at an interface
S	Cross-sectional area
t	Time coordinate
$T_{(\ )}$	Amplitude of transmitted wave
T	Temperature, K

NOMENCLATURE (Continued)

TL	Transmission loss, dB
u'	Perturbation in axial velocity component, m/sec
U	Mean axial velocity component, m/sec
v'	Perturbation in transverse velocity component, m/sec
V	Mean transverse velocity component, m/sec
W_R	Rotor physical speed, m/sec
x	Axial Cartesian coordinate, fixed to blade row
X_o	Reactive component of impedance at an interface
y	Transverse Cartesian coordinate, fixed to blade row
α	Upstream relative flow angle, degrees
β	Downstream relative flow angle, degrees
γ	Ratio of specific heats
Δ	Increment or decrement
ε	Acoustic energy density
η	Strouhal number (dimensionless frequency)
$\theta_{( )}$	Wave propagation angle
μ	$(1 + \frac{\gamma-1}{2} M^2_{abs})$
ν	Dimensionless velocity
ξ	Dimensionless length parameter
π	3.14159
ρ	Density, kg/m^3
σ	Hub/tip (radius) ratio
ϕ	Absolute flow angle relative to axial direction, degrees; also, dimensionless pressure in Section 3.2, $\phi = p'/\gamma p$
ψ_1, ψ_{21}	Angle of inclination of acoustic wave incident on a shock
ψ_2	Angle of inclination of refracted wave leaving shock
ψ_3	Angle of inclination of vorticity wave behind shock
ω	Circular frequency, $2\pi f$

NOMENCLATURE (Concluded)

Subscripts

abs	Absolute flow parameter
$B_{( )}$	Backward-travelling wave parameter
c	Cut-on
f	Final value in passage problem
F	Coordinate frame moving with fluid
$F_{( )}$	Forward-travelling wave parameter
i	Initial value in passage problem
I	Incident wave parameter
m	Value downstream of n-th blade row
n	Value upstream of n-th blade row
$Q_{( )}$	Vorticity wave parameter
$R_{( )}$	Reflected wave parameter
s	Static value
T	Transmitted wave parameter
x	Axial component
y	Transverse component
o	Stagnation value
1	Station upstream of turbine

Superscripts

$( )'$	Perturbation quantity
$( )^*$	Root mean square value

REFERENCES

1. Stone, J.R., "Flight Effects on Exhaust Noise for Turbojet and Turbofan Engines - Comparison of Experimental Data with Prediction," NASA TM X-73552, November, 1976.

2. Matta, R.K., Sandusky, G.T., and Doyle, V.L., "GE Core Engine Noise Investigation - Low Emission Engines," FAA-RD-77-4, February, 1977.

3. Emmerling, J.J. and Bekofske, K.L., "Experimental Clean Combustor Program - Noise Measurement Addendum - Phase II Final Report," NASACR-135045, January, 1976.

4. Strahle, W.C. and Shivashankara, B.N., "Combustion Generated Noise in Gas Turbine Combustors," ASME paper 75-GT-27.

5. Plett, E.G. and Leshner, M.D., "Combustion Intensity and Distribution Relation to Noise Generation," AIAA Paper No. 75-524.

6. Hassan, H.A., "On the Origin of Combustion Generated Noise," Internal memo written at North Carolina State University, Department of Mechanical and Aerospace Engineering.

7. Doyle, V.L. and Matta, R.K., "Attenuation of Upstream-Generated Low Frequency Noise by Gas Turbines," NASA CR-135219, July, 1977.

8. Bekofske, K.L., "Attenuation of Acoustic Energy Across a Blade Row," General Electric Report No. 73CRD342, December, 1973.

9. Mani, R. and Horvay, G., "Sound Transmission Through Blade Rows," J. Sound and Vibr. Vol. 1., No. 1, pp. 59-83, 1970.

10. Cummings, A., "Sound Transmission in Curved Duct Bends," J. Sound Vibr. Vol. 35, No. 4, pp. 451-477, 1974.

11. Tsien, H.S., "The Transfer Function of Rocket Nozzles," Journal of the American Rocket Society (May - June 1952), pp. 139-143.

12. Candel, S.M., "Analytical Studies of Some Acoustic Problems of Jet Engines," Ph.D. Thesis (California Institute of Technology), 1972 (Chapter II).

13. Marble, F.E., "Acoustic Disturbance from Gas Nonuniformities Convected Through a Nozzle," Proceedings of Interagency Symposium of University Research in Transportation Noise, Stanford Univ., Vol. II of Proceedings, pp. 547-561, March 28-30, 1973.

14. Davis, S.S. and Johnson, M.L., "Propagation of Plane Waves in a Variable Area Duct Carrying a Compressible Subsonic Flow," Paper Presented at the 87th Meeting of the Acoustical Society of America, New York, N.Y., April 23-26, 1974.

15. Kaji, S. and Okazaki, T., "Study of Plane Sound Waves Passing Through a Compressor Blade Row," Paper F-5-1, Proc. 6th Intl. Congress on Acoust., Tokyo, Japan, August 21-28, 1968.

16. Cumpsty, N.A., and Marble, F.E., "The Generation of Noise by the Fluctuations in Gas Temperature into a Turbine," University of Cambridge Report No. CUED/A TURBO/TR57, 1974.

17. Shapiro, A.H., Compressible Fluid Flow, Vol. I, The Ronald Press Co., New York, 1953.

18. Blokhintsev, D.I., "Acoustics of a Nonhomogeneous Moving Medium," NACA TM 1399, 1956 (Russian original Leningrad 1946).

19. Morfey, C.L., "Rotating Pressure Patterns in Ducts: Their Generation and Transmission," J. Sound Vibr. vol. I, pp. 60-87, 1964.

20. Mani, R., "Refraction of Acoustic Duct Waveguide Modes by Exhaust Jets," Q. Appl. Math., Vol. 30, No. 4, pp. 501-520, January, 1973.

21. Kinsler, L.E. and Frey, A.R., Fundamentals of Acoustics, John Wiley and Sons, Inc., New York, 1962.

22. Landau, L.D. and Lifshitz. E.M., Fluid Mechanics, Pergamon Press, London, 1959.

23. Moore, F.K.; "Unsteady Oblique Interaction of a Shock Wave with a Plane Disturbance," NACA Report No. 1165, 1954.

U.S. DEPARTMENT OF COMMERCE
Technology Administration
National Technical Information Service
Springfield, VA 22161 (703) 605-6000